ABSTRACT

Title of dissertation: A VALIDATED MODELING FRAMEWORK FOR PERFORMANCE ANALYSES OF EXPERIMENTAL AND PROVEN DESALINATION TECHNOLOGIES

Sebastian Antonio Romo Duenas,

Doctor of Philosophy Mechanical Engineering, 2022

Directed by: Professor Jelena Srebric, Ph.D.

Department of Mechanical Engineering

There is a wide array of desalination methods available for treating water at different salinities and production rates, but there are no systemic approaches on how to directly compare performance of different desalination systems. Existing comparison efforts focus solely on isolated performance metrics for a single desalination system, resulting in segregated case studies and/or incomparable systems. Numerical models for desalination systems can bridge this gap as they can take account of specific deployment needs. However, models in the literature are not mutually compatible, and they seldom disclose all the parameters or equations necessary for development and validation. This dissertation conceives a cross-comparison enabling simulation framework for the most relevant desalination processes. To achieve this, modeling approaches and thermophysical property

correlations are curated from volumes of literature and used to create metamodels for six relevant desalination methods. The models are integrated into a simulation framework based on parameter hierarchies imposed in the model structures. The simulation suite is validated with data from the literature and actual operational data from desalination facilities in the field.

The results show that the cross-comparison across equal parameter hierarchies is possible for all desalination technologies. A comparative analysis between the dominant technologies in the thermal and molecular transport families, Multi-Effect Distillation (MED) and Reverse Osmosis (RO), respectively, shows that energy intensity in MED is an order of magnitude greater for equivalent operational conditions, but actual operational costs are comparable. The models are further refined to reflect conditions from actual systems in the field and an iterative sampling algorithm is developed to find plausible operation scenarios given the scarce data from the field. This method achieves excellent agreement with data from four desalination plants with percent differences ranging between 2.5% and 9.3%. Furthermore, the results identify two plants performing 20% below their theoretically achievable recovery. Apart from evaluating existing deployments, the simulation suite helps identify a niche in the operational map of existing desalination methods characterized by high recovery rates and high feed salinities that is generally unfulfilled by conventional desalination.

A VALIDATED MODELING FRAMEWORK FOR PERFORMANCE ANALYSES OF EXPERIMENTAL AND PROVEN DESALINATION TECHNOLOGIES

By

Sebastian Antonio Romo Duenas

Dissertation submitted to the Faculty of the Graduate School of the
University of Maryland, College Park in partial fulfillment
of the requirements for the degree of
Doctor of Philosophy
2022

Advisory Committee:

Professor Jelena Srebric, Ph.D. (Advisor/Chair)
Professor Reinhard Radermacher, Ph.D.
Professor Bao Yang, Ph.D.
Professor Dongxia Liu, Ph.D.
Professor Peter Sunderland, Ph.D. (Dean's Representative)

Dedication

To my parents,

German and Ivette

Acknowledgements

This dissertation is the culmination of four years of graduate work which at times were intense and emotionally draining. This work could not have been possible without the help of many who helped me push through these challenges and helped making this experience positive, memorable, and worthwhile.

First, I would like to sincerely express my gratitude to my advisor, Dr. Jelena Srebric, for her guidance and support. Dr. Srebric was the first person to give me an opportunity in the research world when I was in my third year of undergraduate studies. And since then, she has helped me exploit my strengths, address my weaknesses, and help me grow in the personal and professional aspects of life.

I would like to extend my gratitude Dr. Bahman Abbasi for trusting me to contribute to the project "Zero Liquid Discharge Water Desalination Process Using Humidification-Dehumidification in A Thermally Actuated Transport Reactor" sponsored by the US Department of Energy (DE-EE0008402). Special thanks to Dr. Matt Bauer, our project manager for his timely inputs and constructive feedback that helped strengthen the impact of my research.

I am immensely thankful to my family, who made themselves constantly present despite the distance. Specifically, I would like to acknowledge my parents, German and Ivette, who could not have been more supportive of my endeavors and have always been my guides and role models. Thank you to my sisters Carla and Paola for their support and encouragement. I would also like to warmly

acknowledge my adoptive family in Maryland, Laura, Gustavo, Didac and Gerard for all their help and kindness.

I would like to thank my team at CITY@UMD who have helped my work with their expertise, feedback, and for creating a warm and welcoming environment. During my undergraduate, Dr. Mohammad Heidarinejad guided me through my first research endeavors which contributed to my desire to pursue a doctoral degree, and Daniel Dalgo warmly welcomed to the team and provided valuable guidance through my studies. Thank you to Nick Mattise, Dr. Shengwei Zhu, Lingzhe Wang, Avery Layne, Michael Raad, Tong Lin, Gautam Vanama, Nicholas Rabchevsky, Michael Storch, Kenny Scheer, and Elaine Sanico.

I would like to thank my grad school friends Water Arias, Camila Correa, Chris Howard, Rafi Wiesel, Matt Arace, Derek Bussman, Mike Hopkins and Rafi Ropelato for making this experience worthwhile. Special thanks to Sergio Cofré, for sharing your friendship, experience, and for the many laughs that made this time memorable.

Finally, thank you to my partner, Oriane Rütsche, for her support, patience, and incessant confidence in me. Thank you for encouraging me to give my best through my work and in the same way, fervidly enjoy life.

Table of Contents

List of Tables

List of Figures

List of Abbreviations

CAOW – Closed Air, Open Water
CDI – Capacitive Deionization
CR – Compression Ratio
CWOA – Closed Water, Open Air
EDS – Electrodialysis
ERD – Energy Recovery Device
GR – Gain Ratio
HDH – Humidification-Dehumidification
HTC – Heat Transfer Coefficient
LCD – Limiting Current Density
MDT – Multi-effect Distillation with Thermocompression
MED – Multi-Effect Distillation
OAOW – Open Air, Open Water
RO – Reverse Osmosis
ROX – Reverse Osmosis with Pressure Exchange
RR – Recovery Ratio
PX – Pressure Exchanger
SI – Salinity Increase
STEWARD – Solar Thermal Extraction of Water by Atomization and Recuperative Desalination
TDS – Total Dissolved Solids
TVC – Thermovapor Compression
XLE – Extra Low Energy
ZLD – Zero Liquid Discharge

Chapter 1: Introduction

This chapter presents the background and motivation for the presented research.

1.1. Background

The deployment of desalination systems worldwide has been rapidly increasing since the mid 1900's when it became not just a convenience in remote locations but rather a necessity for sustaining human activities. These rising are fueled by population trends, economic growth, and depletion of current freshwater sources [1]. For instance, it is was estimated in 2018 that 40% of the global population faced severe water scarcity, with projections rising to 60% by 2025 [2]. In the United States alone, the population has doubled over the past 50 years, and the demand for water has tripled with at least 40 states anticipating water shortages by 2024 [3]. Figure 1-1 shows the rapidly rising trends in deployments of desalination systems. By the beginning of 2020, the global desalination capacity for freshwater production stood at 97.2 million m^3/day [4]. Furthermore, predictions suggest that the global desalination market size will reach USD 32 billion by 2025 [5].

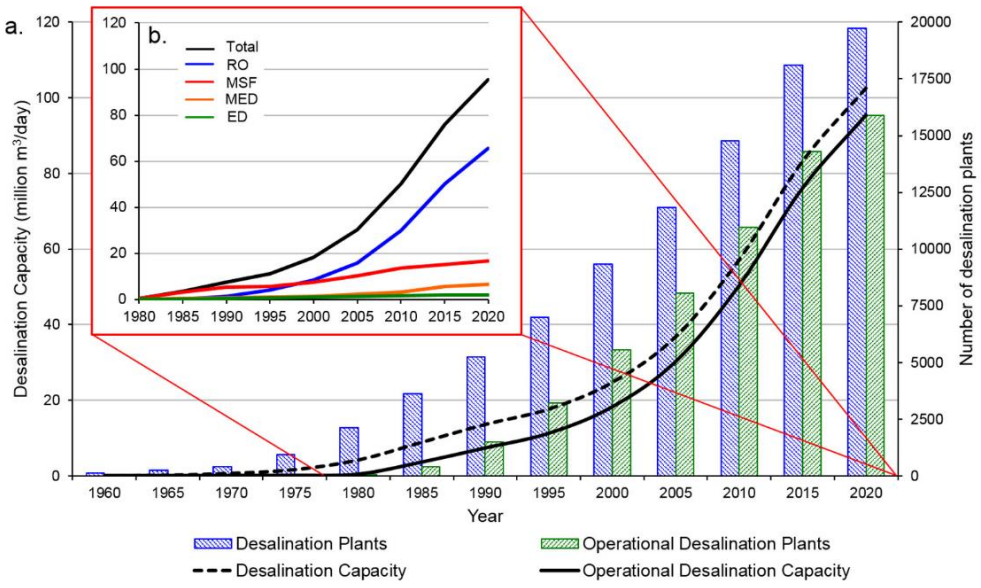

Figure 1-1: Global desalination trends by (a) total capacity and number of plants and (b) desalination capacity by method [2]

In principle, the desalination process consists of separating ions, predominantly sodium chloride, and water from a single stream so the product water at a lower salinity can be suitable for specific uses. Figure 1-2 shows the conventional schematic of a desalination process that has feed water and energy as inputs and product water and concentrate for outputs. Some processes can have an additional cooling water output that has the same salinity content as the feed water stream and is rejected to the environment. Desalted water is widely utilized for human consumption or activities related to the energy, industrial, agricultural, and municipal sectors. Water can be classified according to its salt contents, specifically, fresh or pure water contains less than 0.5 g/kg and it is suitable for

human consumption[1], brackish water ranges from 0.5 to 20 g/kg, sea or saline water ranges from 20 to 50 g/kg and brine for concentrations greater than 50 g/kg [2], [6]. Although there is no technical consensus in the literature about what range is defined by the term *hypersaline* brine or water, it is used in this work to describe water with salt contents above 70 g/kg in accordance to most studies that employ the term [7]–[10] and up to its solubility limit of 360 g/kg at 25°C.

[1] The World Health Organization, while not proposing health-based guidelines, recommends concentrations lower than 0.25 g/kg for chloride and 0.20 g/kg for sodium for taste thresholds [169].

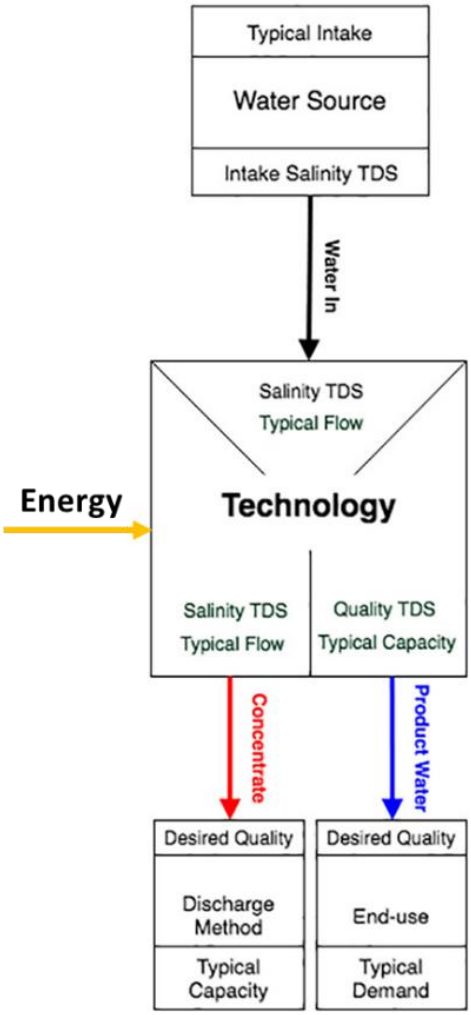

Figure 1-2: Conventional desalination process flowchart. Adapted from [11]

In a conventional desalination process, producing water at a lower salt content than the feed implies, by mass conservation, that a salt-loaded brine stream is also outputted as a byproduct. Discarding brine is problematic because increased salinity, temperature and the presence of chemical additives can damage marine ecosystems and pollute water reservoirs [12]. Furthermore, brine disposal usually involves expensive transportation, post-treatment and potentially hazardous disposal methods such as deep-well injection [13]. This practice consists in injecting the brine into an underground aquifer, however besides its elevated cost,

deep-well injection is restricted to areas with low seismic activity due to the risk of underground water contamination [14].

The estimated global brine production from desalination plants in 2019 was 141.5 million m^3/day with almost 80% being produced within a 10 km distance from the coastline [2]. There are no standard regulations for important factors involved in brine rejection towards sea environments such as excess salinity and discharge jet characteristics [15]. While specific cases carefully monitoring marine life indicators show short-term sustainability in this practice, the ecosystem response is seasonal, region dependent, and would further be challenged by climate change and increased brine production in the long-term [16], [17]. In addition, brine salinity, temperature and chemical content is highly dependent on the desalination method employed which makes brine disposal control and implementation further complicated [18]. It must be noted that the growing desalination number deployments are not the only contributors to the global brine production. The hypersaline water byproduct from the oil and fracking industry is a predominant problem that requires careful consideration. The United States alone produces about 8.7 million m^3/day from oil and gas fracking in which can reach up to 210 g/kg, and is usually disposed through ocean discharge or deep-well injection [8].

Zero Liquid Discharge (ZLD) desalination has emerged as a strategy to overcome the issues associated to brine disposal. ZLD desalination incorporates additional mechanisms to the underlying desalination process so that the effluent byproduct stream is solid salt [19]. It must be noted that ZLD implementation does not necessarily involve that full recovery achieved in the desalination step, but

mainly additional concentration and crystallization of the brine stream. Thus the first step in ZLD is practically desalination, ideally at the highest possible recovery, which acts as a brine concentrating process, followed by either a brine crystallizer or an evaporation pond [12]. A brine crystallizer flashes vapor from the brine stream to further concentrate it until solid crystals begin to form, the salt sludge can eventually be mechanically separated, however, pumping the viscous sludge incurs in high operation costs [20]. An evaporation pond on the other hand makes use of a large land space to let the water evaporate over time [21]. Some experimental implementations intensify evaporation using additional solar or wind energy systems, nevertheless, the cost of land space and time required renders the process rather expensive [22].

There are important implementation constraints for desalination systems that must be considered given the established background. First, the feed water concentration can vary tremendously depending on the water source and the purpose of the desalination process. Second, water production rates can range from small, localized facilities to municipal-scale plants. And third, the deployment location provides spatial, financial, brine-disposal and energy-source constraints for the system. Several desalination methods have been designed over the years to balance these factors. Currently, the experimental domain and the commercial marketplace offer a wide array of technologies that are not cross compared or adequately classified. Therefore, there is a great challenge in decision-making for addressing needs of actual installations which can translate to missed opportunities to saving energy and operation costs.

Many methods have been developed over the years to target water at different salinities, serve different production requirements, increase efficiency, and harness different types of available energy. Today, there are over ten well-established desalination methods available [23], [24], in addition to many experimental processes focusing on hypersaline brine processing [7], [10], [25], [26]. While each method has its corresponding strengths and weaknesses, many of them often overlap in desalination capabilities, or can do so under specific operating conditions. Furthermore, additional pre- and post-treatment as well as energy recovery options can be implemented within each base method to suit individual project needs. The vast array of desalination methods available, myriad of external factors that affect the desalination process and customization possibilities make cross-comparison very difficult.

1.2. Motivation

There are many desalination systems available in the desalination market and in development stages, however, there are no well-established and clear guidelines for choosing among them. A robust cross-comparison framework can help decision-making in deploying and retrofitting a desalination system to prevent severe consequences including compromising water security, hazards due to poor brine management, and capital expenses for underperforming plants. However, cross-comparison of desalination systems can appropriately help decision-making only if the specific requirements of the deployment are included. Traditionally, published cross-comparison efforts compare energy intensities and associated costs [24]. Nevertheless, such studies survey plants that are not necessarily optimized for

the required operating ranges and result in biased comparisons while disregarding additional strengths and limitations inherent to each system. Therefore, cross-comparison of desalination systems must occur from a holistic approach, while considering the specific operation conditions and implications in a case-by-case basis. User requirements can be accounted for using thermodynamic models for desalination systems because they can provide reliable estimations on the performance at variable input conditions. Therefore, the first step in addressing the cross-comparison of desalination systems numerically is to organize the scattered knowledge into adaptable models.

This work focuses on six relevant desalination methods including both established and experimental technologies. These methods include Thermovapor Compression (TVC), Multi-Effect Distillation (MED), Humidification-Dehumidification (HDH), Reverse Osmosis (RO), Electrodialysis (EDS), and Capacitive Deionization (CDI). The dominant methods in the industry are based on MED and RO processes but incorporate energy recovery devices. Therefore, Multi-Effect Distillation with Thermocompression (MDT) and Reverse Osmosis with Pressure Exchange (ROX) are also considered.

The decision-making chaos created by the wide assortment of desalination options available and affecting factors can only be addressed numerically mainly due to data unavailability from both the literature and the field. Models for desalination systems, are therefore a suitable option to undertake this challenge as if they were compatible and generalizable. Several modeling efforts have been undertaken in the literature, and they do an excellent job in analyzing, optimizing,

and advancing the state-of-the-art within each desalination system individually. However, simulation is rarely conducted in conjunction with models for other desalination methods. Overall, most published desalination models are developed in isolation as the information flow from inputs to outputs, as well as algorithm structures are only applicable for each specific study. Furthermore, critical parameters in most modeling studies are known or determined a-priori, restricting the model to the particular operating conditions in each case. The latter is evident in models that employ empirical correlations valid only for the ranges in which the correlations are developed. Unfortunately, there is limited experimental data on the matter as most modeling studies do not disclose the full set of parameters or equation coefficients to complete simulations and reproduce published work.

1.2.1. Approaches to Desalination System Modeling

There are numerous approaches for modeling desalination systems across the published literature. These are related to the purpose for simulation and therefore affects the flow of information within each model. Some studies focus on optimizing a system size to meet a specific recovery ratio [27]–[29], understanding transient operation [30], [31], optimizing with respect to energy [32], and/or replicating mechanistic phenomena [33]–[35] that occurs at a finer scale within the desalination systems. In addition, there are many published studies of data-driven modeling approaches to optimize, control, maintain and predict performance of desalination systems, however, field data is scarce and the vast majority of models developed with small datasets (number of datapoints in are usually the lower hundreds) [36]. Modeling is further complicated by the specific assumptions and

levels of abstraction that different publications employ. These are usually linked to the modeling objectives presented such as integration with renewable energy [37], [38], optimization of a novel system [39], [40], or a high-level overview from a thermodynamic perspective [41]–[43]. Although these varied approaches, underlying assumptions, and modeling objectives embedded are essential to advancing the state-of-the-art within each individual desalination method, it is important to not overlook an integrating and generalizable approach that would enable the cross-comparison of desalination systems.

1.2.2. Model Validation

There is a limited number of published simulation studies in which all the required equations and parameters are disclosed to construct a model. In these cases, validation is important as it demonstrates that a model can accurately reproduce the observed desalination operation. However, the models required for cross-comparative analyses must be generalizable to accurately reproduce a variety of operation conditions. This can be particularly challenging for the models that rely on numerical correlations because their range of validity is limited. In these cases, a desalination model for cross-comparison must employ different empirical correlations to increase the overall simulation range. Validation with multiple published studies, therefore, is crucial because it ensures the model can reproduce an array of operation conditions, and multiple validation points compensate for the cases where not all the parameters are disclosed.

The value of the model lies in its applicability to actual desalination systems as opposed to constraining it to reproducing theoretical case studies. Thus,

validation must also be conducted using data from desalination systems in the field. This introduces another challenge because there are certain input parameters required for simulation that can only be obtained experimentally, others that are usually manufacturer's proprietary data, or variables whose measurement would require additional and expensive instrumentation. Nevertheless, this endeavor is worth pursuing as field-validated models would bring great value to the field. Validated models not only can be deployed to help decision-making and optimization but can also be used to map the operation and performance of existing systems to guide new technology developments.

1.2.3. Need for rapid introduction of novel technologies

Research and development in the desalination field is an expensive and lengthy process. New systems must propose better alternatives to well-established desalination plants that often involve long-term investments. Desalination systems are often characterized by operation metrics such as average energy intensity, typical product flow rates, or feed salinities [23], [24], [44]. A common problem in the literature and the industry is that these metrics are reported in isolation without highlighting their interdependence within system operation. This can result in benchmarks for new desalination developments because it inaccurately conveys that such reported features or limitations are intrinsic to the desalination method itself rather than the underlying operation conditions. Therefore, most benchmarks for desalination systems are arbitrary "rules of thumb" rather than well-defined operation and performance bounds.

Instead of focusing on few performance metrics, the best desalination system is the one that matches the specific requirements at the deployment site such as production needs, infrastructure, feed water conditions and type of energy available [45], [46]. The only way to investigate this at early development stages of a desalination system is through numerical models based on first principles of mass and energy conservation and thermodynamics. By employing simulations one can develop an operational map for each desalination method including the ranges the system can cover and the resulting performance. This would help identify opportunities for new systems rapidly and provide early guidance within the design process.

Chapter 2: Research Hypotheses, Objectives and Tasks

This chapter presents the research hypotheses, objectives and tasks completed in this work.

2.1. Research Hypotheses, Objectives and Tasks

The following hypotheses are formulated to guide the research presented in this dissertation:

- There is a common framework that can integrate simulation of desalination systems to enable cross-comparison.
- The validity of the framework needs to be verified through a rigorous case study assessment of actual desalination plants.
- The validated framework can enable introduction of novel desalination technologies such as HDH-ZLD by mapping its operational performance onto the performance of existing technologies.

The following research objectives (O) are conceived to evaluate the hypotheses:

- **O1:** Develop a cross-comparative simulation framework
- **O2:** Validate the framework with actual data from desalination plants
- **O3:** Map an HDH-based ZLD system operation with the validated framework

The following Research Tasks (RT) are derived from each research objective and are undertaken in this dissertation:

Objective 1: Framework Development

- **RT1:** Develop physics-based models for the most relevant desalination methods.
- **RT2:** Design a simulation framework that incorporates the developed models and allows for cross-comparison.

Objective 2: Case Studies

- **RT3:** Recruit desalination plants in the field to serve as case studies to evaluate the developed models.
- **RT4:** Adapt the previously developed baseline desalination models to fit the configuration presented by the case study systems.
- **RT5:** Deploy the adapted models to replicate case study data

Objective 3: Mapping an HDH-based ZLD system

- **RT6:** Develop a physics-based model for a novel desalination system
- **RT7:** Conduct a simulation-based analysis to assess performance of the new system, costs, and deployment opportunities from a technical standpoint

2.2. Research Summary

There is an abundance of desalination systems but no clear approach on how to choose among them. Numerical simulations can provide a viable approach to cross-comparison of desalination systems because they can implement the specific requirements of each deployment. However, existing desalination models are not suitable for cross-comparison because they have incompatible input-output structures, validity ranges, and underlying assumptions. This is further complicated because the complete set of parameters or equations for building a model are

seldom available in published studies. Therefore, this thesis focused on the three identified objectives, each organized in a progression.

Objective 1 focused on the development of the cross-comparative simulation framework based on desalination models in the existing literature. Specifically, this dissertation developed metamodels for six relevant desalination methods, namely Thermovapor Compression (TVC), Mulit-Effect Distillation (MED), Humidification-Dehumidification (HDH), Reverse Osmosis (RO), Electrodialysis (EDS), and Capacitive Deionization (CDI). These models are grouped into thermal and molecular transport families and validated within 9% difference of published data. The models are implemented in a novel cross-comparison enabling simulation framework based on the analytical hierarchy of parameters. A comparison of the studied methods was conducted at their designed operational conditions specified by feed salinity ranges of 1.6 to 2.4 g/kg for CDI and RO, 2.8 to 4.2 g/kg for EDS, 28 to 42 g/kg for TVC and HDH, and 37 to 55 g/kg for MED. Despite different operational conditions, all models exhibit a non-linear, positive correlation between energy consumption and system size in response to feed salinity and production rate. The framework is also employed in an in-depth cross-comparative analysis between MED and RO which are the dominant technologies in the market. The results suggest that energy intensity for MED is an order of magnitude greater than RO for the same operational conditions, but actual operational costs are comparable.

Objective 2 focused on validation using case studies from the field. The value of a desalination model lies in its applicability to actual systems as opposed

to constraining it to reproducing theoretical case studies. However, validation with actual desalination systems in the field is challenged by unavailable parameters required for simulation that can only be obtained experimentally or are manufacturer's proprietary data. To solve this, the MED and RO are adapted to include thermocompression and pressure exchange, respectively, for energy recovery as featured in most plants in the field. These new models are employed by a novel semi-supervised algorithm that implements data-driven iterative sampling and optimization schemes to find the most plausible operation scenarios given only partially available operational data. This procedure is deployed in four case studies of actual desalination plants: two Multi-Effect Distillation with Thermocompression (MDT) and two Reverse Osmosis with Pressure Exchange (ROX). The maximum differences between simulated and collected data are 5.5% and 2.5% for the two MDT plants as well as 6.4% and 9.3% for the two ROX plants. Then, a new theoretical efficiency metric is introduced to define optimal operation of a desalination plant. This metric allowed to highlight two plants operating around 20% below their theoretically achievable recovery.

Objective 3 focused on using the developed framework to map a novel desalination system onto the operational map of existing technologies. A model based on first-principles can be used to bound operation of a Humidification-Dehumidification-based system concept featuring Zero Liquid Discharge and off-grid capabilities. The model employs conservation laws to find feasible state points that meet baseline operation with a 100 g/kg hypersaline feed stream and 10 kg/h of product water. The system presents a baseline energy intensity of 954 kWh/m^3

for water desalination and zero liquid discharge. The system can tolerate variations of 25% in product flowrate and 75% in feed salinity with energy demands virtually unaffected. Although the energy requirements are high compared to other desalination technologies, the proposed system operating costs of 81 to 93 USD/m^3 of produced water are comparable to those of existing brine disposal techniques. The proposed system could cater to a niche within the operational map of existing desalination technologies characterized by high recovery rates and high feed salinities that is generally unfulfilled by conventional desalination methods.

2.3. Dissertation Outline

The first research objective associated to the development of the simulation framework sets the foundation for validation, case study replication and characterization of new technologies. These objectives are aligned with three publications that form a chapter in this dissertation. Figure 2-1 shows the structure of the chapters with their underlying objectives and tasks. The remainder of the present dissertation is organized as follows:

Chapter 3 – metamodel development and framework for cross-comparison enabling simulations. The framework is demonstrated through a comparative analysis of MED and RO. This chapter is based on the following publication: "S. A. Romo, N. Mattise, and J. Srebric, "Desalination metamodels and a framework for cross-comparative performance simulations," *Desalination*, vol. 525, no. 1 March 2022, p. 115474, Mar. 2022, doi: 10.1016/j.desal.2021.115474." [Journal Impact Factor: 9.501].

Chapter 4 – adaptation of the metamodels to incorporate ERD, development of a methodology to construct simulations from case studies with partially available data and recover missing parameters. Validation and demonstration of this methodology in four desalination plants from the field. This chapter is based on the following publication: "S. A. Romo, M. Storch Jr., and J. Srebric, "Operation Modeling of Actual Desalination Plants," *Desalination*, 2022, Under peer-review." [Journal Impact Factor: 9.501].

Chapter 5 – development of a model for a HDH-based zero-liquid discharge desalination methodology embodied in a novel system. Evaluation of deployment opportunities in the field using case study data and positioning it within the operational map of existing desalination technologies. This chapter is based on the following publication: "S. A. Romo, M. A. Elhashimi Khalifa, B. Abbasi, and J. Srebric, "Mapping of a Novel Zero Liquid Discharge Desalination System based on Humidification-Dehumidification onto the Field of Existing Desalination Technologies," *Water*, Special Issue: Advanced Technologies for Seawater Desalination, 2022, Manuscript Number: water-1707191. Under peer-review." [Journal Impact Factor: 3.103].

Chapter 6 – Personal takeaways and lessons learned from the doctoral experience

Chapter 7 – Conclusion, summary of contributions and future work.

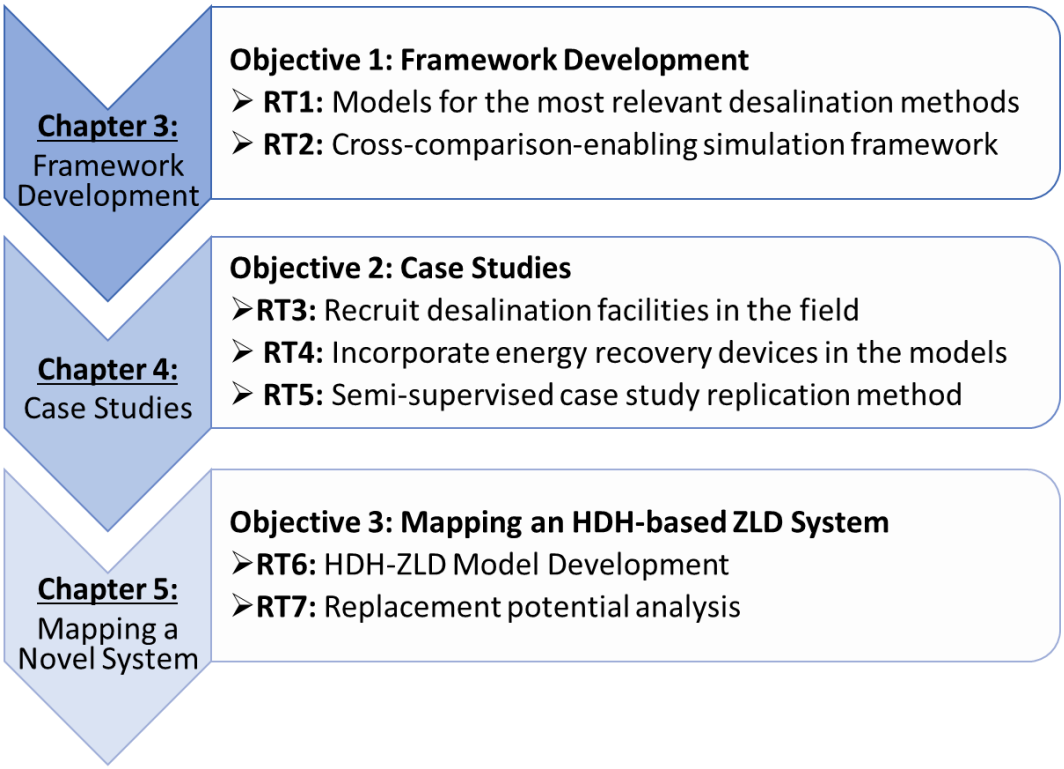

Figure 2-1: Structure of completed research tasks and dissertation

Chapter 3: Development of Metamodels for Desalination Methods

This chapter is reproduced from the following journal paper:

> S. A. Romo, N. Mattise, and J. Srebric, "Desalination metamodels and a framework for cross-comparative performance simulations," *Desalination*, vol. 525, no. 1 March 2022, p. 115474, Mar. 2022, doi: 10.1016/j.desal.2021.115474. [Journal Impact Factor: 9.501].

3.1. Introduction

Different desalination processes have been developed over the years to increase efficiency, reduce equipment maintenance, or target water with higher salt contents. There are more than ten different desalination methods and countless system variations within each method, each one particularly useful for specific feed water characteristics and production requirements. While there have been many efforts to model each process individually for optimization, cross-comparison of desalination technologies remains a major challenge due to several factors including: the lack of standardization in modeling algorithms, difficulties in reproducing modeling approaches because of undisclosed parameters or equations, and models learned with data from a specific system but that cannot be generalized to broader operational ranges.

The starting point towards overcoming this challenge is to correctly implement the models of the most common desalination technologies under a common framework with matching computational structures and parameters. The literature presents volumes of case studies and technological developments with

scattered models. Furthermore, most studies do not disclose all required variables or correlations involved in the simulation algorithm and make the model replication and validation particularly challenging. Although some cases perform comparison of two desalination technologies side-by-side and find equivalent metrics, there is still no standard framework to equalize the input domains of multiple desalination processes simultaneously.

The literature reflects a lack of cohesion in modeling purposes among the different desalination studies. There are commonly accepted desalination models that are predictive in nature, but there is no common algorithm structure that allows for cross-comparison. The greatest challenge in achieving this lies in the lack of knowledge on the physics behind some sub-processes that take place in different desalination systems. Most modeling approaches resort to regression and empirical correlations that are valid for the specific operational conditions and particular system that data is measured from. This is complicated by the lack of disclosure of modeling equations, important parameters, or correlation coefficients in published literature which challenges collaboration among the desalination community. Further research is required into developing such mechanistic equations to expand the predictive capabilities of desalination models. On the other hand, the literature presents many models with different simulation objectives and different input-output structures, which cannot be executed in parallel and therefore do not allow direct comparisons of the results. It is important to organize model algorithms to follow similar input-outputs structures to impose similar constraints to the system and enable meaningful cross-comparison of different desalination technologies.

Few research efforts have focused on comparison between different desalination technologies, and the extent to which such cross-comparison methodologies are implemented present great differences. The majority of studies enumerate and review the general operational ranges such as the feed concentration and product water flow rate that different technologies are able to process [23], [24], [47]–[50]. However, the implementation of such findings is limited to general statistical models that might not be representative of the actual system performance at the required operational conditions [51]. Later research efforts recognized the importance in evaluating energy consumption of desalination technologies and consider the high-level breakdown in heat and electricity requirements [52]. Comparing energy consumption is an initial step into finding universal parameters among desalination technologies that can provide meaningful insights. Finally, a few more recent studies simulate energy consumption from a thermodynamic law analysis [53], [54]. In general, cross-comparison studies in the literature are limited to pairwise comparisons between desalination methods focusing on energy and cost at discrete operation points [29], [45], [46], [55]. A more robust comparison of different desalination systems can be conducted through an exergy analysis, which captures the effects of different operation conditions [56]. Although correct from a theoretical standpoint, reducing system operation to a single operation term is often not enough for practical decision making. Pairwise comparison approaches are valuable and can be an excellent complement to a holistic comparison that considers all involved parameters such as flow rates, concentrations, system sizes and performance metrics. To the best of our knowledge, a modeling framework that

enables a holistic and direct cross-comparison between different desalination methods has not yet been proposed. The first step towards implementing such framework is to classify the different desalination models and establish hierarchical input-output structures that dictates the extent to which different desalination processes can be cross-compared.

The present study proposes a framework for cross-comparison between desalination technologies centered on a standard hierarchical structure for model inputs and outputs, consistent model computational structures, and standardized sets of thermophysical property correlations that include temperature, pressure, and salinity dependence. We first organize the knowledge of desalination modeling to develop metamodels for six different desalination processes including Thermovapor Compression (TVC), Multi-Effect Distillation (MED), Humidification-Dehumidification (HDH), Reverse Osmosis (RO), Electrodialysis (EDS) and Capacitive Deionization (CDI). Then, we deploy the proposed framework in a generalized comparison between the aforementioned desalination methods whose similar energy consumption patterns and responses to product flow rate and feed salt concentration suggests that apparent differences between desalination processes are superficial and that they actually share compatible transport processes. Finally, we apply our framework in a full cross-comparative analysis between MED and RO which are currently the most relevant desalination methods and identify the benchmarks that developing technologies must cater to in the desalination market.

3.2. Methodology

The first step in developing a cross-comparison enabling simulation framework is to correctly implement the models available in the literature. The systematized process of literature review and implementation is shown in Figure 3-1. We used scientific publication databases like ScienceDirect and Google Scholar to search for the desalination method name plus the key words "modeling" and "desalination." We considered peer-reviewed research articles, book chapters, and theses for this review.

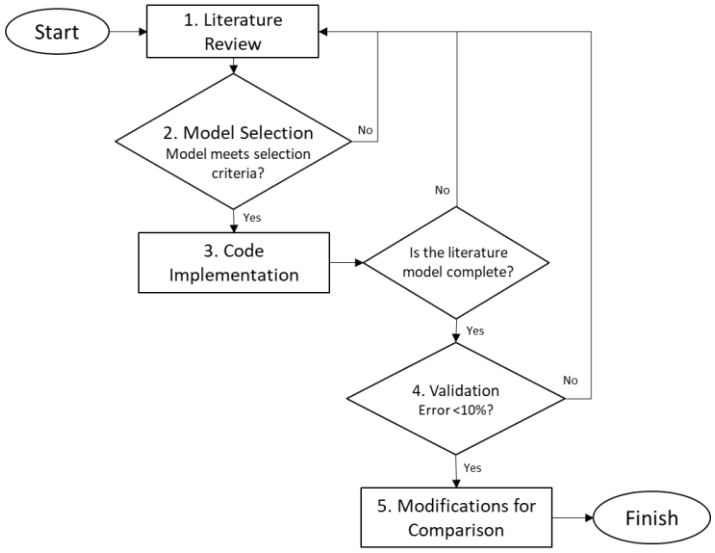

Figure 3-1: Meta-study research and implementation process.

Most published models unfortunately do not disclose all the required parameters or equations, and many can only simulate a single specific set of operational conditions. To resolve this, we develop metamodels that supplement a representative model structure with sub-component models from different studies. The metamodel development process, therefore, is iterative in nature and dictates the direction of the literature review. The most representative model is the literature

model where the complete modeling equations are disclosed, and reference values are provided. Additionally, the selection criteria for the most representative model prioritizes reduced-order models, which have low algorithmic complexity and computational intensity requirements but are still capable of capturing specific differences between operation conditions. The most representative model serves as a guide for the main code structure and provides numerical inputs and outputs for validation. Most models available in the literature unfortunately do not disclose the complete set of variables or equations to close the water/energy/product balance equations needed for implementation in an analytical framework. In the cases where equations, coefficients, or parameters are missing, we conducted further literature review from other references found in the initial search or a new targeted search for the specific unknowns. This iterative process continued until all the initial number of references were reviewed and the metamodel was completed. The resulting metamodel is validated with the values of the most representative model targeting a maximum allowable difference of 10% in the inputs and outputs associated to flow rate, concentration, energy intensity, and system sizing. If the target was not met, we returned to reviewing literature in search of more detailed sub-models.

After successful validation, we standardized the computational structure and matched the hierarchical set of inputs and outputs proposed in this section to enable cross-comparison among different models. In this step, the thermophysical properties of the working fluids are also standardized using correlations that cover the largest validity ranges and consider temperatures, pressures, and salt

concentrations when appropriate [57]–[63]. The resulting metamodel is an improved version of the original literature model re-engineered for the specific purpose of design and cross-comparison between different technologies. Finally, we use the incomplete sets of numerical inputs and outputs found through the literature review process, when available, to test the metamodel with a wider range of inputs. The unknown parameters are supplemented by other studies that disclose them and have the most similar operation conditions. This testing does not impose a maximum allowable difference but rather shows how generalizable the resulting metamodel is.

Table 3-1 shows the total number of studies reviewed through the development of each metamodel presented in this paper and the selected literature models that guided validation.

Table 3-1: Number of curated references used for each developed desalination model.

Desalination Process	**Ref. No.**	**Selected Lit. Model**
Thermovapor Compression (TVC)	34	[43]
Multi-Effect Distillation (MED)	28	[64]
Humidification-Dehumidification (HDH)	19	[65]
Reverse Osmosis (RO)	50	[66]
Electrodialysis (EDS)	40	[67]
Capacitive Deionization (CDI)	64	[68]
TOTAL	235	

3.3. Results

We present the results of our research in two parts. The first part considers metamodel development for each desalination method including thermovapor compression, multi-effect distillation, humidification-dehumidification, reverse osmosis, electrodialysis and capacitive deionization. All equations necessary to

model the corresponding system are disclosed within each section. The relevant equations of the metamodels provided within each description are implemented in an open-source, cloud-based application [69].

The second part elucidates on the cross-comparison enabling simulation framework that controls the execution of the proposed metamodels. The complete list of inputs and expected outputs for each model under the proposed simulation framework are listed in Table 3-9 at the end of the section. The framework is then deployed on all developed metamodels to support that almost identical patterns can be observed in the energy intensity response to changes in product flow rates and feed salinity. Finally, a full cross-comparison between the most commercially competitive processes, multi-effect distillation and reverse osmosis, suggests that the cost of energy process benefits of multi-effect distillation must justify its considerably larger energy intensity.

3.3.1. Metamodels for Desalination Processes

All metamodels integrate submodels and thermophysical property functions from a variety of studies to expand the validity of the model while maintaining computational simplicity. These metamodels are classified according to the separation process featured in each method, which is also aligned with the type of thermophysical properties involved in the calculations. For instance, the thermal family involves properties such as enthalpies and latent heat, while the molecular transport family involves properties like permeability and conductivity. Table 3-2 summarizes the high-level simulation parameters validated within 9% with the relevant parameters from the most representative literature model. In the case of

intermediate parameters for MED and HDH, there is a maximum difference of 15% with the flashed distillate flow rate, and 64% difference with the cooling water flow rate. For MED, the difference is caused because the literature model assumes constant thermophysical properties while all our metamodels incorporate temperature, pressure, and salinity dependence [57]–[63]. The discrepancy in HDH, on the other hand, is not clearly labeled in the published study and is likely a simple typographical error. It must be noted however, these parameters have minimum impact in energy consumption calculations. All other parameters in all the developed models show excellent agreement with literature data overall. The complete validation tables with the selected model and additional studies are found in the paper appendix.

The successful validation of the metamodels with their corresponding representative model from the literature demonstrates they satisfactorily meet their intended purpose. However, the parameters shown in Table 3-2 represent only one possible operation point of each desalination system. Therefore, further validation is conducted with additional studies that show different operation conditions, including product flow rates and feed water salinities. The reader is encouraged to refer to the complete validation tables which list the complete sets of inputs, outputs, and relevant intermediate parameters in the Appendix. The unknown input fields in these cases are supplemented with values from other studies. Priority is given to the studies with most similar operation conditions for the cases where multiple options to supplement an unknown input exist. It is expected that the additional validation points have a larger percent difference from the metamodel

because the correlations, modeling algorithm and unknown values would differ slightly. Nevertheless, the metamodel results show great agreement with all independent studies.

Table 3-2: Validation summary of the metamodels with their corresponding most representative model literature from the literature (Full table in the appendix).

	TVC	**MED**	**HDH**	**RO**	**EDS**	**CDI**
Selected Lit. Model	[43]	[64]	[65]	[66]	[67]	[68]
Family	**Thermal**			**Molecular Transport**		
Product flow rate, M_d (kg/s)	0.5787 [0%]	137.9 [0%]	1.156 [0%]	2.087 [0%]	4.051 [0%]	6.138e-5 [-]
Intake salinity, C_f (g/kg)	35 [0%]	46 [0%]	35 [-]	2 [0%]	3.5 [0%]	2 [0%]
Intake temp. T_{in} (°C)	25 [0%]	28 [0%]	25 [0%]	20 [0%]	20 [-]	25 [-]
Feed water flow rate, M_f (kg/s)	1.360 [2%]	366.9 [4%]	16.87 [0%]	3.472 [-]	5.401 [-]	6.138e-5 [-]
Brine flow rate, M_b (kg/s)	0.7811 [-]	234.4 [4%]	15.48 [1%]	1.383 [-]	1.360 [-]	6.138e-5 [-]
Product water salinity, C_p (g/kg)	0 [-]	0 [0%]	0 [0%]	0.023 [-]	0.35 [0%]	0.70 [-]
Brine salinity, C_b (g/kg)	60.9 [4%]	72 [0%]	38.2 [-]	4.99 [0%]	13.0 [3%]	2.54 [-]
Specific energy, E_{des} (kWh/m^3)	239.9 [-]	66.37 [-]	486.5 [-]	0.9099 [-]	0.3688 [9%]	0.5594 [8%]

[%]: Percent difference. This value is not calculated for the parameters that are not provided explicitly in the literature model

3.3.1.1. Thermovapor Compression

A Thermovapor Compression (TVC) desalination system has three main components: a condenser, one or more evaporators, and a thermoejector. For the interests of this study, we consider only a single evaporator system although there are models in the literature that include multiple cascading evaporators [70], [71]. As shown in Figure 3-2, TVC desalination is driven by a motive steam flow rate (M_p) which mixes and is ejected in the thermocompressor with an entrained water vapor flow (M_e), extracted from the vapor stream produced in the evaporator side. The resulting mixed steam stream that supplies necessary heat in the evaporator to

separate feed water flow rate (M_f) into water vapor and brine (M_b) flows by overcoming the boiling point elevation caused by salt presence in the fluid [72]. The proposed TVC metamodel does not consider circulation pump energy consumption as it is insignificant when compared to the total heat input to the system. Table 3-3 describes the relevant TVC metamodel equations which are solved in a forward sequential algorithm and implemented through the proposed simulation framework at the end of the Results section.

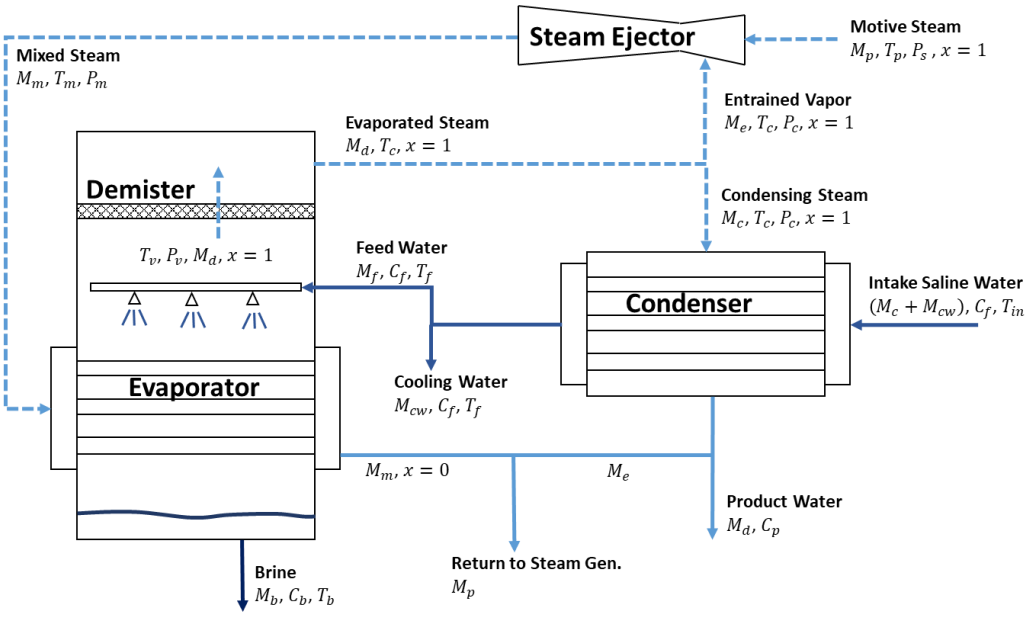

Figure 3-2: TVC process schematic.

The steam ejector is a key component of TVC with contrasting modeling approaches. Several desalination steam ejector models are available in the literature, each one with different assumptions and modeling detail. While recent studies present physical models with great validity [35], [73], they require additional inputs that are not available in published TVC models. There are other high-level empirical models [74], [75], based on graphical operational curves [76], that are suitable for the present application but have narrow operational ranges. We

found the most appropriate model for this study to consist of empirical correlations that expand the validity range of the aforementioned operational curves while maintaining a relevant level of abstraction [77].

The ejected steam from the thermocompressor supplies heat in one side of the evaporator to separate the saline feed water into a water vapor and brine streams in the other side. Part of this generated water vapor is eventually recirculated in the thermoejector, and the remaining is condensed into the product water in the condenser. Heat transfer coefficients (HTC's) are modeled trough empirical correlations consistently used throughout the literature. El-Dessouky et al. [62] compiled evaporator and condenser HTC's with different fouling or flow characteristics. We employ the overall temperature-dependent HTC correlations that combine such variations and can be found across several desalination models with slight variations in significant digits [38], [43], [78], [79].

The water vapor stream produced in the evaporator may have entrained saline water droplets produced from the impact of the saline water jets onto the evaporator tubes. A wire-mesh demister is often used to capture such saline droplets in the flow and induces a pressure drop in the vapor flow. The demister pressure drop is modeled through empirical correlations that consider demister properties such as pad density, thickness or wire diameter, and the vapor velocity through the demister [62], [80]–[82]. We found that these correlation coefficients were often modified without explanation; therefore, we opted to use the correlations from a study that provides a reference pressure drop value so that we could verify coefficients and units [43].

These different approaches to modeling TVC systems can be due to different research objectives in each study. For instance, some of the early models focus on parametric analysis of a generic TVC system [75], [82], while the more recent models propose a parametric study with updated thermoejector modeling strategies [43]. The models used in more recent studies focused on optimization strategies for real-life desalination plant models that feature more than a single evaporator [71], [74]. Finally a different study highlighted another use of a TVC model in analyzing the performance of the system in response to feed water seasonality changes [70].

Table 3-3: TVC Metamodel Key Equations.

Component	Equation		Variables		Ref.
Condenser	$M_c\lambda_c = (M_f + M_{cw})c_p(T_f - T_{in})$	(3-1)	M_c λ_c M_f M_{cw} c_p T_f T_{in}	Vapor flow rate Latent heat Feed water flow rate Cooling water flow rate Specific heat Feed water temperature Intake water temperature	[43]
Evaporator	$M_m(h_m - h_{x=0}) = M_f c_p(T_b - T_f) + M_d\lambda_d$	(3-2)	M_m h_m $h_{x=0}$ T_b M_d λ_d	Mixed steam flow rate Mixed steam enthalpy Mixed steam saturation enthalpy Brine temperature Vapor product Latent heat	[43]
Demister	$\Delta P_{de} = 9.583 \times 10^{-5}\rho_{de}^{1.597}V_{de}^{0.7197}L_{de}^{1.388}$	(3-3)	ΔP_{de} ρ_{de} V_{de} L_{de}	Pressure drop Demister packing density Vapor velocity in demister Demister thickness	[43], [82]
Thermoejector	$M_r = \sum_{n=0}^{3}\left(A_n C_r^n + \frac{B_n}{E_r^n}\right) + \frac{C_r}{E_r}\boldsymbol{C}\cdot\begin{bmatrix}1\\ C_r\\ 1/E_r\end{bmatrix}$ $If\ E_r \geq 100,\ 100 \geq E_r \geq 10$ $M_r = \sum_{n=0}^{3}\left(A_n \ln(C_r)^n + \frac{B_n}{E_r^n}\right) + \frac{C_r}{E_r}\boldsymbol{C}\cdot\begin{bmatrix}1\\ \ln(C_r)\\ 1/E_r\end{bmatrix}$	(3-4) (3-5)	$\boldsymbol{A}$ $\boldsymbol{B}$ $\boldsymbol{C}$ C_r E_r M_r	Regression constants Regression constants Regression constants Compression ratio Expansion ratio Mass ratio	[76], [77]

	$If\ 10 \geq E_r \geq 2$				
Evaporator HTC	$U_e = 1969.5 + 12.057T_b - 8.5989 \times 10^{-2}T_b^2 + 2.5651 \times\times 10^{-4}T_b^3$	(3-6)	U_e	Evaporator heat transfer coefficient	[43]
Condenser HTC	$U_c = 1719.4 + 3.2063T_c + 1.5971 \times 10^{-2}T_c^2 - 1.9918 \times 10^{-4}T_c^3$	(3-7)	U_c T_c	Condenser heat transfer coefficient Steam temperature at the condenser inlet	[43], [82]

3.3.1.2. Multi-Effect Distillation

Multi-Effect Distillation (MED), like TVC, is based on the evaporation of water from a feed saline stream, however, this process features several evaporators denominated "effects" which are connected in series. Motive steam flows into the first effect only in one side of the heat exchanger and the other effects intake the water vapor generated in the prior effect (i.e. steam generated in the first effect supplies heat to the second effect, the latter into the third effect, and so on through all the effects). Electricity consumption in pumps is neglected in the proposed MED metamodel as it is insignificant in comparison to the heat input to the system. Table 3-4 details the relevant MED metamodel equations which are solved in a forward sequential algorithm that iterates through each effect within the system.

There are three configurations of MED that differentiate in how the feed saline water flows with respect to the generated vapor in each effect. Forward feed is the most extensively modeled configuration [62], [78], [83], in which all the saline feed is directed to the first effect, and the brine generated in each effect is then directed as feed into the subsequent effect. This configuration, however, is not practical in the desalination industry because it features the most complex layout [62]. In the backward feed configuration, the saline feed is directed to the last effect, and the generated brine is passed backwards from each effect until the first effect is reached. This implementation has a high risk of scaling because the highest

salinity of the feed stream occurs in the first effect, which also has the highest temperature [84], [85]. In addition, backward feed systems require higher pumping power as the saline feed must be pumped from lower to higher pressure effects [62], [86]. Parallel feed is the most reliable MED configuration for desalination because it allows the highest distillate production per motive steam consumed and generally requires less heat exchanger area [86]. In this configuration the feed water stream is split and directed into all effects simultaneously. We model a parallel feed MED system with no thermoejector for the purposes of this study, as shown in Figure 3-3.

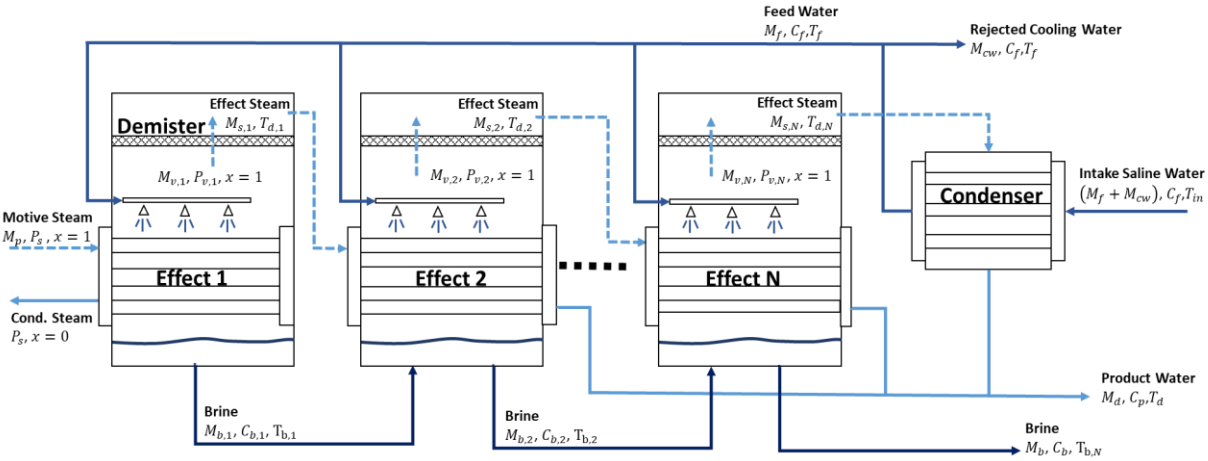

Figure 3-3: MED process schematic.

Published MED models present different assumptions regarding fluid thermophysical properties. For instance, some models assume constant properties such as or average boiling point elevation (BPE), specific heat capacity, and latent heat [64]. Others use a combination of constant properties for the water vapor or saline streams and temperature dependent correlations for the water stream [87], [88]. Finally, there are models that feature temperature-based correlations for water

and water vapor and include salinity effects for seawater thermophysical properties [78]. Like all metamodels presented in this paper, the MED metamodel features thermophysical function libraries that include temperature, pressure, and salinity dependence. Most saline and pure water properties are calculated using the Thermophysical Properties of Seawater library [57], [58], and two-phase vapor-steam properties are calculated using the XSteam library [61]. Both XSteam and the Seawater libraries, however, could be used interchangeably at zero salinity. MED effects generally have a decreasing pressure profile which can promote vapor flashing as brine water is transferred from a previous effect at higher temperature into the subsequent effect. [64], [89]. In some instances, MED units include flashing boxes to redirect steam for feed preheating or to add into the steam stream that is directed into the next effect [78], [88], [90]. It must be noted that flashing is not the main process through which vapor is generated, and therefore, some studies do neglect it [87]. Our metamodel implements flashing within each effect according to the saturation pressure that each effect maintains.

There are further differences between literature models regarding the modeling approach of each effect and the components within. There are models that assume constant heat transfer coefficients and fixed heat exchanger areas [64] while other models assume equal areas only [78]. In these calculations several studies employ the same vapor temperature-dependent HTC correlations as the models, described in the previous TVC section [87], [91]. Within the reviewed MED models, few consider small pressure drop caused by the demister within each effect [91]–[93]. Finally, some MED models consider feed preheaters, which are

heat exchangers before one or more effects that use steam (in some cases from an external process) to heat the feed water stream before entering the effect [64], [83], [87]. The energy required in the preheaters is generally small compared to the energy involved in water distillation but is found in actual case study data [94], [95]. Our metamodel incorporates temperature-dependent HTC correlations commonly found in thermal desalination models [38], [43], [78], [79], and correlations for the demister pressure drop [81]. For simplification, we assume preheating does not factor into the system's energy intensity and overwrite the constant feed temperature with the target preheat temperature at the desired effect. Nevertheless, considering the energy for feed preheating in this case can account for an increase in energy intensity of up to 20%.

These different modeling approaches have been developed to analyze different aspects of MED desalination. Early models were used in parametric studies of generic systems [78], [92]. In the following years, studies used MED models to conduct studies of real-life desalination plants [87], [96], [97] and parametric analysis of MED systems with thermocompression [88], [93], [98]. The latest modeling studies focused on analyzing the performance of MED desalination coupled with power cycles [90], [91], [99], and exploring the integration with solar energy [89], [100].

Table 3-4: MED Metamodel Key Equations.

Component	Equation		Variables		Ref.
Condenser	$(M_{cw} + M_f)c_p(T_f - T_{in}) = M_{d,end}\lambda_{d,end}$	(3-8)	$M_{d,end}$ $\lambda_{d,end}$ M_f M_{cw}	Vapor flow rate from last effect Latent heat Feed water flow rate Cooling water flow rate	[64], [101]

			c_p	Specific heat	
			T_f	Feed water temperature	
			T_{in}	Intake water temperature	
Evaporator	$M_p\lambda_p = M_{f,i}c_{p,i}(T_{b,i} - T_f) + D_{b,i}\lambda_{b,i}$	(3-9)	M_p	Steam flow rate	[64], [101]
			λ_p	Steam latent heat	
			$M_{f,i}$	Feed water flow rate at *i*th effect	
			$c_{p,i}$	Specific heat	
			$T_{b,i}$	Brine temperature in *i*th effect	
			T_f	Feed water temperature	
			$D_{b,i}$	Distillate produced by boiling in the *i*th effect	
			$\lambda_{b,i}$	Latent heat	
Demister	$\Delta P_{de} = 3.88178\rho_{de}^{0.375798}V_v^{0.81317}L_p d_p^{-1.56114147}$	(3-10)	ΔP_{de}	Pressure drop	[62], [81]
			ρ_{de}	Demister packing density	
			V_{de}	Vapor velocity	
			L_p	Packing length	
			d_p	Packing diameter	
Evaporator HTC	$U_e = 1969.5 + 12.057T_s - 8.5989 \times 10^{-2}T_s^2 + 2.5651 \times 10^{-4}T_s^3$	(3-11)	T_s	Saturation temperature of steam	[43], [102]
			U_e	Evaporator heat transfer coefficient	
Condenser HTC	$U_c = 1719.4 + 3.2063T_c + 1.5971 \times 10^{-2}T_c^2 - 1.9918 \times 10^{-4}T_c^3$	(3-12)	T_c	Vapor temperature at condenser inlet	[43], [82], [102]
			U_c	Condenser heat transfer coefficient	

3.3.1.3. Humidification-Dehumidification

Humidification Dehumidification (HDH) desalination makes use of the capacity of dry air to absorb and release moisture through psychometric processes. An Open-Air Open-Water (OAOW) HDH system, shown in Figure 3-4, contains three main components including the dehumidifier, which fulfills a similar role to the condenser in TVC and MED desalination, a heater, and a humidifier. Cool saline water flows into the dehumidifier and gets preheated as hot humid air condenses in the other side. The intake stream flow is regulated by rejecting some of the preheated water as cooling water, and the remaining flows into the heater.

The feed saline water is heated using the energy released from saturated steam inside the heater. The hot saline water is then sprayed in the humidifier, where it mixes with dry intake air. In this component the air absorbs moisture and exits as hot humid air into the dehumidifier, and the remaining water is rejected as saline brine. In the dehumidifier, the moisture from the humid air is collected as product water and the remaining air is exhausted. Circulation pump and fan energy consumption are neglected like the other thermal desalination metamodels. Table 3-5 shows the relevant HDH metamodel equations which are solved in a forward sequential algorithm through each component in the system.

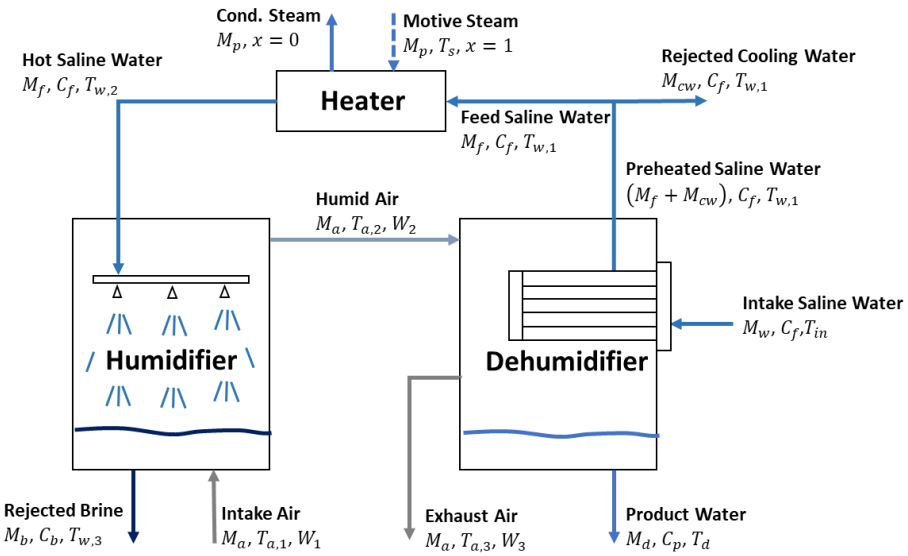

Figure 3-4: HDH process schematic.

The OAOW HDH system can be modified by changing the stream in which the heater is located or by closing and recirculating either the air or water loop. In addition, there is an air-heated configuration where the intake air, as opposed to the feed saline water flows through the heater. Both water-heated and air-heated cycles have similar production rates and energy input requirements, nevertheless, the air-

heated cycle needs a larger air flow rate compared to the water heated cycle, and thus requires a larger fan and dehumidifier than the water-heated system [32]. The air loop in the system can remain open if the intake air temperature and humidity are low enough to facilitate moisture absorption, if this is not viable, the exhaust air can be recirculated to replace the intake air. Fewer instances of closed-water loop systems are found in the literature; while Closed-Air Open-Water (CAOW) and Closed-Water Open-Air (CWOA) water-heated systems have similar production rates of desalted water per steam consumed, recirculating saline water within the system requires additional control mechanisms to prevent scale formation [103]–[105]. Therefore, we implement the OAOW configuration for our proposed HDH metamodel.

The HDH process deals with saline water and moist air streams whose thermodynamic properties present different assumptions in the published studies. While all studies use common psychrometric property equations for moist air, they differ in saline water thermodynamic property calculations with increasing degrees of complexity. For instance, there are cases that employ correlations that do not consider the presence of salt in the fluid [106] and some that consider salt as the only independent variable [27]. The majority of desalination models employ either temperature and salinity dependent thermodynamic property correlations for saline water [65], [107] or correlations that consider pressure effects in addition to temperature and salinity [32], [108]. Like the other desalination processes, we incorporate thermophysical property functions that consider temperature, pressure

and concentration for saline water [57], [58], and moist air property functions with temperature, pressure and humidity dependence [63], [109], [110].

The literature presents different modeling approaches to the components of a HDH system, predominantly in the humidifier. The earlier HDH models use humidifier correlations that consider air and water flows and temperatures, and mass transfer coefficients [37]. The vast majority of studies use either standalone empirical correlations [106], [111] or a combined approach between energy conservation assisted by numerical correlations [112], [113]. And finally, one of the more recent studies employ iterative numerical methods for modeling the humidifier [32]. Similar differences are observed for modeling the heat transfer coefficients in the system including constant heat transfer coefficients [65] or the use of temperature-dependent empirical correlations [107]. We implement humidifier sizing calculations through semi-empirical correlations highlighted in the literature model as it is one of the few studies that discloses parameters for validation [65].

The versatility of HDH desalination is reflected in the different objectives for which models have been constructed. Many studies present a parametric analysis of a theoretical system for comparing different system configurations or showcasing a different modeling methods [32], [65], [105], [107], [111]. However, there is a wide range of models that have been developed to analyze and optimize real life systems, including small experimental deployments [27], [108], [114]. Transient modeling approaches enable the simulation of HDH systems at variating conditions such as feed water changes due to weather [113] or energy supply

variations such as solar power [112] or waste heat from refrigeration [115]. Finally, there are also cases that employ HDH modeling for statistics-based optimization [106].

Table 3-5: HDH Metamodel Key Equations.

Component	Equation		Variables		Ref.
Dehumidifier	$M_a(h_{a2} - h_{a3}) = M_w(h_{w1} - h_{w0})$	(3-13)	M_a h_{a2} h_{a3} M_w h_{w1} h_{w0}	Air flow rate Moist air enthalpy Moist air enthalpy Intake water flow rate Saline water enthalpy Saline water enthalpy	[65]
Humidifier	$M_a(h_{a2} - h_{a1}) = M_f c_p(T_{w3} - T_{w2})$	(3-14)	M_f c_p T_{w3} T_{w2}	Feed water flow rate Specific heat Brine temperature Inlet water temperature	[65], [111]
Humidifier (Sizing)	$L_h = \frac{M_f c_p M_a^2 (C_1 - C_2)}{C_s k A_h}$	(3-15)	L_h C_1 C_2 L_p d_p C_s k A_h	Humidifier length Demister packing density Vapor velocity Packing length Packing diameter Fitting parameter Mass transfer coefficient Cross-sectional area	[65], [107]
Heater	$M_f(h_{w,2} - h_{w,1}) = M_p \lambda_p$	(3-16)	M_p λ_p	Motive steam flow rate Latent heat	[65]
Dehumidifier HTC	$U_c = 1719.4 + 3.2063T_c + 1.5971 \times 10^{-2}T_c^2 - 1.9918 \times 10^{-4}T_c^3$	(3-17)	T_c U_c	Vapor temperature at condenser inlet Condenser heat transfer coefficient	[43], [82], [102]

3.3.1.4. Reverse Osmosis

Reverse Osmosis (RO) is the most widely used desalination method due to its relatively low energy consumption and adaptability for large scale production requirements. Pump energy consumption is considered as the main energy input to drive desalination in this process. The main component of a RO system is the membrane module, which in most cases contains a spiral-wound membrane used

to filter product water high salinity feed. RO uses electricity as its energy source through a high-pressure pump. When the system pump exerts enough pressure on the feed side of the membrane to overcome the net pressure difference, which includes the hydraulic and osmotic pressures, water is forced through the membrane, resulting in a permeated product water and a leftover brine stream at a higher concentration. The RO metamodel is based on a single-pass, tapered arrangement system as shown in Figure 3-5.

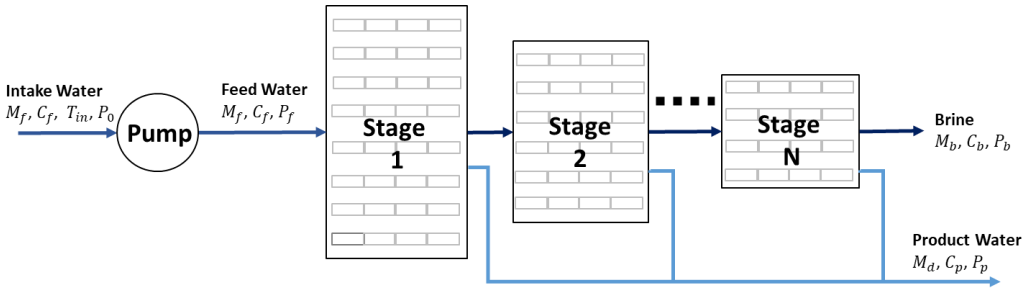

Figure 3-5: RO process schematic.

The RO process extracts water from a saline stream through physical separation as opposed to phase change; therefore, the osmotic pressure calculation becomes particularly important in modeling. Different studies present disparate assumptions in calculating colligative properties of saline water. Most published models assume linear dependence between osmotic pressure and salt concentration with a constant empirical coefficient of proportionality [116]–[118]. These approaches are based on van't Hoff's correlation, which involves temperature and salinity and is widely used in RO modeling [119]. Linearization, however, is mostly applicable to low salt content and can deviate at higher concentrations [120]. Other approaches consist in fitting a concentration-dependent regression to tabulated data [121]. The proposed RO metamodel employs a subroutine based on van't Hoff's

expression in combination of other equations and approximations to expand the validity range [122].

Table 3-6 shows the relevant RO metamodel equations that are solved in a forward iterative algorithm by adding differential membrane elements to the system until the required desalination objective is achieved.

Like most RO models, our proposed metamodel employs a solution-diffusion model that makes the water and salt fluxes proportional to the net force and concentration difference, respectively, across the membrane [123]. The proportionality constants in these equations are water and salt permeability coefficients that depend on the specific membrane and operation of the system. These parameters are not usually included in membrane catalogues and therefore the approaches to implementing these coefficients vary across the literature. It is common among published models to assume constant permeability coefficients [121]. These are often deduced from actual system measurements through regression analysis [116], [117], [119], or adjusted to match results from commercial simulation packages [118]. It is important to note that these coefficients tend to be strongly dependent on the feedwater characteristics, system specifications, and operational conditions, therefore these values are not necessarily interchangeable among models.

The RO membrane blocks most salt ions from permeating; therefore, a high concentration layer is formed at the interface between membrane surface and the feed water stream. This phenomenon is called concentration polarization and can have significant effects on the water and salt fluxes through the membrane as they

factor into a mass transfer coefficient through the membrane [124]. Concentration polarization is usually modeled as a factor given by the ratio of the wall-permeate and brine-permeate concentration differences through thin film theory [123]. This poses a challenge since the actual product concentration cannot be known *a-priori* unless measured and regressed from an actual system. There are modeling cases in the literature that concentration polarization is not considered [125], or the value for product water concentration is assumed to simplify the equations [126]. In many cases, the models simplify the calculation by assuming a linear increase in brine concentration with respect to the flow path length and using a mass balance approach [117], [118], [121]. The RO metamodel incorporates different empirical correlations for calculating this mass transfer coefficient, which can be averaged or individually selected according to the membrane type and system setup [66], [127], [128]. In the model validation we choose the correlation that best fits the available data.

There are several analytical levels at which RO systems are modeled in the literature. A common approach to modeling single stage systems involves treating the flow channel as bulk [30], [42], [129]. Within this simplification there are several approaches, such as statistical-mechanical models, that require several fitting constants from experimental data [28], [62], or solving for simultaneous equations in the simplified control volume [118], [121]. Models based on empirical correlations, however, are only valid for the operating conditions, membrane modules, and plant configuration used in the statistical regressions, so they do not allow for flexibility in terms of modeling different desalination requirements or

systems. Simplifying the system might not be appropriate for large, multi-stage systems since the effects of concentration polarization are diminished. More detailed analytical models use finite element approximations and follow an iterative calculation process through the discretized membrane elements [66], [126]. Higher detail on fluid transport can be studied through CFD-based models [130]. The different modeling approaches and assumptions are tailored to specific modeling objectives. For instance, many studies use RO models to conduct parametric studies with different purposes such as exploring theoretical system tradeoffs [42], [125], [126], process optimization [118], or developing case studies with actual desalination plants [121]. In addition, RO models have been used to study transient effects through dynamic simulations [30]. Alternatively, numerical method-based models aim to explore more detailed and mechanistic modeling options that do not rely on common modeling assumptions [130].

Table 3-6: RO Metamodel Key Equations.

Component	Equation		Variables		Ref.
Membrane permeation	$J_w = K_w\left[\left(P_b - P_p\right) - \left(\beta\pi_b - \pi_p\right)\right]$	(3-18)	J_w K_w P_b P_p β π_b π_p	Water flux Water permeability Feed (brine of previous element) pressure Permeate pressure Concentration polarization factor Feed (brine of previous element) osmotic pressure Permeate osmotic pressure	[66], [119]
Concentration polarization	$\beta = Rej \exp\left(\frac{J_w}{k_{cp}}\right) - Rej + 1$	(3-19)	Rej k_{cp}	Observed salt rejection Mass transfer coefficient	[30], [66], [123], [131]
Local salt rejection	$Rej = 1 - \frac{C_p}{C_f}$	(3-20)	C_p C_b	Permeate concentration Feed (brine of previous element) concentration	[30], [66]

Mass Transfer Coefficient	$k_{cp} = 0.023\left(\frac{D_T}{dH}\right)(Re)^{0.875}(Sc)^{0.25}$	(3-21)	dH λ	Hydraulic diameter Empirical multiplier	[132]
	$k_{cp} = \lambda\left(\frac{D_T}{dH}\right)(Re)^{0.50}(Sc)^{1/3}$	(3-22)	v l	Flow velocity Element length	[133]
	$k_{cp} = 0.664\left(\frac{D_T}{dH}\right)(Re)^{0.5}(Sc)^{0.33}\left(\frac{dH}{L}\right)^{0.5}$	(3-23)	h D_{25}	Channel thickness Diffusivity of salt through membrane at 25°C	[134]
	$k_{cp} = 0.808\left(\frac{6vD_{25}^2}{hl}\right)^{\frac{1}{3}}\left(\frac{D_T}{D_{25}}\right)^{\frac{2}{3}}$	(3-24)	D_T	Diffusivity of salt at actual temperature	[127]
Pump	$P_m = \frac{Q_f(P_f - P_0)}{\eta_{pump}\eta_{motor}}$	(3-25)	P_m Q_f P_0 η_{pump} η_{motor}	Motor power Feed flow rate Intake pressure Pump efficiency Motor efficiency	[125]

3.3.1.5. Electrodialysis

Electrodialysis (EDS) is a desalination method that is still in the early phases of large-scale commercialization. The EDS process uses an electrical driving force to transport salt ions across ion selective membrane arrays. The lack of a thermal process and low fouling potential due to flow reversal ability make EDS an attractive option for desalination [135]. The process is mostly viable for low production capacity and low salinity ranges. In this desalination process, two different saline flows, a dilluate stream and a (saline) concentrate stream, flow into several channels in the EDS stack. An EDS stack contains many alternating anion and cation exchange membrane pairs, and the spaces in between are called cells. When a voltage is applied to the stack through a pair of electrodes located at each end, negatively charged salt ions flow through the anion permeable membranes towards the cathode and are stopped by the cation permeable membranes. Conversely, positively charged salt ions flow through the cation permeable membranes towards the anion and cannot flow through the cells that contain anion

permeable membranes. This process results in the formation of cells with alternating concentration where the dilluate and concentrate solutions are simultaneously desalted and concentrated, respectively, as shown in Figure 3-6. The main energy consumption in the system occurs through the electrical input in the EDS stacks. Circulation pump energy is not considered in this analysis as it is insignificant in comparison the operational conditions from the literature.

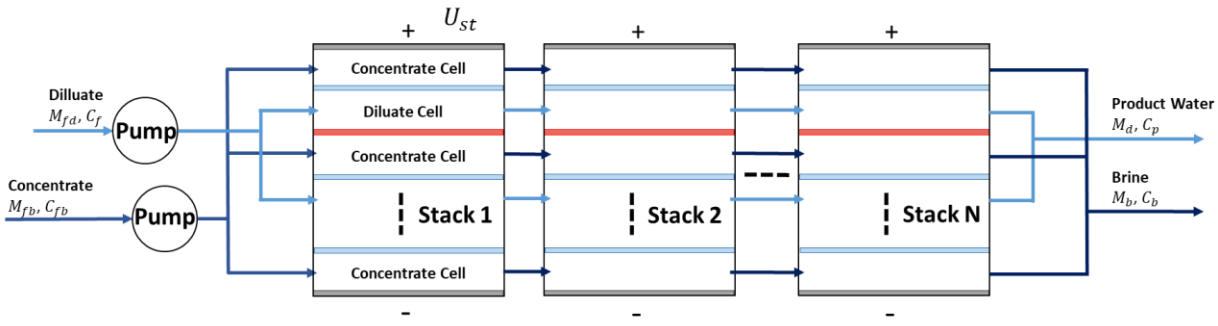

Figure 3-6: EDS Process schematic.

The EDS process involves ion transport within channels in the stack as a response to an electrical force; therefore, the electrical conductivity of the fluid is one of the most important thermophysical properties to consider. Some studies use a linear equation between conductivity and fluid concentration using ion conductance [67], [136], while other studies propose higher order numerical correlations [137], [138]. There are also models that include temperature effects through regression approach [139]. It must be noted that for all the instances, the employed correlations are limited to relatively low concentrations, which corroborates the most common concentration ranges this method usually operates in. Table 3-7 describes the relevant EDS metamodel equations which are solved in a forward sequential algorithm.

The EDS process is constrained by the Limiting Current Density (LCD), which occurs at the maximum voltage for which water molecules begin to dissociate. Thus, if exceeded, it can result in a significant drop in overall efficiency of the system and increasing the risk of scaling [140]. This phenomenon occurs in the dilluate channel at the interface between the desalted stream and the membrane surface, therefore, it is highly dependent on the boundary layer formed which involves the specific flow and surface characteristics [141]. There are few studies that propose models that do not consider LCD explicitly; however, its effect is factored into their numerical correlations as a data-driven coefficient [136], [138]. Thus, it must be noted that while there are several approaches to LCD modeling, these solutions are valid only on a case-by-case basis and might not be appropriate to be used interchangeably. In some studies, LCD is calculated through a polynomial regression [142], [143]. Most EDS models in the literature, however, assume a power law relation that involves flow velocity and salt concentration and fit the equation to measured data from a bench system [144]–[146]. Some complex analytical solutions based on boundary layer analysis have been proposed; however, this still requiring the input of measured parameters [147]. Our EDS metamodel calculates the LCD through a power law relation as the literature model provides the necessary coefficients and exponents that are usually undisclosed in other studies [67].

There are several differences in the computational approach between EDS models. The majority opt for defining a control volume for either a single EDS stack or multiple stacks in series and solving the transport equations as a bulk

process [40], [67], [138], [139], [148]. Others maintain the large control volume in the EDS stacks but use numerical approaches that require iterations for a solution to converge [137], [149]. A more recent modeling approach discretizes the EDS stack into finite elements and applies the modeling equations through the flow channel length [33]. Considering EDS modeling equations are largely based on empirical correlations that are tailored to specific operational conditions, it is unlikely yet that a single modeling approach can successfully represent other studies.

The EDS modeling approach and underlying assumptions are related to the modeling objective in each study. There are some cases for parametric analysis or optimization of a theoretical system [40], [138], design of an actual plant [67], or dissemination of modeling approaches for alternate operational methods [137], [150]. The latest studies propose new modeling methods with the aim of expand operational ranges or generalize applicability to a wider range of systems [33], [139].

Table 3-7: EDS Metamodel Key Equations.

Component	Equation		Variables		Ref.
Limiting Current Density	$i_{lim} = saC_{\Delta}u^{b}$	(3-26)	i_{lim} s a C_{Δ} u b	Limiting current density Safety factor Regression constant Degree of desalination Linear flow velocity Regression constant	[67]
Cell Pairs	$N_{cp} = \frac{Q_d}{\alpha w \Delta * u}$	(3-27)	N_{cp} Q_d α w Δ	Number of cell pairs Product flow rate Volume factor Cell width Cell thickness	[67]
Electrical Current	$I_{st} = \frac{zFQ_dC_{\Delta}}{\zeta N_{cp}}$	(3-28)	I_{st} z F	Stack current Valence number Faraday constant	[67]

			ζ	Current utilization factor	
Stack	$L_{prac} = \frac{\left(\ln\left(\frac{C_b C_f}{C_{fb} C_d}\right) + \frac{\Lambda \rho C_\Delta}{\Delta}\right) zF C_d u \Delta \alpha}{\left(\frac{C_d}{C_b} + 1 + \frac{\Lambda C_d \rho}{\Delta}\right) i_{lim} \beta \zeta}$	(3-29)	L_{prac} C_b C_f C_{fb} C_d Λ ρ β	Flow path length Concentrate outlet salinity Dilluate feed salinity Concentrate feed salinity Dilluate outlet salinity Equivalent conductivity Membrane area resistance Area factor	[67]

3.3.1.6. Capacitive Deionization

Capacitive Deionization (CDI) is a relatively new technology that makes use of an electrochemical force to adsorb ions from aqueous solutions [151]. A conventional CDI system consists in a cell made by two parallel porous electrodes with a separator in between through which saline water flows. As shown in Figure 3-7, during the charging phase, a voltage difference is applied and salt ions in the solution migrate into the electrical double layers that are formed along the inner surfaces of the porous electrodes [152]. Adsorbed ions are retained in the electrodes until the applied voltage is reversed or the electrodes are shorted. This releases the ions back into the saline water stream regenerating the electrodes for the next cycle [153]. Thus, desalination through CDI consists of alternating charging and discharging cycles in a CDI cell to produce an alternating desalted water and brine stream, respectively. There are several variations of CDI cell architecture. For cases where the flow is parallel to the electrodes configuration, it is common to implement ion selective membranes between the flow channel and the electrode, and there are also instances where the flow occurs perpendicular and through the electrodes [152]. Although CDI technologies remain largely experimental with a

lot of theoretical work done in the field, we believe it is important to include them in this study to explore how it compares to benchmark operation of conventional desalination processes.

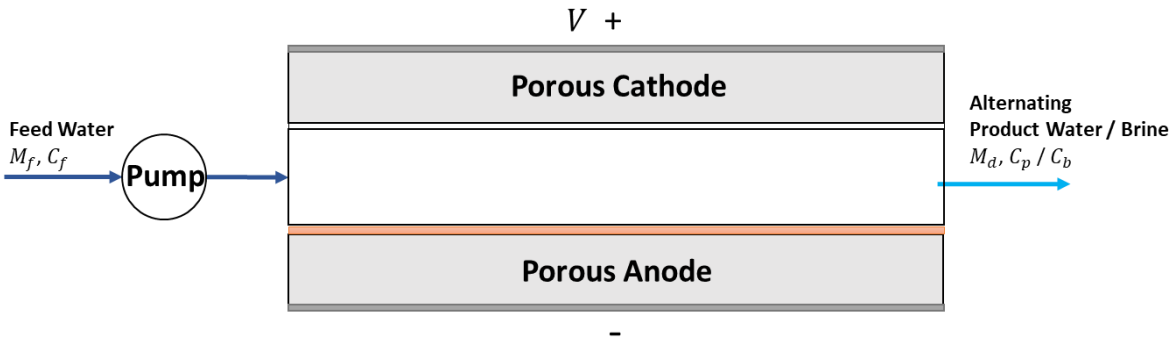

Figure 3-7: CDI process schematic.

Modeling the mechanism through which ions are retained within the porous electrode is still a matter of ongoing research. The latest modeling approaches consider an electrical double layer composed of a constant ionic surface formed by the salt ions adherence to the electrodes, and a diffusive layer where the electric potential decreases exponentially toward the center of the flow [154]. The implementation of electrical double layer theory in CDI is still under development, and there are several approaches in the literature models. Reduced-order models in the literature consider voltage drops across the whole CDI stack through a higher analytical resolution [68], [155], [156]. The subsequent tier in analytical resolution employ bulk modeling of the fluid without considering the boundary layer effects at the electrode interface [157]. The majority of models found in CDI, however, employ a mechanistic approach to electrical double-layer modeling [39], [158], [159].

CDI desalination is inherently a dynamic process as operation alternates between charging and discharging as desalination and concentration, respectively, occurs. There are different modeling approaches to considering time dependence at different spatial resolutions in the literature, and this is still a topic of current research. The literature presents design models that consider time marching only by executing the modeling algorithm at a system level through each time step [39], [68]. Within this approach, some studies propose models that require measuring an experimental system and fitting equation parameters [157], [158], [160]. Other approaches discretize the flow channel into differential elements and execute the modeling algorithm through spatial iterations [159], [161]. Mechanistic models employ numerical method schemes to iterate through discretized space and time [162], [163]

CDI desalination is still in experimental stages, so therefore most models focus on mechanistic approaches at a fluid flow analytical scope that would help understand ion transport and concentration changes. The alternative approaches to modeling scope and methods cater to the particular objectives of the study. These include parametric optimization [39], dynamic modeling to investigate transient effects [153], [157], determining electronic resistances across the stack [160], and the study of constant current or constant voltage operation [161], [164]. On the other hand, there are several studies where generalized models are deployed with the purpose of modeling CDI at a system scope; for instance, exploring options of stack coupling for energy recuperation [159]. It is important to note that these objectives aim to advance the knowledge in CDI desalination and there is still not

a robust system-level model although a modeling framework has been proposed [165] and generalized models have been used to determine contributions to energy consumption [68]. For this reason, we implement a generalized modeling approach in our metamodel which simplifies the CDI stack into an equivalent Randles circuit [68] where the ion exchange membranes, current collectors, and solution are modeled as a resistor with resistance R_1, and the electrodes are modeled as a charging capacitor with fixed capacitance C and fixed resistance, R_2, connected in parallel as shown in Figure 3-8. The circuit is solved using a forward sequential algorithm for every timestep during charging and discharging. The variation in salt concentration in the product stream are calculated through the changes in R_1 at each timestep using the CDI metamodel equations described in Table 3-8. This assumption neglects energy of the circulation pump which is minimal in comparison to the energy input in the CDI stack at the operation conditions from the literature.

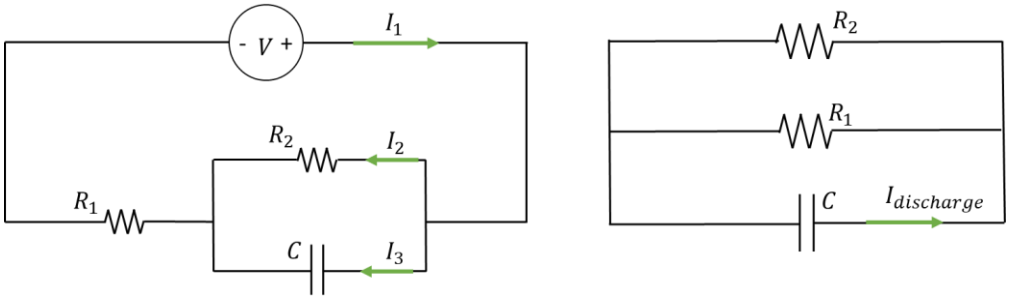

Figure 3-8: Randles circuit equivalent of a MCDI system charging (left) and discharging (right).

Table 3-8: CDI Metamodel Key Equations.

Component	Equation		Variables		Ref.
Membranes, current collectors, and solution	$R_1 = s + \frac{l}{kA_e}$	(3-30)	R_1 s l k	Equivalent resistance Internal resistance Stack length Electrical conductivity at time t	[68]

			A_e	Electrode area	
Stack operation	$t_{discharge} = t_{charge}\left(\frac{1}{RR} - 1\right)$	(3-31)	$t_{discharge}$	Discharging time	[68]
			t_{charge}	Charging time	
			RR	Recovery ratio	
Stack (Charging)	$V = I_1(R_2 + R_1) - I_1 R_2\, exp\left(\frac{-t}{R_2 C}\right)$	(3-32)	V	Applied voltage	[68]
			I_1	Applied current	
			R_2	Equivalent electrode resistance	
			t	Operation time	
			C	Equivalent electrode capacitance	
Stack (Discharging)	$V_{discharge} = -V\, exp\left(\frac{-t}{R_t C}\right)$	(3-33)	$V_{discharge}$	Discharge voltage across CDI stack	[68]
			R_t	Equivalent stack resistance	

3.3.2. Simulation Framework

Standardizing desalination modeling algorithms involves defining common sets of inputs and outputs for all desalination models. There is a notion in previous studies of defining an operational range for desalination processes according to the production flow rates and feed water concentrations [23], [24], [48], [53]. These parameters impose practical limits of operation and therefore would be appropriate to group them as common inputs to the models. Furthermore, these parameters represent the same physical concept in all methods and therefore can be directly compared. Defining which parameters can be compared and the order of relevance in which analysis should be directed is the basis for the proposed cross-comparison framework. Therefore, we propose a standard classification of inputs and outputs which include the General, Family and Specific analytical hierarchies. Such standardization resolves the computational order discrepancies in existing models and thus enables cross-comparison.

3.3.2.1. General Variables

Any desalination process intakes a feed stream of saline water (M_f) at a certain intake temperature (T_{in}) with salt concentration (C_f) and through an energy input extracts a product water stream (M_d) with negligible salt concentration (C_d) and a brine stream flow rate (M_b) with a higher salt concentration (C_b). Therefore, a mass balance for water can be written as:

$$M_f = M_d + M_b \tag{3-34}$$

And salt:

$$M_f C_f = M_d C_d + M_b C_b \tag{3-35}$$

Equations (3-34) and (*3-35*) hold for any desalination method.

The molecular transport desalination processes, RO, EDS, and CDI are driven by either an external physical or electrostatic force inputted through a pair of electrodes or a pump. This force must be high enough to overcome intermolecular forces, such as osmotic pressure or intermolecular electrostatic attractions that are higher than those of pure water due to the presence of salt. This separation results in two liquid streams, the product stream with a lower salt content and the brine stream with a higher salt concentration. Thermal desalination systems, including TVC, MED, and HDH, extract water from the saline feed through a phase change, therefore, the product concentration can be assumed zero and the salt balance reduces to:

$$M_f C_f = M_b C_b \tag{3-36}$$

A recovery ratio (RR), which indicates the proportion of product water flow rate (M_d) recovered from feed water flow rate (M_f), can be defined for all desalination processes such that:

$$RR = \frac{M_d}{M_f} \tag{3-37}$$

The parameters M_f, M_b, M_d, C_f, C_b, C_d, T_{in} ,and RR form part of the "General" parameter hierarchy. This category corresponds to variables that are numerically equivalent in all desalination methods and therefore can be directly compared with one another.

3.3.2.2. Family Variables

The proposed framework for cross-comparison between distinct desalination processes takes into first consideration the clear distinction between thermal desalination processes, which use thermal energy to induce a phase change to separate water from salt, and molecular transport processes, which conversely use an external force to separate water and salt through molecular dynamics. All desalination processes have a power input (P_{des}) to the system required to overcome intermolecular attractions so that separation can occur. This input can be either thermal, electrical, or mechanical energy depending on the method and can be normalized by M_d to obtain an energy intensity of desalination:

$$E_{des} = \frac{P_{des}}{M_d} \tag{3-38}$$

It is important to note that electrical and thermal power cannot be directly compared as they are region and market dependent. Therefore, although the numerical value of E_{des} describes the same parameter within desalination, it must

be considered as a Family Variable. Future research can investigate appropriate conversion factors to complement the direct comparison of General desalination-related operation variables such as flow rates, salinities, and end performance ratios as presented in this study.

Thermal desalination processes including TVC, MED, and HDH desalination in this study are driven by the heat released from condensation of motive steam inputted to the system at a pressure P_s. This must supply enough heat to evaporate water from the saline feed. The produced vapor must later be condensed using cooling water or brine acting as a heat sink. The nature of this process suggests metrics for cross-comparison that include motive steam flow rate, heat exchanger area, and cooling water flow rate. The relevant metrics of performance are the Gain Ratio (GR) and the Specific Cooling Water (sM_{cw}):

$$GR = \frac{M_d}{M_p} \tag{3-39}$$

$$sM_{cw} = \frac{M_{cw}}{M_d} \tag{3-40}$$

Where M_p is the motive steam flow rate, and M_{cw} is the cooling water flow rate. The parameters P_s, M_p, GR, and sM_{cw} are numerically equivalent only within the desalination methods corresponding to the thermal family. Therefore, it is appropriate to cross-compare these metrics and parameters directly only between TVC, MED, and HDH. The formal separation of these desalination families is further corroborated by the thermophysical properties involved in the desalination process. Thermal desalination models employ, for instance, specific heat capacities,

latent heat of evaporation, and boiling point elevation while molecular transport models involve other properties, such as osmotic pressure and conductivity.

3.3.2.3. Specific Hierarchy

The remaining parameters inherent to each desalination method form part of the Specific Hierarchy. These variables are numerically compatible only within the specific desalination method and cannot be cross compared with different methods as they are not related. This hierarchy becomes particularly useful when analyzing different operation conditions for the same desalination system. The full list of specific parameters corresponding to each model are given in Table 3-9 of the following section.

3.3.2.4. Cross-Comparison Enabling Simulation Framework

The proposed simulation framework imposes that cross-comparison between different desalination technologies can only occur across equal hierarchy levels for which the parameters have the same numerical and physical meaning. It is necessary to maintain constant input-output structures in the metamodels to enable a direct cross-comparison at the different hierarchy levels and facilitate sequential algorithm solution. All desalination processes can be cross-compared at the General Hierarchy level, while only models of the same desalination family can be cross-compared across the Family Hierarchy level. Finally, only variations within the same desalination process can be compared using data corresponding to the Specific Hierarchy level as it has the same representation across technologies and thus allows for fair and meaningful and fair comparisons. It is important, however, to consider parameters that are incompatible for cross-comparison but

could still provide valuable insight on system operation and performance. For instance, when comparing two different methods, there will not be direct cross-comparison of specific variables; however, identifying them can yield valuable information about the system that can factor into an indirect comparison. Table 3-9 summarizes the inputs and outputs for each model under the proposed analytical hierarchy structure.

Table 3-9: Input and Output Hierarchy for Cross-Comparison.

<table>
<tr><th>Hierarchy Level</th><th colspan="6">Parameters</th></tr>
<tr><td>1. General
Parameters that are numerically compatible among all desalination technologies</td><td colspan="6">Inputs:
• Target product Flow rate, M_d (kg/s)
• Intake Salinity, C_f (g/kg)
• Intake Temp. T_{in} (°C)

Outputs:
• Product Flow rate, M_d (kg/s)
• Feed water flow rate, M_f (kg/s)
• Brine flow rate, M_b (kg/s)
• Product water salinity, C_p (g/kg)
• Brine salinity, C_b (g/kg)
• Recovery ratio, RR</td></tr>
<tr><td rowspan="2">2. Family
Parameters that are numerically compatible only among desalination technologies within the same family</td><td colspan="3">Thermal Desalination</td><td colspan="3">Molecular Transport Desalination</td></tr>
<tr><td colspan="3">Inputs
• Motive steam pressure, P_s (kPa)
Outputs
• Specific energy (thermal), E_{des} (kWh/m^3)
• Motive steam flow rate, M_p (kg/s)
• Gain ratio, GR
• Sp. cooling water flow rate, sM_{cw} (kg/kg)</td><td colspan="3">Inputs
• Target recovery ratio, RR
Outputs
• Specific energy (electrical), E_{des} (kWh/m^3)</td></tr>
<tr><td>3. Specific
Parameters that are valid only with a particular desalination method and is not compatible with any other.</td><td>TVC
Inputs
• Operating temperature, T_v (°C)
• Cond. area, A_c (m^2)
• Compression ratio, CR
• Condenser effectiveness, η_c
Outputs
• Evap. area, A_e (m^2)
• Sp. Area, sA, (m^2/(kg/s))</td><td>MED
Inputs
• Top brine temp. Tbt (°C)
• Last effect brine temp. T_b (°C)
• Feed water temp. T_f (°C)
• Brine salinity, C_b (g/kg)
Outputs
• Cond. area, A_c (m^2)
• Sp. Area, sA, (m^2/(kg/s))</td><td>HDH
Inputs
• Heater outlet air temp., T_{high} (°C)
• Hum. air inlet temp., T_{a1} (°C)
• Humidifier outlet air temp., T_{a2} (°C)
• Condenser outlet air temp., T_{a3} (°C)
• Hum. air inlet rel. hum. φ_1
• Humidifier outlet air rel. hum. φ_2
• Condenser outlet air rel. hum. φ_3</td><td>RO
Inputs
• Feed pressure, P_f (bar)
• Feed velocity, v_f (m/s)
• Permeate pressure, P_p (bar)
• Module length, l (m)
• Channel width, h (mm)
• Module area, a (m^2)
• Module head loss, hl (bar)
• Module design velocity, v_0 (m/s)
• Membrane water</td><td>EDS
Inputs
• Product Concentration, C_d (g/kg)
• Linear flow velocity, u (m/s)
• Cell thickness, del (m)
• Cell width, w (m)
• Length per stack, L_{st} (m)
• Anion selective membrane resistance, ρ_a (Ohm.m^2)
• Cation selective membrane resistance, ρ_c (Ohm.m^2)
• LCD Constant, a</td><td>CDI
Inputs
• Normalized Current, I_{norm} (A/m^2)
• Normalized Capacitance, C_{norm} (F/g)
• Normalized Internal resistance, s_{norm} (Ohm.m^2)
• Normalized electrode resistance, $R_{2,norm}$ (Ohm.m^2)
• Electrode area density, m (g/m^2)
• Charging step time, t_{charge} (s)</td></tr>
</table>

			• Feed water flow rate, M_f (kg/s) • Condenser outlet water temp. T_{w1} (°C) • Cond. HT coeff. U_c (kW/m^2°C) • Humidifier crossectional area, A_h (m^2) • Vapor mass transfer coefficient, k (kg/(sm^3)) Outputs • Cond. area, A_c (m^2) • Hum. Height, L_h (m) • Air mass flow rate, M_a (kg/s) • Total intake water flow rate, M_w (kg/s)	permeability at 25°C, K_{w25} L/(m^2.h.bar) • Membrane salt permeability at 25°C, K_{s25} (m/h) • Temperature coefficient for water transport, K_{wt} (K) • Temperature coefficient for salt transport, K_{st} (K) Outputs • Number of stages, N_{stage} • Number of modules, $N_{modules}$ • Membrane area, A_m (m^2) • Average water flux, J_w (L/(m^{2}h))	(A.s^{b}m$^{(1-b)}$/keq) • LCD Constant, b • Safety factor, s • Volume factor, α • Area factor, β • Current utilization factor, ζ Outputs • Concentrate feed mass flow rate, M_{fb} (kg/s) • Concentrate feed concentration, C_{fb} (g/kg) • Stack current, I_{st} (A) • Stack voltage, U_{st} (V) • Number of cell pairs, N_{cp} • Number of Stacks, N_{st}	• CDI Stack volume, V_{cdi} (L) • Channel thickness, l (mm) • Charge efficiency, η_{charge} • Discharging efficiency, $\eta_{discharging}$ • Max. Salt adsorption capacity, SAC (mg/g) • Electrode area, A_e (m^2) Outputs • Desorption Capacity, (%) • Max. Voltage, (V)

3.4. Discussion

In the first part of this section, we deploy the proposed simulation framework using the base representative literature model inputs in a high-level, cross-comparative analysis. The similar energy consumption patterns observed, even though the operational regimes are disconnected, justify the framework as appropriate for joining seemingly disconnected models. The similar operation patterns throughout the six studied desalination processes suggest that conservation laws form a theoretical performance curve that represents ideal operation. However, actual performance depends on system design and operating conditions, which in this analysis, are expressed as energy intensity patterns based on meta-analysis of the literature. The performance curves provide evidence that a system can operate in sub-optimal regimes.

For the second part of this section, we apply the framework in a full cross-comparative study between MED and RO; the desalination methods that currently have one of the largest market shares in seawater desalination, greatest maximum production capacity per unit, and highest technology growth trends [166]. Furthermore, we chose MED and RO to highlight that new desalination technologies must outcompete these processes in terms of operation and costs. The resulting cross-comparative analysis highlights that MED has energy consumption that is an order of magnitude greater than that of RO but uses a different type of energy. Such difference is justified by the cost of energy and maintenance for MED which must be an order of magnitude smaller than RO for it to be competitive. The results help define a technical benchmark that upcoming desalination technologies must overcome in order to be competitive.

3.4.1. Application of the Analytical Framework in Intended Operation of Desalination Methods

Figure 3-9 shows the distribution of M_d and C_f values collected from the reviewed literature. We consider operation points from studies that describe an actual desalination plant, model, or bench-scale system. Each study does not necessarily disclose all these parameters; therefore, the resulting median points only suggest typical operation from the literature. The meta-analysis shows that thermal desalination methods have a very similar C_f median with an average of 38.5 g/kg. Conversely, EDS and CDI in the molecular transport methods have close C_f medians with an average of 1.74 g/kg. RO is the only molecular transport desalination method with instances in the literature that spans from molecular

desalination to thermal desalination feed salinity ranges. Unsurprisingly, product salinity is negligible for the thermal processes while the molecular transport methods typically result in concentrations around the potable water limits of 0.6 g/kg. The distributions show that generally MED and RO can achieve similar product flow rates from the highest feed salinity levels while incurring in the lowest E_{des}.

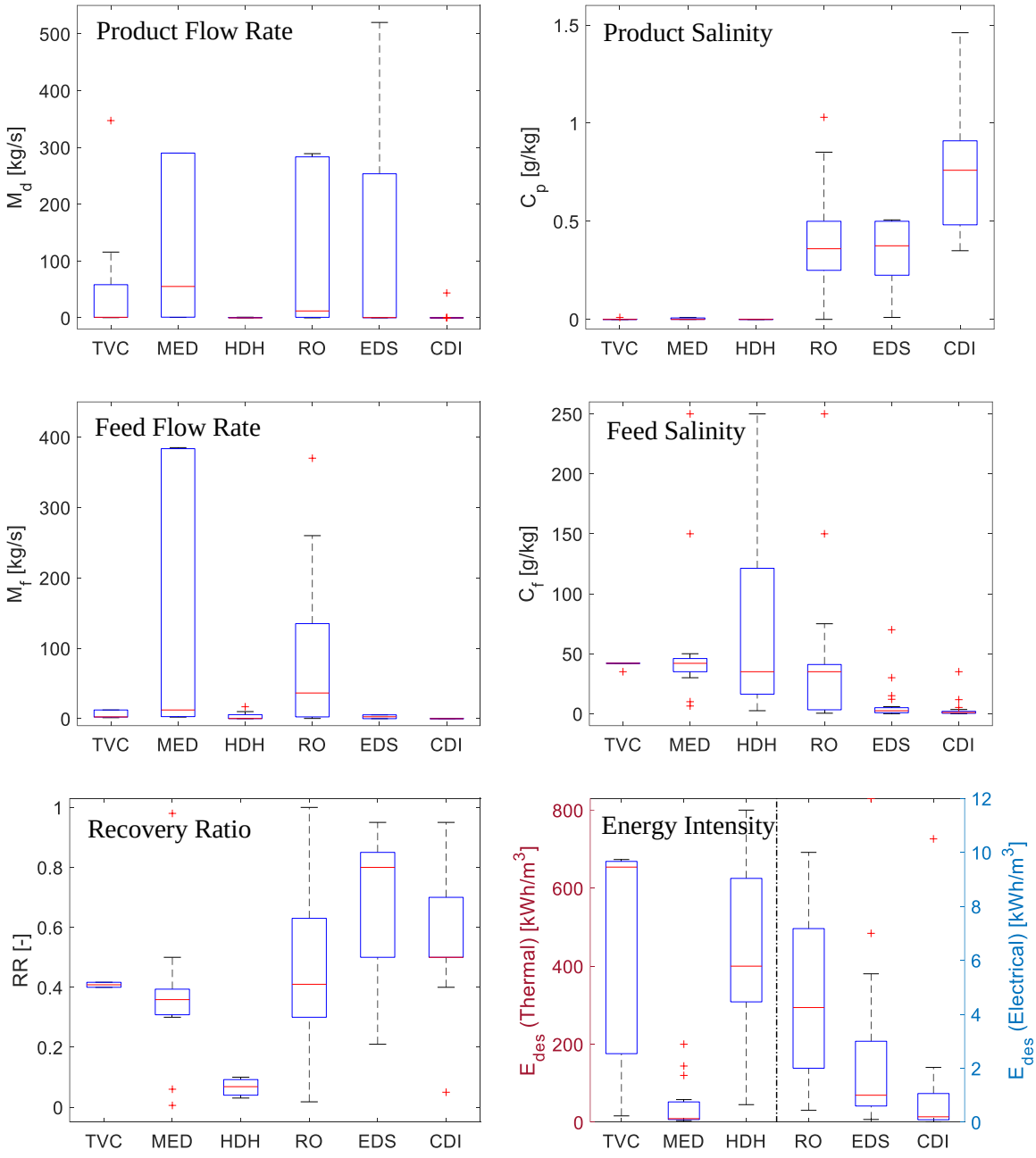

Figure 3-9: Distribution of operation parameters in the literature for each desalination method.

Table 3-10 shows the metamodel simulation results using the most representative models as particular case studies from the literature. These could be considered optimal operation conditions. Thermal desalination methods show

significantly greater energy intensity and lower recovery ratios but higher feed salinities than the molecular transport methods.

Table 3-10: Outputs overview of cross-comparative simulations at case study operation points.

Method	M_f [kg/s]	$\boldsymbol{C_f}$ **[g/kg]**	C_p [g/kg]	$\boldsymbol{M_d}$ **[kg/s]**	$\boldsymbol{RR}$ **[-]**	$\boldsymbol{E_{des}}$ **[kWh/m^3]**	M_b [kg/s]	C_b [g/kg]
TVC	1.360	35	0	0.5787	0.43	239.9	0.7811	60.9
MED	366.9	46	0	137.9	0.38	66.37	234.4	72
HDH	16.87	35	0	1.156	0.069	486.5	15.48	38.2
RO	3.472	2	0.023	2.087	0.60	0.9099	1.383	4.99
EDS	5.401	3.5	0.35	4.051	0.75	0.3688	1.360	13.0
CDI	6.138×10^{-5}	2	0.70	6.138×10^{-5}	0.50	0.5594	6.138×10^{-5}	2.54

Figure 3-10 shows the simulation points and the operation ranges from the meta-study. The system performance is summarized by recovery ratio and energy intensity where desirable operation is located close to $RR = 1$ and lowest E_{des}. The molecular transport desalination methods show on average better performance as they achieve high recoveries with the lowest salinity values. MED and CDI exhibit typical recovery ratios but at a higher energy intensity. TVC has smaller energy intensity but also smaller water recovery. A limitation in this approach is that neither RR nor E_{des} captures the degree of desalination in the feeds stream, and a better metric could include E_{des} be normalized by $(C_f - C_P)$. This, however, cannot be conducted with the range values from the meta-study as they do not correspond to a single desalination system constrained by mass transfer and energy equations. Specific recovery ratios, energy intensity, and other important parameters can be calculated using the metamodels for a given desalination system. Comparison to typical operation can help decision making between desalination

methods or identify cases suboptimal operation, and simulation can provide more valuable insights into the tradeoffs within a system.

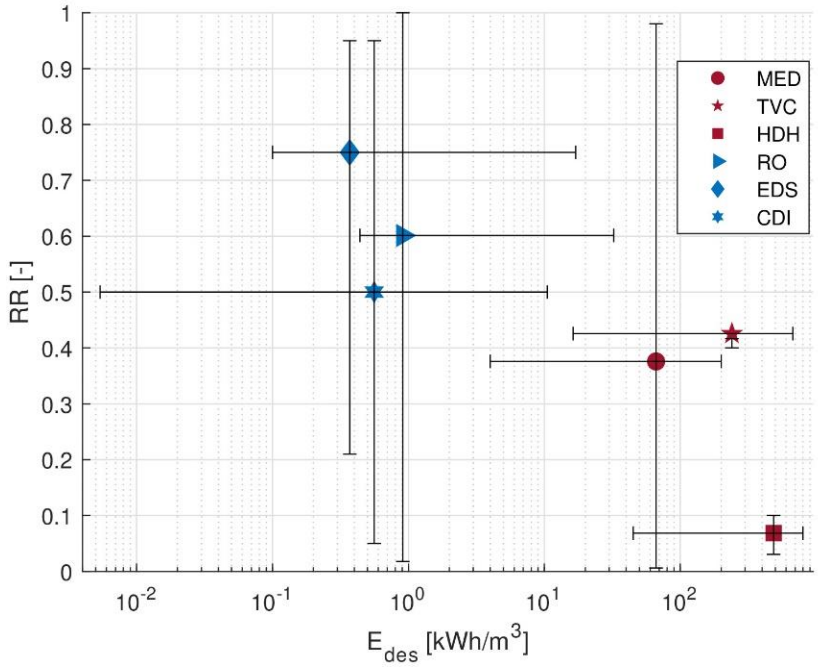

Figure 3-10: Operational Map: RR and Energy Intensity (with operation ranges from Figure 3-9).

Figure 3-11 shows the resulting surfaces formed by the response of energy intensity (E_{des}) to changes of ± 20% in M_d and C_f from the base case operation described in the most representative model for each desalination method. The magnitude of a representative parameter of the system's size is represented by the diameter of the gray circles included in each point within the surface. All desalination technologies follow a similar sensitivity to variations M_d and C_f regardless of the operational space they were designed for and independent from the physical phenomena that drives salt and water separation.

The TVC surface shown in Figure 3-11.A. is the exception to the direct proportionality between C_f and E_{des} presented in other desalination technologies.

In this analysis, the compression ratio (CR) is always fixed at 2.68, and the motive steam pressure (P_s) remains constant at 1002 kPa according to the reference model inputs. The motive steam flow rate input to the system (M_p) must be adjusted to supply the required energy for desalination. There is a very small increase of the required M_p in response to increasing C_f. A greater C_f elevates the boiling point of the solution; however, this additional energy demand is compensated for by recirculating some of the produced steam as entrained steam into the thermoejector. The saturation temperature of the entrained steam increases in response to the boiling point elevation. Thus, the implementation of a thermocompressor stabilizes the energy demands of the desalination system with respect to changes in C_f. Since the entrained steam flow rate is adjusted to supply the required energy, the expansion ratio and the mass ratio remain constant, and the output is always superheated steam. The system size follows a similar response pattern to changes M_d as larger flow rates demand larger systems to provide enough surface area for the required heat exchange.

The implemented simulation framework imposes common design constraints across all the desalination metamodels. There is an exception in the HDH metamodel because, unlike the other metamodels, HDH has M_f as an input with a numerical value much greater than M_d that remains constant through all the calculated points in the surface. Thus, a constant, large saline water stream is unnecessarily heated independent from the specified M_d, resulting in a large, constant energy consumption that becomes smaller when normalized by larger values of M_d as shown in Figure 3-11.C. The model energy consumption does not

present a strong response to changes in C_f because the additional energy required due to the variation in the specific heat capacity is insignificant within the studied C_f range in comparison to the energy involved in heating the bulk flow of the specified M_f stream. The marker diameter is scaled according to the dehumidifier area, which positively correlates to the product flow rate as the other desalination technologies.

The intended operational surface for MED, RO, EDS, and CDI presents similar responses of a direct proportionality between feedwater salt concentration and energy intensity as shown in Figure 3-11.B, 3-11.D, 3-11.E, and 3-11.F. This agrees with the response of colligative properties: boiling point elevation for MED, osmotic pressure for RO, and electrochemical potential for EDS and CDI to changes in salt concentration. Practically, energy intensity (E_{des}) only depends on C_f is the in these desalination models. Conversely, E_{des} does not show a significant dependence on M_d; instead, the product water flow rate drives the system size: condenser area for TVC and MED, dehumidifier area for HDH, membrane area for RO, and theoretical (not rounded) number of cell pairs for EDS and electrode area for CDI.

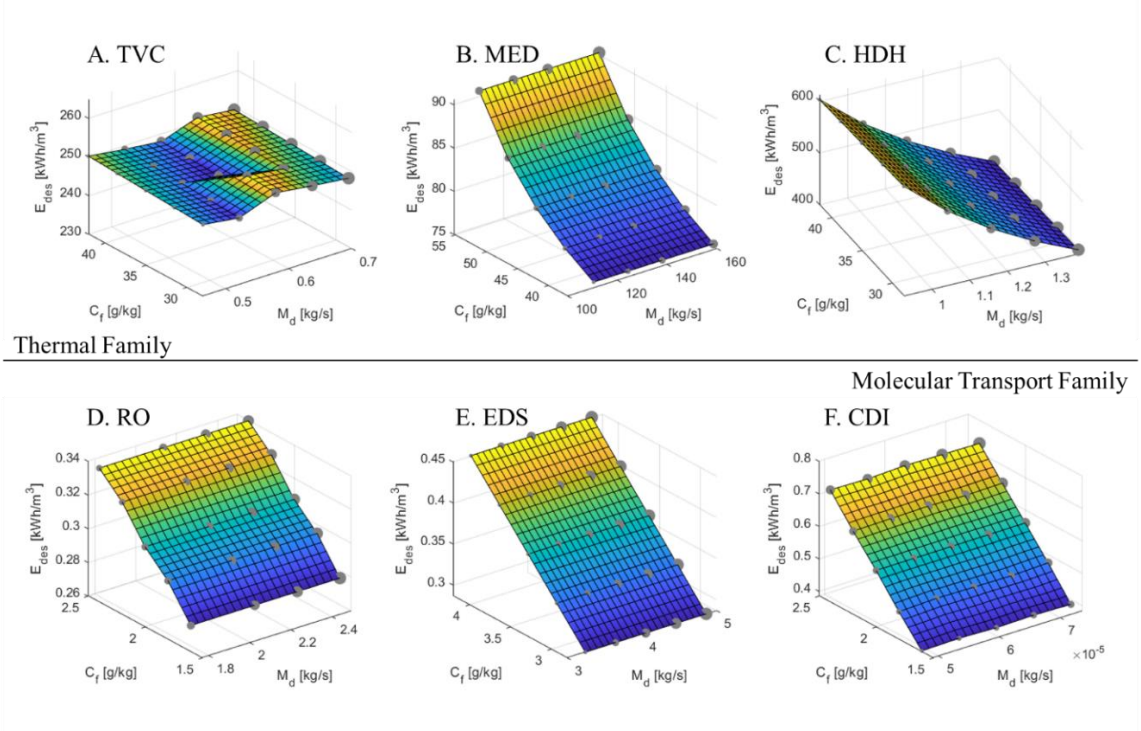

Figure 3-11: Surface plots at ±20% from the design point for different desalination methods, all plots are optimized to minimize system size. (A): TVC – base case ($M_d = 0.5787$ kg/s, $C_f = 35$ g/kg) [43], (B) MED – base case ($M_d = 137.9$ kg/s, $C_f = 46$ g/kg) [64], (C) HDH – base case ($M_d = 1.156$ kg/s, $C_f = 35$ g/kg) [65] , (D) RO – base case ($M_d = 2.087$ kg/s, $C_f = 2.0$ g/kg) [66], (E) EDS – base case ($M_d = 4.051$ kg/s, $C_f = 3.5$ g/kg) [67], (F) CDI – base case ($M_d = 6.138 \times 10^{-5}$ kg/s, $C_f = 2.0$ g/kg) [68].

Advantages in some desalination methods lie on the practical limits to the system size, such as fouling or scaling potential, maintenance, and space availability as well as the quality and type of energy available on site to run the process. It is particularly evident in the molecular transport processes, whose representative cases have similar C_f, M_d and E_{des} magnitudes, that the advantages corresponding to system size are associated to the system's capital costs. Constraints indicated by the energy intensity of each process are associated to energy availability and cost. For instance, the magnitudes of energy intensity become irrelevant for the practical deployment of MED and HDH as these systems

can be optimized to run on low-grade steam. TVC, on the other hand, requires high-grade steam which can incur higher operating costs. Finally, RO, EDS, and CDI use electricity, which is the most refined form of energy between these desalination methods and depending on the market and location, could be significantly more expensive.

3.4.1.1. Modeling regimes

The scalability of both the actual desalination methods and the corresponding models play a key role in dictating which can handle specific M_d and C_f ranges and therefore pose limitations in their deployment. The MED and RO processes are modular, as system size can be easily increased by adding an additional effect or stage to increase the heat transfer or membrane area, respectively, and adjusting the corresponding operation conditions to satisfy production requirements. Furthermore, these metamodels do not rely on numerical correlations that constrict them to a specific operational point. The other metamodels, on the other hand, present limitations in the validity of the correlations used to model key components such as the thermoejector in TVC, the humidifier in HDH, the limiting current density in EDS, and the equivalent resistances in CDI. It must be noted that most of these correlations are regressed from measured data valid for the specific component at the specific operational conditions and extrapolating to different C_f and M_d ranges might not be appropriate.

The operational regime plots in Figure 3-11 include a ±20% deviation from the intended operational point that the literature model is designed for. It is important to highlight that even with this expanded operational ranges, the

desalination models present no overlap in M_d. Specifically, the smallest range corresponds to CDI, which is found as a bench scale system with a M_d ranging from 4.9×10^{-5} to 7.4×10^{-5} kg/s. Then, there is a large gap of four orders of magnitude for the M_d ranges where most of the models for small scale systems operate without any intersection. TVC ranges from 0.46 to 0.69 kg/s, HDH from 0.92 to 1.39 kg/s, followed in increasing order by RO with an M_d range from 1.66 to 2.49 kg/s and EDS with a range from 3.24 to 4.86 kg/s. Finally, the operational range for MED is an order of magnitude greater ranging from 110 to 159 kg/s. On the other hand, the simulations present significant overlap in C_f. CDI and RO have complete intersection of C_f values ranging from 1.6 to 2.4 g/kg. This is followed by EDS with a C_f range from 0.29 to 4.2 g/kg. TVC and HDH have a complete intersection of C_f ranging from 28 to 42 g/kg. Finally, the MED simulations have partial intersection of about 37% with TVC and HDH because it ranges from 36.8 to 55.2 g/kg.

It is important to emphasize that these ranges specify the operational ranges for the representative literature models and not the possible operational range for each desalination method. Further research within each desalination method is required to find more accurate correlations that are applicable in wider operational ranges to minimize the modeling range gaps. All desalination models exhibit similar responses to variations of C_f and M_d and are observed despite the completely different operational ranges that each simulation case presents. Therefore, the second part of this analysis deploys the proposed simulation framework and evaluates performance of the desalination methods within similar

operational ranges. The models for CDI and EDS remain highly experimental while TVC and HDH are intended for very low production rates imposed by practical constraints that are not inherent to the desalination process. MED and RO are the most scalable technologies for both actual systems and theoretical modeling. Given that these two technologies are the predominant desalination processes in the desalination market, analyzing their performance at low, middle, and high C_f and M_d ranges would set an appropriate benchmark in both modeling capabilities and desalination efficiency that other technologies would compete with.

3.4.2. Cross-Comparative Simulation in Common Operational Spaces

The first step for a fair assessment of MED and RO desalination performance is defining common operational conditions for deploying the developed simulation framework. The notion of classifying models according to a Low, Normal, and High production capacity has been previously documented among the thermal desalination processes [24]. We deploy the metamodels usingC_f values of 2, 18, 35, and 50 g/kg for this study, which correspond to the limit for conventional irrigation, brackish water, sea water and brine processing, respectively. At each salinity level, we simulate product water flow rates of 2.3, 70, 138, and 1157 kg/s which correspond to common ranges for bench scale systems, industrial processing, municipal and large-scale systems, respectively. The feed water temperature is maintained at 24 °C for all the simulations. For each RO simulation case, the model attempts the maximum recovery ratio RR while minimizing feed pressure P_f. On the other hand, the MED simulations maintain a constant P_s at 31.2 kPa while minimizing the required steam flowrate M_p. Brine

salt concentration C_b is fixed at 72 g/kg for all operational MED regimes. This limit corresponds to the maximum solubility limit of $CaSO_4$ at common parallel feed MED operating temperatures [167]. At each $[C_f, M_d]$ regime (16 total), variations of ±5% and ±10% in both C_f and M_d (total of 25 simulations per $[C_f, M_d]$ pair) to account for variations that can occur in actual operation. Table 3-11 shows the results of the cross-comparative simulation, $[C_f, M_d]$ pair results are averaged in this analysis.

Table 3-11: Cross-Comparative Simulation Results.

		MED					RO				
M_d [kg/s]	C_f [g/kg]	M_b [kg/s]	C_b [g/kg]	C_p [g/kg]	RR [-]	$E_{des,th}$ [kWh/m^3]	M_b [kg/s]	C_b [g/kg]	C_p [g/kg]	RR [-]	$E_{des,el}$ [kWh/m^3]
2.3	2	0.065	72	0	0.97	68.5	0.14	45	0.05	0.95	3.3
	18	0.76	72	0	0.76	70.7	0.73	86	0.25	0.78	4.5
	35	2.2	72	0	0.53	75.2	2.0	90	0.53	0.57	6.5
	50	5.7	72	0	0.32	86.5	4.0	90	0.90	0.39	1.2
70	2	2.0	72	0	0.97	68.5	4.2	42	0.05	0.95	3.3
	18	23	72	0	0.76	70.7	27	86	0.32	0.77	4.5
	35	67	72	0	0.53	75.2	59	88	0.53	0.57	6.5
	50	175	72	0	0.32	86.5	126	90	0.90	0.39	1.2
138	2	3.9	72	0	0.97	68.5	8.5	43	0.09	1.0	3.3
	18	46	72	0	0.76	70.7	45	89	0.26	0.78	4.5
	35	132	72	0	0.56	75.2	120	89	0.53	0.57	6.5
	50	343	72	0	0.32	86.5	241	89	0.90	0.39	1.5
1157	2	33	72	0	0.97	68.5	76	47	0.13	1.0	3.3
	18	382	72	0	0.77	70.7	348	83	0.25	0.78	4.5
	35	1109	72	0	0.53	75.2	963	88	0.52	0.57	6.5
	50	2888	72	0	0.32	86.5	1951	81	0.89	0.38	3.3

3.4.2.1. General Hierarchy

Following the proposed cross-comparative framework, we first analyze the parameters within the General Hierarchy. The variables M_d, C_f, and T_{in} are fixed for MED and RO simulations within the same operational space. The motive steam pressure (P_s) remains constant for all MED simulations, and the motive steam flow rate (M_p) is optimized to supply enough heat for evaporation.

Figure 3-12 shows the fitted linear regression recovery ratio for different feed water salt concentrations and different product flow requirements. The metamodels consistently find an optimum system performance for most of the simulation cases. The RO metamodel shows a small numerical instability at 2 g/kg feed salinity and 1157 kg/s resulting from the mass transfer coefficient calculation at those opposing extreme values. Future research would be required to produce general, unified mass transfer coefficient correlations. The results show that optimized MED and RO systems can achieve similar RR at low salinities. At higher concentrations, however, RO consistently shows higher RR values than MED with the largest difference being 10% at 50 g/kg. For both MED and RO, the system can extract less water as feed higher salinity increases while incurring in greater energy intensity.

The average RR for all M_d scenarios can be approximated an inverse linear relationship to C_f which define optimal mass transfer capabilities. Ideal recovery can be described as a linear relationship with slopes of -0.012 and -0.014 for RO and MED, respectively, and an intercept of 1.0. In the case of MED, greater feed water concentrations lead to higher boiling point elevation. The operating temperatures of the system, however, are constrained by the temperature of motive steam and thus RR decreases for higher C_f. Conversely in the case of RO, this tradeoff occurs because greater concentrations lead to higher osmotic pressure to overcome by the high-pressure pump. Operating pressure is constrained by the maximum allowable pressure in the membrane module to prevent membrane rupture. The total drop in recovery ratio from the lowest to highest C_f values is

about 60% for RO and almost 70% for MED. The regressed intercept is 1.0 suggesting that, theoretically, zero salinity levels would make full recovery possible.

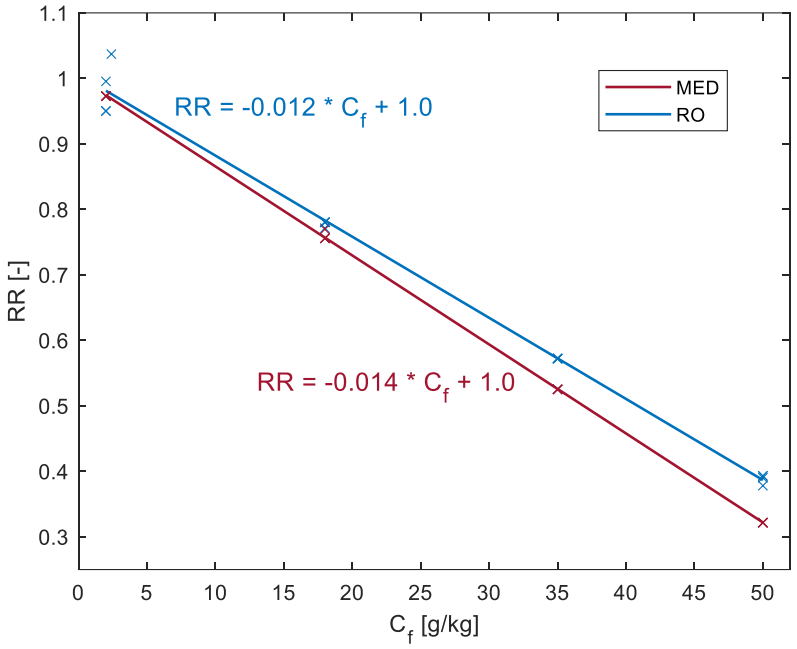

Figure 3-12: Recovery Ratio for RO at different feed salinities.

Both MED and RO have a similar response of M_b to changes in C_f at all the studied M_d regimes. A direct proportionality is maintained for which the greater C_f results in larger brine production. At the M_d range between 2.3 and 138 kg/s, MED and RO have comparable brine production for all C_f values. However, at higher production rates of 1157 kg/s this similarity only holds up to 35 g/kg feed concentration. At the higher C_f ranges, MED shows significantly higher M_b values that can be about to 50% greater than the magnitude of M_b in RO. This is an important difference to consider as brine disposal can have negative environmental effects and result in expensive treatment processes.

Brine concentration in MED is constant at 72 g/kg as it is imposed in the system design as a safe maximum salinity limit to prevent fouling. On the other hand, RO presents lower C_b values for lower concentrations up to brackish water ranges. The operation conditions for MED and RO are dictated by solubility limits of salt to prevent fouling or scaling. From a modeling standpoint, brine concentration in MED can be defined *a priori* based on solubility limits of salts in the feed water stream [167]. RO, on the other hand, requires iterative simulations because solubility limits occur at membrane interface where concentration polarization takes place [168]. The resulting brine concentrations in RO are not consistently proportional to the magnitude of M_d because the model employs an iterative procedure involving discrete increments of membrane area. For RO cases of greater salinity, the discharged brine can have concentrations close to 90 g/kg. This could be problematic as increased concentrations lead to precipitation and therefore localized fouling [85]. Furthermore, disposal of brine at greater concentrations increases the risk of pollution and could be subject to regulation depending on the location.

The final parameter of interest within the general hierarchy is the product salt concentration C_p. It is expected to have no salt concentration in MED as it employs a distillation process with demisters that prevent entrained saline droplets from combining with the produced water vapor. However, salt ions can permeate the membrane in RO and result in a flow with non-negligible C_p. MED, as expected, results in negligible product concentrations independent of M_d or C_f. RO, on the

other hand, presents product concentrations ranging from 0.05 g/kg up to 0.90 g/kg at feed concentrations of 2 g/kg and 50 g/kg, respectively.

The General Output analysis results also suggest it is important to consider what the product water will be used for after desalination. While MED consistently results in water with negligible salt content, the RO permeate product can have salt concentrations up to 0.90 g/kg at high C_f. As a reference point, the World Health Organization defines palatable concentration limits for human consumption as follows: 0.2-0.3 g/kg for chloride, 0.2 g/kg for sodium, and 0.6 g/kg for total dissolved solids [169]. If the product water is used as municipal water, it must go through a post-desalination process regardless of what desalination method is used, however, the MED process will consistently produce water with negligible salt content as opposed to RO which could involve additional desalination.

3.4.2.2. Family Hierarchy

MED and RO correspond to the thermal and molecular transport desalination families, respectively, and therefore, their family parameters cannot be directly cross-compared. However, it is important to consider them independently to understand potential tradeoffs associated to each system.

Figure 3-13 shows the relation between mean E_{des} across the studied M_d ranges and C_f. All curves are superimposed for each desalination method indicating that P_{des} and M_d are directly correlated with a 1:1 ratio. E_{des} is the main point for cross-comparison in other studies whose analyses are usually restricted to sea water salinity ranges between 35 and 42 g/kg. The results closely match the energy consumption found at these concentrations for both MED and RO [45], [46], [170].

Furthermore, the results lie within the generalized ranges of 73 kWh/m^3 and 2-4 kWh/m^3 for MED and RO, respectively, determined in a previously conducted life cycle assessment analysis [171]. The change in E_{des} is positively correlated to C_f for both technologies. This can be expected from the increase in boiling point elevation and osmotic pressure that result from increasing feed concentration in MED and RO, respectively. It is important to note that E_{des} in both methods has a similar gradient with respect to C_f at low concentrations; however, while energy intensity in RO remains linear with a constant gradient, the gradient for MED starts increasing after roughly 25 g/kg thus, deviating from a linear relation.

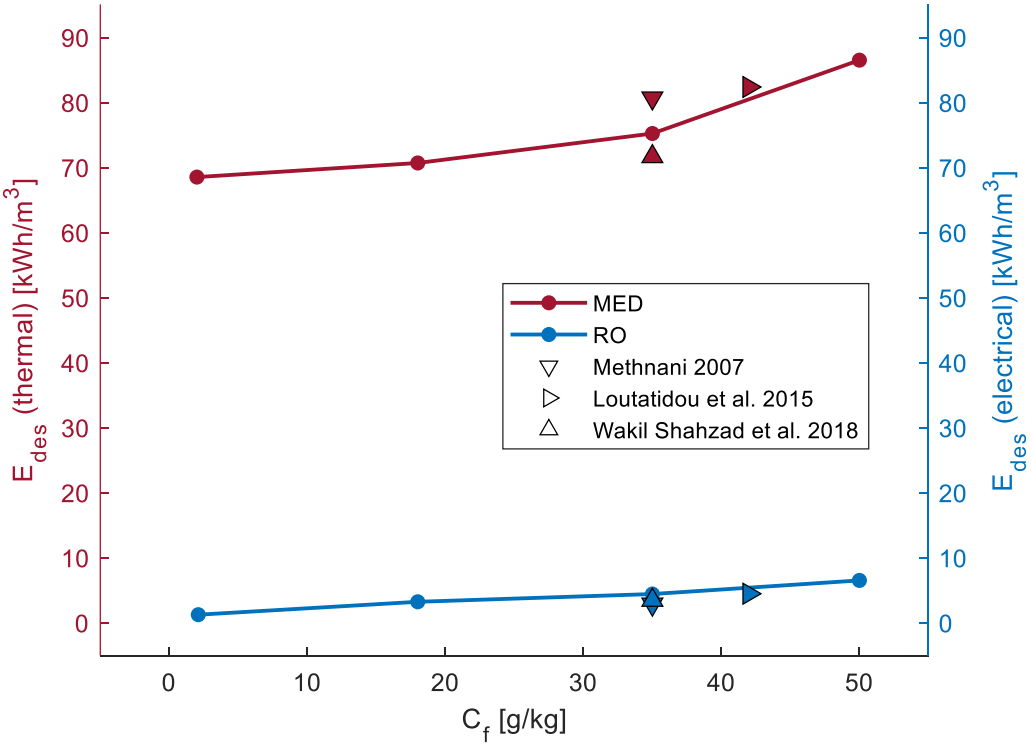

Figure 3-13: Energy intensity (E_{des}) averaged across the studied M_d ranges in response to changes in feed water concentration.

Overall, E_{des} remains between 51 and 13 times larger for MED than RO. This difference is attributed to the greater energy requirements involved in phase

change which is inherent to the MED process. Despite the fact MED consistently shows a larger energy intensity, it must be noted that unlike RO, the process can run on low-grade energy. This could make the cost irrelevant if heat from a different process is available at a lower cost. For instance, in the MENA region, the average operating cost for RO can be about 4.6 times greater than MED, presumably due to low oil prices; however, the average total costs for both methods is relatively similar with differences of 0.04 $\$/m^3$ [4]. The difference in the cost of energy is further extended for indirect solar desalination plants where the cost of water produced through RO can be up to about 13 times greater than MED even though the associated specific energy for desalination for RO can be between one and two orders of magnitude lower than that for MED [48]. RO presents a higher risk of fouling as it involves a permeation process, and therefore, preprocessing and maintenance can contribute to greater costs of desalination at higher feed salt concentrations and production rates. About 14% of the operating cost can be attributed to chemicals and post treatment [172] and pretreatment while structural and administrative tasks can add to 46% of the total cost [173]. The large discrepancies in energy consumption and total water cost further support the need of a methodological approach to benchmarking and cross-comparison as opposed to restricting the analysis to energy consumption alone.

Table 3-12 shows the remaining Family Hierarchy parameters for MED. It is evident that to achieve greater product flow rates, the system must generate more water vapor and therefore incur larger energy requirements with motive steam for evaporation independently of the value of C_f. Within a fixed M_d, there is a

consistent positive correlation between M_p and C_f as increased salt concentration leads to a greater boiling point elevation and therefore larger energy requirements for evaporation.

Table 3-12: Thermal Family Hierarchy Results.

		MED		
M_d [kg/s]	C_f [g/kg]	M_p [kg/s]	GR [-]	sM_{cw} [g/kg]
2.3	2	0.25	9.3	2.9
	18	0.25	9.0	2.8
	35	0.27	8.5	2.5
	50	0.31	7.5	1.7
70	2	7.5	9.3	2.9
	18	7.7	9.0	2.8
	35	8.2	8.5	2.5
	50	9.5	7.5	1.7
138	2	15	9.3	2.9
	18	15	9.0	2.8
	35	16	8.5	2.5
	50	19	7.5	1.7
1157	2	124	9.3	2.9
	18	128	9.1	2.8
	35	136	8.5	2.5
	50	156	7.5	1.7

The gain ratio (GR) for MED decreases as C_f becomes greater in all M_d ranges. From an energetic standpoint, the results show that the MED system becomes slightly less efficient as C_f increases, independent from M_d, since less product water can be produced by unit of motive steam used. There is about a 20% drop in GR between the lowest and highest C_f values.

Like GR, the specific cooling water (sM_{cw}), is independent of M_d and decreases with a total drop of about 40%. This highlights the fact that the MED is driven by evaporation and that the system must operate at higher temperatures because the boiling point is elevated with the presence of salt. The larger temperature differences between steam in the last effect and the intake cooling

water improve heat transfer and reduce the requirements for cooling water. This would suggest that the MED process is optimized for larger salt concentrations, regardless of the required production.

The Family Hierarchy can give a notion of the performance of the desalination process and the tradeoffs associated with each method, but it cannot yield comparative conclusions as MED and RO come from different desalination families. The resulting GR from MED indicates that at the system produces about 9.3 times the mass flow rate of motive steam and reduces to about 7.3 with increasing C_f. This occurs due to the increasing energy required to overcome the higher intermolecular attraction between salt ions and water molecules resulting from higher feed salinities. Greater M_d flow requirements and higher C_f consistently result in greater motive steam demand. It is important to note that MED can work with low-grade steam and thus be combined with an existing process. Steam availability can constrain the production flow rates achieved through MED. An external steam generator can supply the full or partial steam load, but this results in additional operating costs. This Family parameter analysis highlights a tradeoff in MED where greater C_f results in lower GR, or increased steam demands per product water flow rate, but also results in a deceasing sM_{cw} and therefore less discharged cooling water. With respect to MED, this hierarchy yields valuable insight on the limitations imposed by energy availability and water supply and discharge.

3.4.2.3. Specific Hierarchy

The Specific Hierarchy is redundant in this analysis since the studied systems are completely different, and therefore, the parameters cannot be cross compared. Nevertheless, a brief independent assessment of the resulting representative system size in response to changes in feed salinity can be important to consider. As shown in Table 3-13, the representative system size is expressed in the condenser area (A_c) in the case of MED and the total membra area (A_m) in the case of RO. In both desalination methods, the larger the production requirements require a larger system. Furthermore, for most cases the system size is also positively correlated to C_f. At 2 g/kg and with a product flow rate of 1157 kg/s, the membrane area for RO is larger and deviates from the trend. This occurs because the model considers such large flow rate as many parallel pressure vessels, therefore increasing one module in series, since adding a membrane module is equivalent to a discrete increase in system area, actually results in a larger total area than required for the desired M_d. It must be noted that the condenser area in MED is the effective area in the tube bundles of the heat exchanger while the system area in RO is the total surface area of the spiral-wound membrane modules. Generally, RO systems are more flexible in terms of size as membrane modules can be added to an existing system with relative ease as opposed to a condenser in MED which would require replacing the entire component.

Table 3-13: Relevant Specific Family Hierarchy Results.

		MED	RO
M_d [kg/s]	C_f [g/kg]	A_c [m^2]	A_m [m^2]
2.3	2	37	53
	18	41	55

	35	49	96
	50	63	155
70	2	1138	1653
	18	1262	1694
	35	1481	2934
	50	1915	4684
138	2	2242	3218
	18	2486	3314
	35	2918	5779
	50	3772	9304
1157	2	18821	128411
	18	20873	28015
	35	24499	48353
	50	31671	78113

3.4.3. Limitations

Although the presented simulations support the viability for integrating different desalination methods into the proposed framework, the major limitation remains at the validity ranges for intake product flow rate (M_d) and intake salinity (C_f) of the representative models. Most of the constructed models, including TVC, MED, HDH, and RO, are validated within a 10% difference of their corresponding literature model and show excellent agreement with more than 24 independent publications in total. However, models such as EDS or CDI that rely on empirical correlations and coefficients that are valid only for the specific system and operating conditions have a much narrower operational range that does not completely intersect with the other models. Therefore, the proposed framework can only be deployed at these reduced ranges potentially showing incomplete results. Bench scale systems will need future modeling upgrades to represent electric energy consumption for a commercial system that could potentially include not only the electric energy for electrodes but also for circulation pumps. More appropriate general models for these desalination processes are a subject of ongoing

research and updating the existing models can solve this limitation. The hierarchical parameter classification framework presented in this paper provides a clear structure to easily incorporate published models which can either expand the capabilities of the current metamodels or incorporate new models for novel desalination methods.

The present study focuses on specific energy consumption and the associated operational cost as a key parameter for cross-comparison. We suggest that the type of energy associated to MED and RO justifies the current market share panorama based on the costs of steam and electricity generation. It is possible that inadequate operation and maintenance are more expensive than energy itself in an actual facility. This is a view of energy which is an important piece of the puzzle, but there are many other aspects of desalination technologies which are out of the scope of this work. Additional studies, such as a full lifecycle analysis can provide insights into levelized cost calculations and therefore better conclusions about the financials associated to each desalination process.

3.5. Conclusions

This work aims to evaluate technologically possible operation conditions for different desalination technologies, which set targets to achieve or exceeds in the development of new desalination systems. This study developed reduced-order desalination metamodels and a framework to conduct a cross-comparative analysis by classifying input and output parameters according to an analytical hierarchy. The metamodels show excellent agreement with published data as the results have a maximum 9% error when compared to the results of models in the existing

literature. The proposed framework compares the general outputs of (a) Thermovapor Compression (TVC), Multi-Effect Distillation (MED), Humidification-Dehumidification (HDH) in the thermal family of desalination methods, and (b) Reverse Osmosis (RO), Electrodialysis (EDS), and Capacitive Deionization (CDI) in the molecular transport family of desalination methods, at different operational condition ranges. The study provided a detailed comparative analysis between the most popular desalination technologies, MED and RO.

The first part of this study used the developed framework for a comparison between the studied desalination methods and their corresponding operational points from the most representative model in the literature. The results highlight the importance of system scalability in catering towards wider ranges of salt concentrations and production flow rates. The simulation results at the operational conditions presented in the literature for each representative model highlights the lack of overlap in product flow rate ranges that the models can simulate, which makes cross-comparison more challenging as some correlations cannot be used beyond the intended operational range. Indeed, there are instances where operation ranges are reported in the literature, but the number of undisclosed parameters make their implementation difficult. Future research would be required to expand modeling capabilities of the presented metamodels by linking additional modeling correlations. Nevertheless, integrating the current metamodels into a single simulation frame is appropriate as the existing models exhibit partial overlaps in feed water salt concentration and show similar sensitivity to feed salinity independent from product flow rate. Specifically, the operation points from the

most representative literature models employ a salinity range of 1.6 to 2.4 g/kg for both capacitive deionization and reverse osmosis, a range of 28 to 42 g/kg for thermovapor compression and humidification-dehumidification desalination, and a range of 37 to 55 g/kg for multi-effect distillation, and there is a common increase in energy intensity for each increase in feed salinity. The presented comparative analysis suggests this relationship is consistent for MED and RO when testing wider operation ranges.

From a modeling perspective, small scale, or newer desalination methods such as TVC, HDH, EDS, and CDI, do not yet offer the required system scalability reflected in ranges for which correlations hold valid, to compete with the established MED and RO processes. This is particularly evidenced in the humidifier calculations for HDH, the limiting current density in EDS, and the ion adsorption in CDI. All of these critical parameters are estimated with empirical relations that are specific to the system and operating conditions and are not generalizable to larger system scales and other operational regimes. MED and RO are constructed in a modular form for either evaporator effects or membrane units governed by less constrained equations that can be easily added to expand capacity and therefore cover the largest operational spaces. Until new developments within the other desalination processes allow such scalability, the commercial competitiveness of TVC, HDH, EDS and CDI would be limited to the specific conditions of low production flow rates and in the case of the molecular transport processes, low salt concentrations that are found in the literature. Further research is required within

each desalination method to enable generalized predictive modeling to facilitate adoption and fair cross-comparison in the long term.

The second part of the study uses the simulation framework in a cross-comparative analysis between MED and RO, which are the most widely used desalination technologies in the current market. We find that recovery ratio can be expressed as an ideal operation line that can be used to assess how far from ideal operation a system is. These functions give targets for existing facility managers to understand if their technology is optimally designed or operated. The first concluding remark from this analysis points at the wide operational regimes in the conducted simulations. The operational space considered in product water flow rates ranges from bench to large scale production, and feed salinity levels concentrations range from irrigation to brine. The ability to cover such a large range of operational regimes is the first objective that experimental desalination technologies need to reach to become competitive in the marketplace. The conducted comparative analysis identified the tradeoffs, strengths, and weaknesses that each system has through a systematic review of General-, Family-, and System-level parameters. This can also be used to identify potential niche opportunities that experimental desalination methods could target. For all ranges, energy intensity is an order of magnitude larger for MED than RO. This difference results from the greater energy requirements involved in phase change in the MED process and can be equalized by the higher cost of electricity compared to low grade steam. Furthermore, at high feed salinities MED shows 50% greater brine production values than RO, whose discharged brine can have concentrations close to 90 g/kg,

while MED restricts brine concentration at 72 g/kg. In addition, MED product concentration is consistently negligible as opposed to RO for which product concentration ranges from about 0.1 g/kg to 0.9 g/kg for feed concentrations of 2 g/kg and 50 g/kg, respectively. Therefore, although MED incurs a larger energy intensity, the lower energy costs and greater controllability of brine and product streams justify such a difference. For actual desalination plants, the thermodynamic differences between MED and RO result in similar utility costs due to the variation in the costs of thermal and electrical energy. Furthermore, besides energy availability and costs, other considerations in selecting the type of desalination plant involve available space for the plant, system lifetime, and local regulations regarding brine disposal, including temperature, quantity, and salinity.

In conclusion, energy intensity alone or isolated model parameters are not appropriate for determining the viability of desalination processes. Instead, an inclusive approach relating model inputs and outputs across the same analytical hierarchy clearly outlines the energetic tradeoffs that a desalination system presents. Taking this into account, the best desalination method is the one that fulfills the operational requirements while recognizing energy availability and its costs. Practical constraints, such as the available space for the desalination facility and the disposal of the brine, also play a major role in establishing the most suitable desalination system. Overall, this study developed an analytical framework to desalination modeling because it allowed for systemic comparisons among all desalination methods.

Chapter 4: Validation with Field Data

This chapter is reproduced from the following journal paper:

> S. A. Romo, M. Storch Jr., and J. Srebric, "Operation Modeling of Actual Desalination Plants," *Desalination,* 2022. Under peer-review. [Journal Impact Factor: 9.501]

4.1. Introduction

Thermodynamic models are powerful tools for development, evaluation, and improvement of actual desalination plants. Existing desalination models allowed investigations of system response to different input conditions [96], [174], [175] optimized system performance [176]–[178] and macro-level cost analyses [179], [180]. However, before implementing a model-aided investigation or decision, a model must be validated to confirm accuracy of simulated parameters. Unfortunately, many published models do not disclose all the necessary thermo-physical parameters to conduct a detailed validation for desalination plants. This lack of disclosure in the literature challenges research efforts that aim to improve existing models, preventing a wider adoption of model-driven strategies for design of desalination systems and plant management. This limits the widespread adoption of desalination systems along with efforts to make desalination more sustainable [181].

The practical application of simulation studies is contingent upon the accuracy with which a model can replicate the operation of actual desalination plants. For this reason, models have been developed based on actual desalination plant facilities [87], [121] whose parameters are known a-priori. For instance, there

are publications that describe desalination plants with enough parameters to build a simulation [95] and several existing studies leveraged such data for building new analytical tools [89], [91], [94]. There are relatively few cases with full set of required system data because of the proprietary nature of most plant operations. Importantly, high fidelity models for specific components found in desalination plants are available in the literature [182], but incorporating them into the desalination plant models can be challenging due to missing thermo-physical input and/or model components. Additionally, review articles generally provide only high level data for a plant operation [94], [166], which are insufficient to construct robust simulations. Therefore, modeling actual desalination facilities remains a challenge and is limited to the few cases where all operation parameters are available.

Simulation and validation of desalination models with incomplete datasets can be defined as an optimization problem in which it is desired to find a set of unknown inputs that result in the best estimate of actual plant operation. The first logical approach toward implementing an optimization algorithm is by conducting a sensitivity analysis. However, this is only possible, in constrained domains because desalination models are nonlinear and do not have a continuous solution space due to physical nature of these systems and associated underlying numerical correlations within each model. This would suggest, therefore, that sampling-based processes can be applied to reduce the bias towards a single disconnected solution space. Several global optimization algorithms [183]–[185] apply adaptive sampling schemes and surrogate models to test problems from the literature. Such

optimization methods have been extensively researched with respect to desalination systems [176]. However, these methods are only feasible in cases where the operation of a system or solution bounds are known a-priori to constrain the solution space such that it remains continuous and connected. Furthermore, collapsing the model into a system of equations is challenging because different correlations depend on the specific plant operation. Finally, most desalination simulations, especially those where most inputs are unknown, require a local calibration of certain parameters, such as supplied steam or feed pressure, to ensure conservation laws are followed.

In this paper, we first expand models of Multi-Effect Distillation (MED) and Reverse Osmosis (RO) desalination by implementing sub-models of energy recovery devices, namely, thermocompression and pressure exchange, respectively. The upgraded models are then validated with corresponding literature data. In the end of this effort, we present a novel methodology that applies these models to recover simulation parameters based on partially available process parameters. The proposed algorithm is demonstrated in four different desalination plants from which we collected field data. Finally, we propose a theoretical efficiency parameter that utilizes the simulation results to quantify the degree of suboptimal recovery in desalination systems.

The contributions of this paper are:

- Fully deployable models for Multi-Effect Distillation with Thermocompression (MDT) and Reverse Osmosis with Pressure Exchange (ROX) desalination systems.

- A novel methodology that combines the proposed models and a sampling scheme to infer plausible operation conditions for actual desalination plants with partially available data.
- Demonstration of the proposed algorithm using data from four different desalination plants, specifically, two MDT and two ROX desalination plants.
- A new theoretical efficiency metric that quantifies how far away from ideal operation a desalination system is.

The remainder of this paper is structured as follows. Section 2 presents the models for MDT and ROX along with their validation with literature data and introduces the desalination facilities serving as case studies. Section 3 elucidates the proposed methodology and its application to each case study. Section 4 discusses the implications of deploying the proposed algorithm as it allows to calculate a theoretical efficiency parameter to quantify the degree of suboptimal recovery for MDT and ROX desalination systems.

4.2. Methodology

Desalination models provide an accurate representation of desalination plants to investigate system response to changes operation conditions and aid in decision making during deployment, maintenance, and upgrades. In this section, we adapt solution algorithms for MED and RO metamodels [186], to incorporate energy recovery devices like those featured in the case studies. This significantly changes the underlying computational scheme of each model. Hence, the presented development focuses on incorporating thermocompression and pressure exchange

as featured in the case study systems. These models are viable for replicating operation from systems in the field since they require less measured variables compared to other computationally intensive simulation approaches. Furthermore, their low running time allows for their fast deployment and rapid automated iterations for calibration.

4.2.1. Model for Multi-effect Distillation with Thermocompression

The Multi-Effect Distillation with Thermocompression (MDT) model features parallel feed MED with a single thermocompressor that aids with heat recovery as shown in Figure 4-1. Desalination takes place in evaporators (called "effects") connected in parallel with respect to the feed water flow and in series with respect to the steam and brine streams.

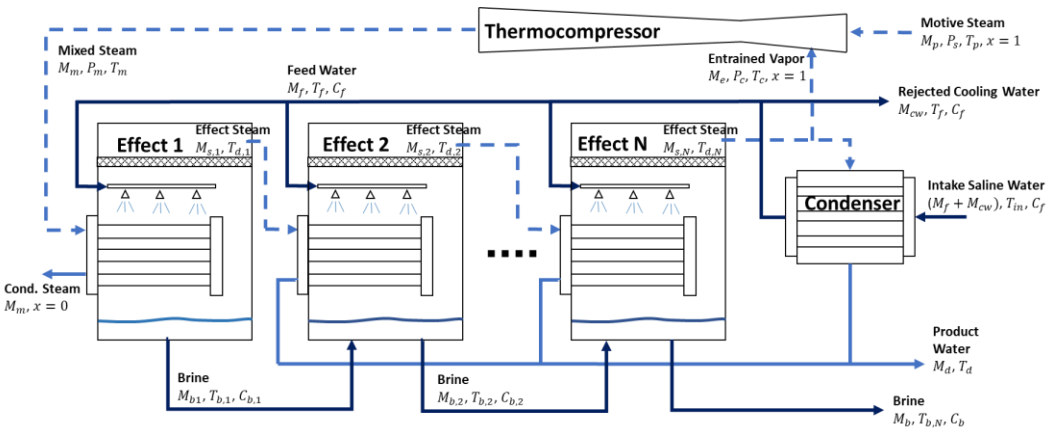

Figure 4-1: MDT process schematic.

Motive steam flow, M_p, entrains part of the vapor produced in the last effect M_e, which is ejected as a mixed steam flow rate M_m directed into the first effect. This flow supplies energy to drive evaporation. The vapor that is not entrained in the thermocompressor, described by $(M_{s,N} - M_e)$ flows through the condenser, where it undergoes a phase change to become condensed liquid water. This

condensate stream is combined with the condensed water produced in each effect as the desalinated water product with flowrate M_d. On the other side of the condenser, the intake water flowrate, constituted by the feed water for desalination M_f and additional cooling water M_{cw}, is preheated. The cooling water is then discarded after acting as a heat sink in the condenser, and the feed water flow rate is divided among the system effects. In each effect the feed is distilled resulting in a brine flow ($M_{b,pass,i}$) that passes into the subsequent effect for flashing while an effect steam flowrate $\left(M_{s,i}\right)$ is directed into the subsequent effect to supply energy for evaporation. The process culminates in the last evaporation effect, where a high-salinity brine flow (M_b) is generated as a byproduct of the desalination process. The MDT model, incorporates equations to model the thermoejector [76], [77] which describe the mass ratio (M_r) as:

$$M_r = \sum_{n=0}^{3} \left(A_n C_r^n + \frac{B_n}{E_r^n} \right) + \frac{C_r}{E_r} \boldsymbol{C} \cdot \begin{bmatrix} 1 \\ C_r \\ 1/E_r \end{bmatrix}, \tag{4-1}$$

for $E_r \geq 100$ or $100 \geq E_r \geq 10$, and

$$M_r = \sum_{n=0}^{3} \left(A_n \ln(C_r)^n + \frac{B_n}{E_r^n} \right) + \frac{C_r}{E_r} \boldsymbol{C} \cdot \begin{bmatrix} 1 \\ \ln(C_r) \\ 1/E_r \end{bmatrix}, \tag{4-2}$$

for $10 \geq E_r \geq 2$. Where the vectors $\boldsymbol{A}$, $\boldsymbol{B}$, and $\boldsymbol{C}$ are regression constants, C_r is the compression ratio, and E_r the expansion ratio.

4.2.2. Model for Reverse Osmosis with Pressure Exchange

The Reverse Osmosis with Pressure Exchanger (ROX) model describes a conventional single-pass RO system with membrane modules in a tapered arrangement and a pressure recovery device as shown in Figure 4-2.

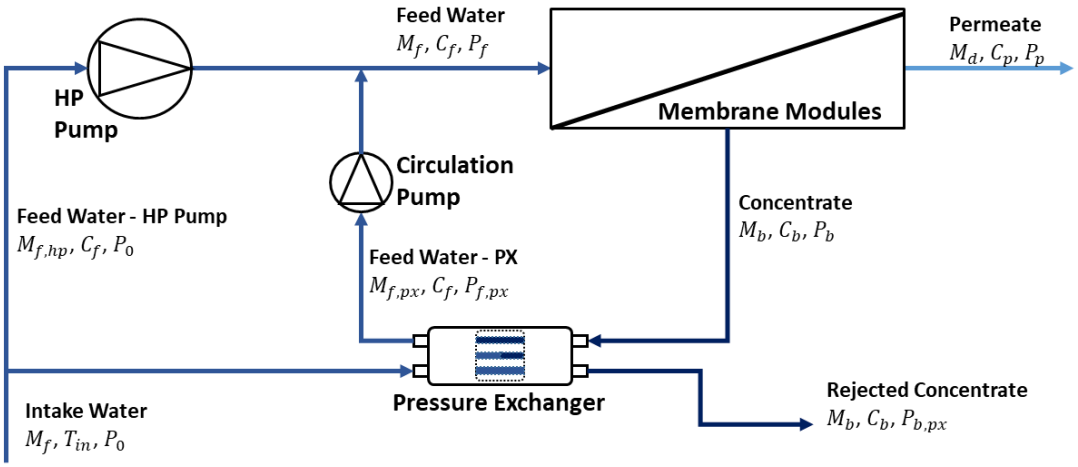

Figure 4-2: ROX process schematic.

The saline intake water stream is split into two streams that undergo pressurization: one by the high-pressure pump ($M_{f,hp}$) and another by the pressure exchanger ($M_{f,px}$). The pressure exchanger is a vessel that contains a rotating cartridge between two end-covers [187]. The end-covers contain inlet and outlet passages that allow water to flow in and out of the rotating cartridge. When the cartridge compartment aligns with the low-pressure side inlet, intake water stream ($M_{f,px}$) enters the cartridge and fills the compartment while displacing the contained water out through the high-pressure outlet as rejected concentrate. As the cartridge rotates, the compartment is closed until it aligns with the high-pressure inlet. At this point, the high-pressure brine (M_b) displaces the water in the compartment through the low-pressure side's outlet, transferring the energy contained within the flow. The cartridge then completes a full rotation and allows

for more intake water, which displaces the contained concentrate into the rejected concentrate stream ($M_{b,px}$). The multiple compartments within the rotating cartridge make this exchange process virtually continuous. Because the two streams have partial mixing, there is a slight salinity increase in the intake water stream fraction in the pressure exchanger. A circulation pump ensures no backflow occurs from the high-pressure side of the system back into the pressure exchanger. The two feed streams are combined and then directed into the RO membrane modules, which separates the feed water stream into the permeate water and concentrate. The relevant equations of the ROX model are detailed in our previous publication [186] under RO key equations. A mass transfer coefficient developed for commercially available XLE modules is implemented as it best matches the membranes used in the ROX systems [66], [127]:

$$k = 0.808\left(\frac{6vD_{25}^2}{hl}\right)^{\frac{1}{3}}\left(\frac{D_T}{D_{25}}\right)^{\frac{2}{3}}, \tag{4-3}$$

where v is the flow velocity, D_{25} is the membrane diffusivity at 25°C, h is the channel thickness, l is the element length, and D_T is the membrane diffusivity at the operating temperature.

The pressure exchanger efficiency (η_{PX}) is described by [187]:

$$\eta_{PX} = \frac{Q_{f,PX}P_{f,PX} + Q_bP_{b,PX}}{Q_{f,PX}P_0 + Q_bP_b}, \tag{4-4}$$

where $Q_{f,PX}$ is the feed portion of the volumetric flow rate that is directed through the pressure exchanger with pressures P_0 and $P_{f,PX}$ at the inlet and outlet, respectively. Q_b is the brine volumetric flow rate with pressures P_b and $P_{b,PX}$, at the inlet and outlet of the energy recovery device, respectively.

Finally, the salinity increase (SI) is described by [188]:

$$SI = RR \times 6.15\%, \tag{4-5}$$

where RR is the recovery ratio of the desalination system.

4.2.3. Model validation

Published studies usually provide more information on the variables relevant to the mechanistic transport processes that are not available in the high-level plant data and, therefore, are appropriate for guiding model adaptation. Validation data is obtained from studies that provide inputs, outputs, and intermediate parameters that can be used to address model validity and identify errors in the model subroutines. Besides aiding model development, literature data provides an initial approximation to the unknown variables in a simulation.

The MDT model is validated with the data published by Temstet et al. [95], which presents a system with feed heaters resulting in different feed temperatures at each effect; however, only the temperatures for the 1st, 5th, 11th, and 12th effects are provided. This is addressed by manually overwriting the feed temperatures and assuming linear interpolation between unknown effect feed temperatures. Feed heater energy is not considered in the desalination energy calculations, which according to our simulations, can potentially result in up to a 20% increase in energy intensity. The gain ratio (GR) is mentioned in a follow-up study [91].

The ROX model is validated with data from a study that details operation of a seawater ROX facility [187]. The model algorithm initially assumes a conventional single pass RO system without the circulation pump or the pressure exchanger to initialize the ROX variables. After the ROX variables are initialized,

the algorithm proceeds to compute energy recovery in the pressure exchanger, and then the membrane modules are solved until convergence is achieved.

Table 4-1 and Table 4-2 show the literature data, the model outputs, and the corresponding percent difference. The models show excellent agreement with the validation data. For MDT, the maximum difference occurs in the brine flow rate due to an accumulated small discrepancy in the amount of distillate generated in each effect that accumulates through the 12 effects of the system. Regarding the ROX model, the greatest discrepancy with validation data occurs in the product salinity. This can be attributed to a small error in the salt passage in each differential membrane element that accumulates with each iteration. An important factor that contributes to this error is concentration polarization, which refers to an increase in concentration at the membrane surface due to accumulation of salt ions that affects the mass balance across the membrane. Concentration polarization effects are typically accounted for in a mass transfer coefficient calculation that is membrane-specific and requires data, typically designated as proprietary by the manufacturers. Thus, we chose to approximate this parameter using an empirical correlation from the literature [127].

Table 4-1: MDT Model validation summary.

Inputs	**Temstet et al.** [95]	**Model Values**	**% Err.**
Product flow rate, M_d (kg/s)	104.17	104.17	0.0
Intake salinity, C_f (g/kg)	40	40	0.0
Intake temp., T_{in} (°C)	[10, 22]	22	0.0
Motive steam pressure, P_s (kPa)	4500.0	4500	0.0
Top brine temp., T_{bt} (°C)		63	
Last effect brine temp., T_b (°C)		38	
Feed water temp., T_f (°C)	[35, 55]	36	2.9
Brine salinity, C_b (g/kg)	59.9	59.9	0.0
No. effects, N_{eff}	12	12	0.0
Motive steam flow rate, M_p (kg/s)	6.25	6.25	0.0

Mixed steam sat. temp, $T_{m,sat}$ (°C)	64.5	64.5	0.0
Entrained vapor target flow rate, $M_{entrained,target}$ (kg/s)	0.4167	0.4167	0.0
Condenser effectiveness, η_c		0.69	
General Outputs			
Product flow rate, M_d (kg/s)	104.17	105.6	1.4
Feed water flow rate, M_f (kg/s)	314.0	298.6	4.9
Brine flow rate, M_b (kg/s)	209.7	193.0	8.0
Product water salinity, C_p (g/kg)	< 0.1	0	
Feed water salinity, C_f (g/kg)	40	40	0.0
Brine salinity, C_b (g/kg)	59.9	59.9	0.0
Recovery Ratio, R	0.3318	0.3537	6.6
Family Outputs			
Specific energy, E_{des} (kWh th/m^3)		43.6	
Motive steam flow rate, M_p (kg/s)	6.250	6.25	0.0
Gain ratio, GR	16.7	16.9	1.4
Sp. cooling water flow rate, sM_{cw} (kg/kg)	0.40	0.41	1.7
Specific Outputs			
Cond. area, A_c (m^2)		2070	
Specific area, sA (m^2/kg/s)		312	
Intermediate Parameters			
Vapor temp. 1st effect, $T_{v,1}$ (°C)	62.2	62.5	0.5
Vapor temp. last effect, $T_{v,12}$ (°C)	37	38	1.6
Distillate by boiling, M_{sb} (kg/s)		99.2	
Distillate by flashing, M_{sf} (kg/s)		6.8	
Cooling water flow rate, M_{cw} (kg/s)	41.56	42.86	3.1
Cond. HT coeff., U_c (kW/m^2°C)		1.9	
Mean evap. HT Coeff., $U_{e,avg}$ (kW/m^2°C)		2.3	

Table 4-2: ROX Model validation summary.

Inputs	**Stover et al.** [187]	**Model Values**	**% Err.**
Product flow rate, M_d (kg/s)	56.11	56.11	0.0
Intake salinity, C_f (g/kg)	[13, 35]	29.5	0.0
Intake temp. T_{in} (°C)	25	25	0.0
Recovery ratio, RR	0.473382266	0.47	0.7
Feed pressure, P_f (bar)	60.3	60.3	0.0
Feed velocity, v_f (m/s)		0.25	
Permeate pressure, P_p (bar)		0.3	
Max pressure, P_{max} (bar)		83	
Max temperature, T_{max} (°C)		45	
Module length, l (m)		1.01	
Channel thickness, h (mm)		0.8	
Module area, a (m^2)		37.2	
Module head loss, hl (bar)		0.15	
Design velocity, v_0 (m/s)		0.5	

Water permeability at 25°C, K_{w25} (L/(m^2.h.bar))		1.056	
Salt permeability at 25°C, K_{s25} (m/h)		0..00007875	
Water permeability correction constant, K_{wt} (K)		-2849	
Salt permeability correction constant, K_{st} (K)		-3281	
PX efficiency, η_{px}	0.966	0.966	0.0
PX fraction, px_f	0.5257	0.5257	0.0
General Outputs			
Product flow rate, M_d (kg/s)	56.11	54.74	2.4
Feed water flow rate, M_f (kg/s)	118.53	119.42	0.8
Brine flow rate, M_b (kg/s)	62.42	64.53	3.4
Product water salinity, C_p (g/kg)	0.341	0.307	10.0
Feed water salinity, C_f (g/kg)	30.6	29.5	3.6
Brine salinity, C_b (g/kg)	57.8	56.2	2.7
Actual Recovery Ratio, R	0.473	0.470	0.7
Family Outputs			
Specific energy, E_{des} (kWh e/m^3)		1.67	
Specific Outputs			
Number of Stages, N_{stage}		1	
Number of Modules, $N_{modules}$	308	337	9.4
Total system area, A (m^2)		12500	
Average Flux, J_w (L/m^2.h)		15.78	
Brine Pressure, P_b (bar)	59.4	59.9	0.8
Feed Stream PX Salinity, $C_{f,px}$ (g/kg)	30.15	30.35	0.7

4.2.4. Case Studies of Existing Desalination Facilities

The following sections contain a brief overview of each desalination plant serving as case studies for this work.

4.2.4.1. Case Study #1: MDT Plant 1

The MDT Plant 1 is located near Jeddah, Saudi Arabia and consists of two MDT desalination systems, each one producing 5000 m^3/day of desalted water [189]. Part of the product water is used in the nearby oil refinery, and part is used as potable water in the local community after a post-treatment process. The plant has been in operation since 2005 and has been consistently producing water at 0.005

g/kg (5 mg/L) or lower concentration. The feed water to the plant comes from the Red Sea and has a total concentration of 41 g/kg. Water preprocessing consists of a series of filters and strainers with different sizes. The system is very similar to the standard parallel feed, multi-effect distillation process with thermocompression with the only difference being that it includes a second thermoejector that redirects some of the steam produced in the last effect to preheat the feed water stream in the first effect.

4.2.4.2. Case Study #2: MDT Plant 2

The MDT Plant 2 is located in Jamnagar, Gujarat, India and features nine multi-effect distillation units with thermocompression: four units with a footprint of 45m x 200m, four units with a footprint of 60m x 120m, and one unit with a footprint of 45m x 45m. The plant supplies the local refinery with approximately 160,000 m^3/day of desalted water. The feed water for the desalination plant comes from the neighboring gulf in the Arabian Sea and has a total concentration of 42 g/kg TDS.

The system presents three groups of effects connected in a backward feed configuration and a parallel feed configuration within each effect. This parallel-backward hybrid feed configuration is not usually found in scientific literature. Because the effects are labeled from left to right as hot, intermediate, and cold, (see effect arrangement in Figure 4-1), we assume the heat from steam travels from left to right, thus reducing its temperature as energy is transferred throughout the effects. Furthermore, the brine from the third effect in the hot group is redirected to a flash chamber before being discharged.

4.2.4.3. Case Study #3: ROX Plant 1

The desalination plant is located in Bimini Island, Bahamas, and consists of three packaged desalination units with a nominal capacity of 1000 m^3/day each. The plant serves a resort complex and supplements municipal water for 300 homes and condominiums since July 2019 [190]. The system intake is sea water with 39 g/kg TDS and the product is potable water with less than 0.4 g/kg TDS. Each unit is housed in a 40 ft shipping container and contains 10 pressure vessels with 50 RO modules manufactured by DOW. The pretreatment process includes disk filtration and an ultrafiltration module. The desalination section includes a RO system with a pressure exchanger as an energy recovery device. Post treatment includes sulfide stripping, calcite remineralization, and disinfection by chlorination.

4.2.4.4. Case Study #4: ROX Plant 2

The ROX Plant 2 is a packaged desalination unit in the Cát Bà island [191]. The plant is a ROX system housed in a 40-foot shipping container; it contains 15 pressure vessels with a total of 75 LG Nano H20 reverse osmosis membrane elements. The plant began operation in 2019 with a nominal production capacity of 1500 m^3/d. The plant intakes seawater at 33 g/kg TDS and produces potable water for the island with less than 0.4 g/kg TDS. Pretreatment includes disk filtration and ultrafiltration modules. The desalination system consists of the RO module and a pressure exchanger energy recovery device. Finally, the post-treatment process consists of disinfection by chlorination.

4.2.5. Available Plant Data

The parameter hierarchy is closely related to the data availability and measurement difficulty. General and Family parameters describe the desalination process from a high-level perspective in the sense that they are not unique to a single system. Usually, General outputs are readily available in most plants and can be calculated by a simple mass balance. The Family outputs are mostly available and explicitly stated in the surveyed plants, except for energy intensity. The parameters in the Specific hierarchy are harder to obtain and are not typically disclosed by manufacturers or other studies. This hierarchy is descriptive of the modeled system because it contains information unique to each desalination process. As a result, this category contains proprietary data or variables that can only be obtained via experiments in a controlled environment. Furthermore, these Specific variables, depending on the model, can contain generalizations at a system level. For instance, salt and water permeability coefficients in RO and ROX models cannot be measured, but are obtained through empirical correlations, and assumed to be uniform through the entire membrane area.

Table 4-3 and Table 4-4 shows the available data for each desalination plant generously provided by the corresponding manufacturers. In the case of the intake temperatures for ROX systems, the ranges are obtained from the highest and lowest 10-year average sea temperatures from a weather forecasting website [192]. As shown, there are several unknown inputs and outputs that pose a challenge for system modeling. This is particularly evident with the Specific set of parameters, which are closely associated to the system and its unique operation. Therefore, it

would not be appropriate to complement the dataset with data from published studies because that data must then come from a system running at similar production and feed salinity levels. In addition, the nonlinear relationships of inputs and outputs in RO-based and MED-based processes further complicate finding appropriate parameters to carry out simulations [91], [193].

Table 4-3: Summary of Case Study Data – Inputs.

Case Study	**MDT Plant 1**	**MDT Plant 2**	**ROX Plant 1**	**ROX Plant 2**
System Family	**Thermal**		**Molecular Transport**	
General Inputs – Low difficulty to obtain				
Product flow rate, M_d (kg/s)	57.87	277.78	11.57	17.36
Intake salinity, C_f (g/kg)	41.5	42	39	33
Intake temp., T_{in} (°C)	[26, 32]	-	[24.4, 30.2]	[22.2, 32.2]
Family Inputs – Medium difficulty to obtain				
Motive steam pressure, P_s (kPa)	350	-	Not Applicable	
Target recovery, RR	Not Applicable		0.5	0.47
Specific Inputs – High difficulty to obtain				
Top brine temp., T_{bt} (°C)	70.9	67.64		
Last effect brine temp., T_b (°C)	46	43.71		
Feed water temp., T_f (°C)	-	-		
Brine salinity, C_b (g/kg)	62.5	70		
No. effects, N_{eff}	6	11	Not Applicable	
Motive steam flow rate, M_p (kg/s)	7.23	24.73		
Mixed steam sat. temp, $T_{m,sat}$ (°C)	-	-		
Entrained vapor target flow rate, $M_{entrained,target}$ (kg/s)	-	-		
Feed pressure, P_f (bar)	Not Applicable		-	-
Feed velocity, v_f (m/s)			-	-
Permeate pressure, P_p (bar)			-	-
Max pressure, P_{max} (bar)			-	-
Max temperature, T_{max} (°C)			-	-
Module length, l (m)			-	-
Channel thickness, h (mm)			-	-
Module area, a (m^2)			41	41
Module head loss, hl (bar)			-	-
Design velocity, v_0 (m/s)			-	-
Water permeability at 25°C, $K_{w,25}$ ($L/(m^2.h.bar)$)			-	-
Salt permeability at 25°C, $K_{s,25}$ (m/h)			-	-

Water permeability correction constant, K_{wt} (K)		-	-
Salt permeability correction constant, K_{st} (K)		-	-
Pump efficiency, η_{pump}		-	-
Motor efficiency, η_{motor}		-	-
PX efficiency, η_{px}		-	-
PX fraction, px_f		-	-

Table 4-4: Summary of Case Study Data – Outputs.

Case Study	**MDT Plant 1**	**MDT Plant 2**	**ROX Plant 1**	**ROX Plant 2**
System Family	**Thermal**		**Molecular Transport**	
General Outputs – Low difficulty to obtain				
Product flow rate, M_d (kg/s)	57.87	277.78	11.57	17.36
Feed water flow rate, M_f (kg/s)	172.22	695.80	23.15	36.94
Brine flow rate, M_b (kg/s)	114.35	417.62	11.57	19.58
Product water salinity, C_p (g/kg)	< 0.005	0	0.4	0.40
Feed water salinity, C_f (g/kg)	41.5	42	39	33
Brine salinity, C_b (g/kg)	62.5	70	77.6	61.9
Actual Recovery Ratio, R	0.3360	0.3992	0.5	0.47
Family Outputs – Medium difficulty to obtain				
Specific energy, E_{des} (kWh/m^3)	-	-	2.50	2.20
Motive steam flow rate, M_p (kg/s)	7.234	24.729	Not Applicable	
Gain ratio, GR	8.0	11.2		
Sp. cooling water flow rate, sM_{cw} (kg/kg)	2.976	-		
Specific Outputs – High difficulty to obtain				
Cond. area, A_c (m^2)	-	-	Not Applicable	
Specific area, sA (m^2/kg/s)	-	-		
Number of Stages, N_{stage}	Not Applicable		-	-
Number of Modules, $N_{modules}$			50	75
Total system area, A (m^2)			2050	3075
Average Flux, J_w (L/m^2.h)			-	-
Brine Pressure, P_b (bar)			-	-
Feed Stream PX Salinity, $C_{f,px}$ (g/kg)			-	-

4.2.6. Modeling assumptions

Both MDT and ROX feature an energy recovery component to utilize some of the energy remaining at the end of the desalination block, consisting of evaporator effects and membrane modules (called "stages") connected in series for MED and RO, respectively. The computational algorithm accounts for these

devices by calculating the mass and energy balances through each component in series, implementing the energy recovery calculation after the last component, and then loops through the system again with the modified energy inputs until the outputs of the last component converge. It must be noted that the simulations in this work focus exclusively on the desalination process and energy recovery within each plant. Pre- and post-treatment processes are not considered in the simulations.

The proposed MDT model implements some assumptions with respect to the studied systems. The MDT Plant 1 second thermocompressor is not considered in this study as it only involves sensible heating in roughly a sixth of the feed stream, which would be small in comparison to the latent load involved in evaporation in addition to the sensible heating of the remaining effects. The proposed MDT model does not consider pumping energy involved as this desalination method is driven by a phase change, which consumes approximately two orders of magnitude more energy than the energy required for water circulation [44].

The MDT Plant 2 features a very specific parallel-backward feed flow configuration. The preheated water from the condenser outlet is directed to effects 8 through 11, denominated “Cold Group” in a parallel configuration, then, the resulting brine from this effect group is directed backwards into previous group of effects, denominated “Intermediate Group”, where it is again fed in parallel to effects 4 through 7. Similarly, the resulting brine from the Intermediate Group is directed backwards into effects 1 through 3, denominated “Hot Group” and fed in a parallel configuration within the group. Generally, backward feed configurations

can present a challenge in scaling in the first effects since the brine with the highest concentration is exposed to the highest evaporation temperatures [167]. However, countercurrent heat exchange presents the most thermodynamic efficient approach to MED. Another simplifying assumption consists of embedding the effects of the flash train within each effect. In doing so, a decreasing saturation pressure is imposed, which is aligned with the vapor temperature in each effect. Finally, like the MDT Plant 1, pumping energy is not considered.

The ROX Plant 1 consists of three packaged desalination units, each one with a nominal capacity of 1000 m^3/day. It is important to note these desalination units are decentralized and can operate independently from one another, therefore, this study considers only a single unit for simplification. The ROX Plant 2, meanwhile, consists of a single packaged desalination system for which no simplifying assumptions on the plant are made.

4.3. Results

Data unavailability is one of the most common problems associated with desalination system modeling. Most published models do not report complete datasets and many actual desalination plants have parameters that are either impossible to measure by the user or are proprietary data for the manufacturer. We propose a case study replication method that relies on model non-linearity, low runtime, and the assumption of optimal operating conditions of the studied system.

The methodology is divided into a data-driven iterative initialization process followed by an error minimization algorithm. The following sections explain each part of the methodology separately.

4.3.1. Iterative Initialization and Sampling-based Optimization

The initialization has the objective of finding a complete set of inputs that result in thermodynamically and physically plausible operation. This is achieved by building a number N of input sets from known and guessed values. Table 4-5 indicates the three possible options and the respective initialization procedure for each variable through an example.

Table 4-5: Example input parameters and corresponding initialization procedure.

Variable	Case Study Data	Guess from literature	Initialization Procedure
$M_d\ [kg/s]$	57.87	-	**Known value from system data** – Plug into input set directly
$T_{in}\ [°C]$	[26, 32]	-	**Known range from system data** – Sample from uniform distribution bounded at range ends
$T_f\ [°C]$	*Unknown*	[35, 71] from Temstet et al. [95] bounded by T_{bt}	**Unknown parameters** – Sample from uniform distribution bounded by literature range ends and physical constraints

Each initialization iteration consists of selecting one variable that corresponds to either a known range from the available system data or an unknown parameter with its associated guess range. As illustrated in Figure 4-3, the variable is sampled from a uniform distribution bounded by the ends of the corresponding range. The variables whose values are known from the system data are directly imported to each model input set. All the other variables given as ranges, known and unknown, are imported as the midpoint value of the corresponding range. The desalination model is then executed for each of the built input sets resulting in N number of output sets. The maximum percent difference is then calculated for each simulation by considering the known and simulated outputs. Finally, the sampled

variable from the input set that results in the lowest percent error is selected as the complete initialized variable. A single iteration, therefore, executes N number of simulations, each with a unique set of inputs with the sampled variable associated to the iteration.

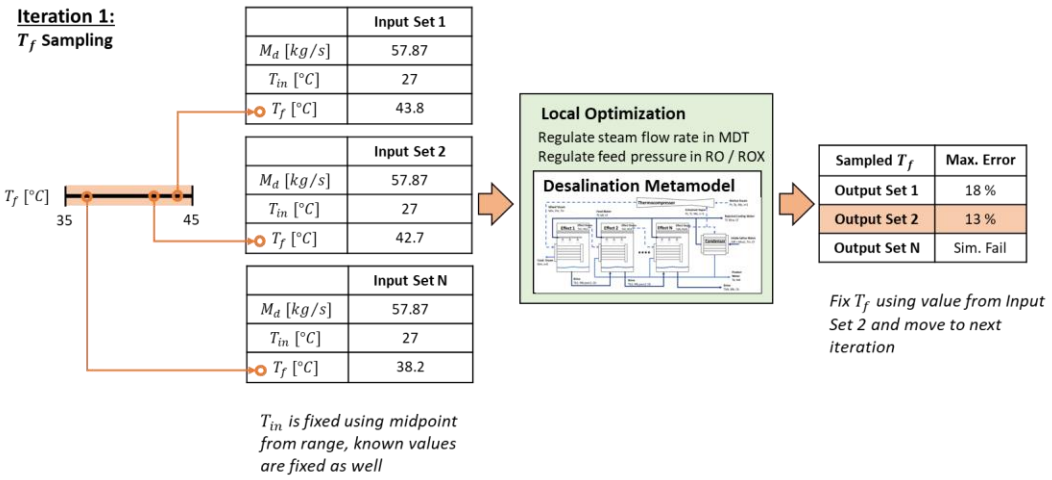

Figure 4-3: An illustrative example of a single iteration of the initialization algorithm.

As shown in Figure 4-4, after a variable is initialized in each iteration, it becomes fixed for subsequent iterations at the value that results in the minimum percent error when compared to available output data. There is one iteration required for each known input range and unknown input variable. The unknown input parameters are initially inferred by using the values from the literature from systems running at similar operating conditions. For the presented case studies, initial input parameters are selected from our previous publication which features an extensive number of simulations and validation points with peer-reviewed studies [186]. It is important to note that valid simulations are regarded as plausible solutions, but not necessarily the most likely operation. Therefore, an optimization process must take place after the input set initialization is completed.

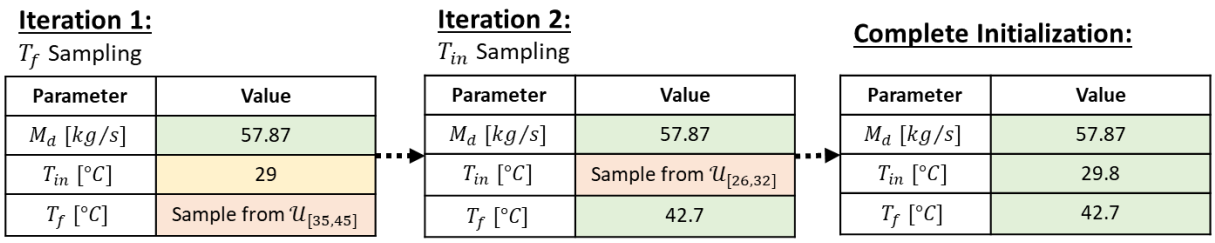

Figure 4-4: An illustrative example of input set initialization.

The optimization part, illustrated in Figure 4-5, in the case study replication involves fixing variables that correspond to known values and ranges, and sampling the rest of the unknown variables from uniform distribution centered at the initialized values. The uniform distributions to sample from in iteration i are defined by the input values that result in the lowest output percent error from the previous iteration, $\widehat{\boldsymbol{X}}_{i-1}$, and a range, r_{i-1}, such that:

$$\boldsymbol{X}_i = \mathcal{U}_{[\widehat{\boldsymbol{X}}_{i-1}(1-r_{i-1}),\ \widehat{\boldsymbol{X}}_{i-1}(1+r_{i-1})]} \qquad \text{for } i = 1, 2 \dots N \tag{4-6}$$

And

$$r_{i+1} = \min \frac{|\widehat{\boldsymbol{X}}_{i-1} * (1 \pm r_i) - \widehat{\boldsymbol{X}}_i|}{\widehat{\boldsymbol{X}}_i} \qquad \text{for } i = 1, 2 \dots N \tag{4-7}$$

For the first iteration, $i = 1$, $\widehat{\boldsymbol{X}}_0$ are the initialized inputs and r_0 is a user-defined sampling range. For the subsequent iterations, $\widehat{\boldsymbol{X}}_i$ is determined by the values of the input set that result in the lower percent error between known and simulated outputs. It is important to note that if none of the built simulations in an iteration result in a lower or equal percent error than the previous iteration, then the sampling range and center values remain unchanged:

$$\widehat{\boldsymbol{X}}_i = \widehat{\boldsymbol{X}}_{i-1} \text{ and } r_i = r_{i-1} \tag{4-8}$$

The algorithm will keep iterating until the error between simulated and known outputs reaches a minimum. When this happens, an early stopping condition

is implemented and the last set of inputs $\widehat{\boldsymbol{X}}_i$ is considered as the most plausible operation scenario. If the early stopping condition is not reached, the algorithm will return the best-found inputs at the last iteration $\widehat{\boldsymbol{X}}_N$. In such cases, improvement can be accomplished by increasing the number of iterations, N, increasing the number of simulations built per iteration, or increasing r_0 in the case that a plausible input value was not covered.

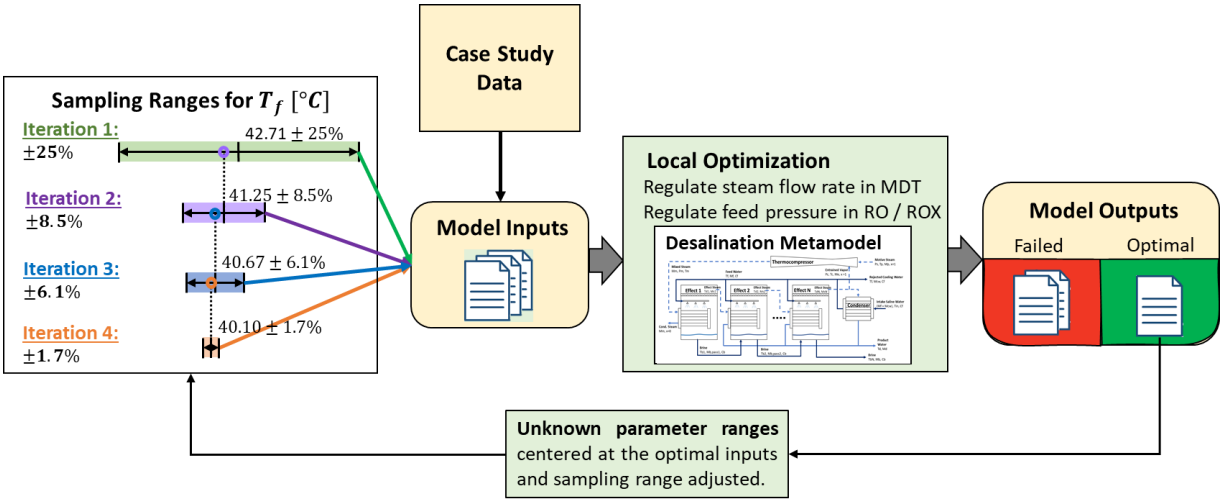

Figure 4-5: Illustrative example of optimization algorithm.

4.3.2. An Application in Four Actual Desalination Facilities

The presented algorithm relies on iterative sampling and reduced-order desalination models that result in a relatively low overall runtime. In the presented deployments for the four desalination plants, initialization takes a less than 10 minutes to complete while optimization takes less than one minute. The initialization incurs the greatest computational time because it explores wider limits of possible operation that might result in either failed simulations or large adjustments of M_p and P_f for the MDT and ROX systems, respectively. We found that 1000 simulations were sufficient during initialization to explore the complete input ranges without incurring excessively large runtimes. In using 1000

simulations to build for all the unknown parameters, there will be: three unknown parameters for MDT Plant 1, five for MDT Plant 2, and eight in ROX Plant 1 and ROX Plant 2, which implies over 20,000 simulations in total for the initialization of all case studies. Table 4-6,

Table 4-7, Table 4-8, and Table 4-9 show the inputs, sampling ranges, and initialized variables for each system.

Table 4-6: MDT Plant 1 Initialization.

Inputs	**Value**	**Source**	$\widehat{\boldsymbol{X}}_0$
Product flow rate, M_d (kg/s)	57.87	Actual system data [189]	57.87
Intake salinity, C_f (g/kg)	41.5		41.5
Intake temp., T_{in} (°C)	[26, 32]		29.8019
Motive steam pressure, P_s (kPa)	350		350
Top brine temp., T_{bt} (°C)	70.9		70.9
Last effect brine temp., T_b (°C)	46		46
Feed water temp., T_f (°C)	[35, 45]	Range [95] limited by $T_b - 1$ to ensure heat transfer	42.7132
Brine salinity, C_b (g/kg)	62.5	Actual system data [189]	62.5
No. effects, N_{eff}	6		6
Motive steam flow rate, M_p (kg/s)	7.233		8.234
Mixed steam sat. temp, $T_{m,sat}$ (°C)	73.9	$T_{bt} + 1$ to ensure heat transfer	73.9
Entrained vapor target flow rate, $M_{entrained,target}$ (kg/s)	[0.96, 5]	10 to 55% of last effect $M_{d,6}$	3.5199

Table 4-7: MDT Plant 2 Initialization.

Inputs	**Value**	**Source**	$\widehat{\boldsymbol{X}}_0$
Product flow rate, M_d (kg/s)	277.78	Actual system data	277.778
Intake salinity, C_f (g/kg)	42		42
Intake temp., T_{in} (°C)	[21.1, 29.9]	10-year max and min [192]	25.5
Motive steam pressure, P_s (kPa)	[350, 4500]	Thermocompressor ranges from MDT Plant 1 case study and published data [186]	350
Top brine temp., T_{bt} (°C)	67.64	Actual system data	67.64
Last effect brine temp., T_b (°C)	43.71		43.71

Feed water temp., T_f (°C)	[35, 42.7]	Range [95] limited by $T_b - 1$ to ensure heat transfer	41.7
Brine salinity, C_b (g/kg)	70	Actual System Data	70
No. effects, N_{eff}	11		11
Motive steam flow rate, M_p (kg/s)	24.7292		22.7292
Mixed steam sat. temp, $T_{m,sat}$ (°C)	[68.64, 70.64]	$T_{bt} + 1$ and $T_{bt} + 3$ to ensure heat transfer	69.64
Entrained vapor target flow rate, $M_{entrained,target}$ (kg/s)	[2.53, 13.89]	10 to 55% of last effect $M_{d,11}$	8.21

Table 4-8: ROX Plant 1 Initialization.

Inputs	**Value**	**Source**	$\widehat{\boldsymbol{X}}_0$
Product flow rate, M_d (kg/s)	11.5741	Actual system data	11.57
Intake salinity, C_f (g/kg)	39		39.00
Intake temp., T_{in} (°C)	[24.4, 30.2]	10-year max and min [192]	29.24
Target recovery, RR	0.5	Actual system data	0.50
Feed pressure, P_f (bar)	70.5	Adjusted per model feedback	70.50
Feed velocity, v_f (m/s)	0.52	Mean between [66] and [129]	0.52
Permeate pressure, P_p (bar)	0.3	[66]	0.30
Max pressure, P_{max} (bar)	83	SW30ULE, SWXLE-440i, SW30XHR-440i specs	83.00
Max temperature, T_{max} (°C)	45		45.00
Module length, l (m)	1.016		1.02
Channel thickness, h (mm)	0.125	Range across published studies [186]	0.125
Module area, a (m^2)	41	SW30ULE, SWXLE-440i, SW30XHR-440i specs	41.00
Module head loss, hl (bar)	0.2	[66]	0.20
Design velocity, v_0 (m/s)	0.5	[66]	0.50
Water permeability at 25°C, $K_{w,25}$ (L/(m^2.h.bar))	1.26	[129]	1.26
Salt permeability at 25°C, $K_{s,25}$ (m/h)	0.0000865	[129]	0.0000865
Water permeability correction constant, K_{wt} (K)	-2849	[66]	-2849
Salt permeability correction constant, K_{st} (K)	-3281	[66]	-3281
Pump efficiency, η_{pump}	0.85		0.85
Motor efficiency, η_{motor}	0.85		0.85
PX efficiency, η_{px}	0.966	[187]	0.97
PX fraction, px_f	0.52	[187]	0.52

Table 4-9: ROX Plant 2 Initialization.

Inputs	**Value**	**Source**	$\widehat{\boldsymbol{X}}_0$

Product flow rate, M_d (kg/s)	17.36	Actual system data	17.36
Intake salinity, C_f (g/kg)	33		33
Intake temp., T_{in} (°C)	[22.2, 32.2]	10-year max and min [192]	32.0
Target recovery, RR	0.47	Actual system data	0.47
Feed pressure, P_f (bar)	61	Adjusted per model feedback	61
Feed velocity, v_f (m/s)	0.52	Mean between [66] and [129]	0.52
Permeate pressure, P_p (bar)	0.3	[66]	0.3
Max pressure, P_{max} (bar)	82.7	LG440 Series membrane specs	82.7
Max temperature, T_{max} (°C)	45		45
Module length, l (m)	1.02		1.02
Channel thickness, h (mm)	0.125	Range across published studies [186]	0.513
Module area, a (m^2)	41	LG440 Series membrane specs	41
Module head loss, hl (bar)	0.2	[66]	0.2
Design velocity, v_0 (m/s)	0.5	[66]	0.5
Water permeability at 25°C, $K_{w,25}$ (L/(m^2.h.bar))	1.26	[129]	1.26
Salt permeability at 25°C, $K_{s,25}$ (m/h)	0.0000865	[129]	0.0000865
Water permeability correction constant, K_{wt} (K)	-2849	[66]	-2849
Salt permeability correction constant, K_{st} (K)	-3281	[66]	-3281
Pump efficiency, η_{pump}	0.85		0.85
Motor efficiency, η_{motor}	0.85		0.85
PX efficiency, η_{px}	0.966	[187]	0.97
PX fraction, px_f	0.52	[187]	0.52

After each input set has been initialized, the optimization algorithm is implemented for each case study with the following settings: 10 simulations to build, 25 training iterations, and an early stop of 5 iterations. The initial sampling ranges for MDT Plant 1, MDT Plant 2, and ROX Plant 1 are $\pm 25\%$ from the initialized values. For ROX Plant 2, this range was too large for the algorithm to converge, so it starts at $\pm 20\%$. Figure 4-6 shows the error evolution for all iterations of the optimization algorithm. Early stop was reached for all cases,

although this was not necessarily guaranteed. The largest percent error occurs in the ROX Plant 2 simulation with 9.3% and the lowest is MDT Plant 2 with 2.1%. The error for most case studies decreases by about 1-3% for with respect to the error at initialization, however, the error in MDT Plant 1 decreases by almost threefold. This suggests that the optimization part is still important even though most unknown input fitting occurs in the initialization. The optimization algorithms were run 10 times for each system and the values presented here are those that resulted in minimum percent error reached for all trials. It is likely that MDT errors are consistently lower than ROX because there is larger proportion of known inputs. Specifically, the MDT systems present 3 unknown specific inputs out of the 8 required, while the ROX systems have 17 unknown specific inputs out of the 18 required.

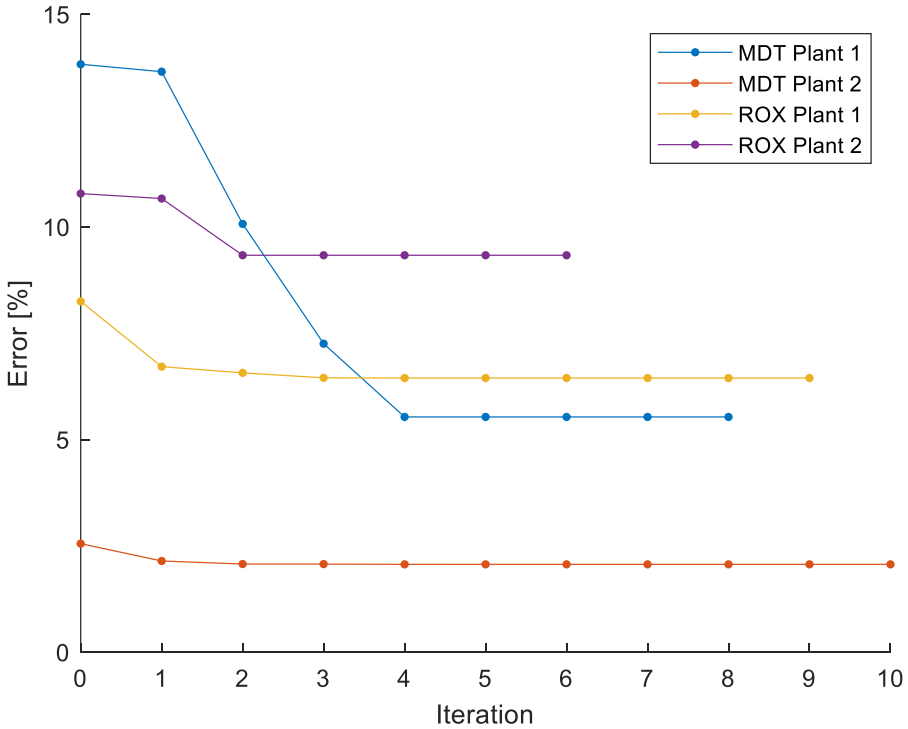

Figure 4-6: Percent error through algorithm iterations after initialization.

For the MDT simulations, M_p is automatically adjusted to supply enough energy for distillation. P_f is automatically adjusted in the ROX simulations to supply enough pressure for reverse osmosis. All other input parameters shown in are sampled from the distributions created by the initialized values and sampling ranges. The most significant corrections occur at the initial iterations due to the larger probability of sampling a value that is further away from the initialized parameter. As the iterations continue, the sampling ranges get smaller, thus, refining the correction resolution. In all cases, the unknown parameter guesses stabilize within the first five iterations, and then converge to the early stopping condition.

4.3.3. MDT Simulation Results

Table 4-10 shows the complete set of parameters for the MDT models deployed in using data from MDT Plant 1 and MDT Plant 2. Overall, the simulations show excellent agreement with the actual system data with most errors falling within 2.5 to 5.5%. The outputs in the General category, which include those related to mass transfer, are all within 4.8% of actual operation.

Table 4-10: MDT simulation results.

	MDT Plant 1			**MDT Plant 2**		
	Plant Data	**Simulation**	**% Err**	**Plant Data**	**Simulation**	**% Err**
Inputs						
Product flow rate, (kg/s)	57.87	57.87	0.0	277.78	277.78	0.0
Intake salinity, (g/kg)	41.5	41.5	0.0	42	42	0.0
Intake temp. (°C)	[26, 32]	30	0.0		26	
Motive steam pressure, (kPa)	350	350	0.0		382.1	
Top brine temp. (°C)	70.9	70.9	0.0	67.64	67.64	0.0
Last effect brine temp. (°C)	46	46	0.0	43.71	43.71	0.0
Feed water temp. (°C)		41.6			38.5	

Brine salinity, (g/kg)	62.5	62. 5	0.0	70	70	0.0
No. effects,	6	6	0.0	11	11	0.0
Motive steam flow rate, (kg/s)	7.23	7.23	0.0	24.73	24.73	0.0
Mixed steam sat. temp, (°C)		77.8			68.8	
Entrained vapor target flow rate, (kg/s)		4.05			7.96	
General Outputs						
Product flow rate, (kg/s)	57.87	55.10	4.8	277.78	283.51	2.1
Feed water flow rate, (kg/s)	172.22	164.00	4.8	695.80	692.51	0.5
Brine flow rate, (kg/s)	114.35	108.90	4.8	417.62	409.00	2.1
Product water salinity, (g/kg)	< 0.005	0		0	0	
Feed water salinity, (g/kg)	41.5	41.5	0.0	42	42	0.0
Brine salinity, (g/kg)	62.5	62.4995	0.0	70	70	0.0
Recovery Ratio,	0.34	0.34	0.0	0.40	0.41	2.5
Family Outputs						
Specific energy, (kWh/m3)		131.74			76.05	
Motive steam flow rate, (kg/s)	7.234	7.2338	0.0	24.729	24.729	0.0
Gain ratio,	8.0	7.6	4.8	11.2	11.5	2.1
Sp. cooling water flow rate, (kg/kg)	2.976	3.031	1.9		0.713	
Specific Outputs						
Cond. area, (m^2)		1035			2655	
Specific area, (m^2/kg/s)		133.2			183.5	
Intermediate Parameters						
Vapor temp. 1st effect (°C)	74.5	70.4	5.5	67.6	67.1	0.8
Vapor temp. last effect (°C)	46.0	45.6	1.0	43.7	43.3	1.0
Cooling water flow rate (kg/s)	172.22	167.03	3.0		202.15	

: From system operation data

The largest error of 5.5% in the MDT Plant 1 simulation occurs in the vapor temperature in the first effect. The top brine temperature is given as 70.9°C from the operation data; this value should reflect the effects of boiling point elevation due to the salt concentration in the water. Therefore, the produced vapor in the first effect would be saturated water at the same pressure, which would be slightly lower at 70.4°C as calculated by the model. The reported value of 74.5°C could be due to a measurement error influenced by the existing feed preheating in the first effect, which is not considered in the model, or part of the uncertainty inherent to temperature measurement in industrial systems. An unlikely but possible source of

this discrepancy is an additional heat source, such as the exposure to the sun or an adjacent component at a higher temperature that makes the effect behave like a heat sink.

The simulation results are within less than 10% error of the known outputs. While the minimum error is consistently reached in all case studies, it is important to note that the discovered operation state might not coincide with actual operation, but rather a plausible operation that matches the available datapoints. Therefore, various model inputs could exist to describe different operation conditions that would still result in a low error. To address this, we conducted a numerical investigation with the MDT Plant 1 case study by running the iterative optimization part five times while maintaining the initialized input set. In all trials, the maximum percent error of the sampling-based optimization rounds was consistently 5.5% with 3 rounds reaching the early stop of 5 iterations, and the others running for the full 25 iterations. The mean results for unknown sampled parameters were 41.62 °C with a standard deviation of 0.56 °C for T_f, 73.79 °C with a standard deviation of 3.24°C for $T_{m,sat}$, and 4.26 kg/s with a standard deviation of 0.19 kg/s for $M_{entrained,target}$. Furthermore, the resulting mean energy intensity was 131.9 kWh/m^3 with a standard deviation of 1.3 kWh/m^3. Such small standard deviations in relation to the mean falling within 0.9 and 4.4%, show that the proposed algorithm can infer unknown operation scenarios consistently, and that the uncertainty generated by the stochastic nature of the algorithm is low enough to compare to the uncertainty in the measured data.

The MDT Plant 2 simulation exhibits the lowest percent error of the four case studies with a maximum difference of 2.1% in the product and brine flowrates, as well as the recovery and gain ratios. The source of this error is the estimation of M_p, which is slightly greater than the value reported in the system data. The source of this discrepancy can be attributed to the simplifying assumption of flow configuration in the model, and the overall heat transfer coefficient correlation for the evaporator. The actual flow configuration in the system divides effects 1-3 into the hot group, effects 4-7 into the intermediate group, and effects 8-11 into the cold group. The system has a backward feed between groups, but parallel feed to all the effects within each group. Therefore, the feed temperature found by the model is likely to be an intermediate value closer to the feed of the intermediate group. Thus, the temperature difference between feed and vapor in the hot and cold groups would be slightly different than the difference calculated by the model. In the actual configuration of the system, the highest salinity brine with the highest temperature in the hot group undergoes heat exchange and evaporation with the heating steam at the highest temperature in the first effects. Because the temperature difference is lower than the simplified intermediate temperature, the amount of actual vapor produced in these first effects is lower at a lower energy expense. Conversely, the vapor produced in the cold group does not offset the discrepancy of the vapor produced in the hot group because evaporation occurs at a lower temperature requiring a larger latent heat.

4.3.4. ROX Simulation Results

Table 4-11 shows the relevant parameters of each ROX model deployed in the ROX Plant 1 and ROX Plant 2 case studies. The outputs in the General category, which include those related to mass transfer, are all within 6% of actual operation. The ROX Plant 2 shows the greatest deviation from the case study data with a 9.3% and 8.8% error in the Family and Specific outputs, respectively.

Table 4-11: ROX simulation results.

	ROX Plant 1			ROX Plant 2		
	Plant Data	**Simulation**	**% Err**	**Plant Data**	**Simulation**	**% Err**
Inputs						
Product flow rate, (kg/s)	11.57	11.60	0.0	17.36	17.36	0.0
Intake salinity, (g/kg)	39	39	0.0	33	33	0.0
Intake temp. (°C)	[24.4, 30.2]	29		[22.2, 32.2]	32	
Recovery ratio	0.5	0.5	0.0	0.47	0.47	0.0
Feed pressure (bar)		70.2			61.0	
Feed velocity (m/s)		0.5			0.6	
Permeate pressure (bar)		0.3			0.3	
Max pressure (bar)		83.0		82.7	82.7	
Max temperature (°C)		45.0		45.0	45.0	
Module length (m)		1.0		1.0	1.0	
Channel thickness (mm)		0.137			0.544	
Module area (m^2)	41	41	0.0	41	41	0.0
Module head loss (bar)		0.154			0.180	
Design velocity (m/s)		0.58			0.58	
Water permeability at 25°C ($L/(m^2.h.bar)$)		1.26			1.26	
Salt permeability at 25°C (m/h)		8.65E-05			8.65E-05	
Water permeability correction constant (K)		-2849			-2849	
Salt permeability correction constant (K)		-3281			-3281	
Pump efficiency		0.85			0.85	
Motor efficiency		0.85			0.85	
PX efficiency		0.98			0.98	
PX fraction		0.5			0.6	
General Outputs						
Product flow rate, (kg/s)	11.57	11.50	0.7	17.36	17.43	0.4
Feed water flow rate, (kg/s)	23.15	23.16	0.0	36.94	36.95	0.0

Brine flow rate, (kg/s)	11.57	11.90	2.8	19.58	20.02	2.3
Product water salinity, (g/kg)	0.4	0.42	6.1	0.40	0.41	3.3
Feed water salinity, (g/kg)	39	39	0.0	33	33	0.0
Brine salinity, (g/kg)	77.6	78.9	1.7	61.9	62.9	1.6
Actual Recovery Ratio	0.50	0.50	0.7	0.47	0.47	0.4
Family Outputs						
Specific energy, (kWh/m^3)	2.50	2.66	6.4	2.20	2.39	8.8
Specific Outputs						
Number of Stages		1			1	
Number of Modules	50	52	4.0	75	82	9.3
Total system area (m^2)	2050	2111	3.0	3075	3344	8.8
Average Flux (L/m^2.h)		19.89			19.06	
Brine Pressure (bar)		69.80			58.68	
Feed Stream PX Salinity (g/kg)		40.20			33.95	

: From system operation data

The largest percent error in the ROX Plant 1 simulation, and a large error in the ROX Plant 2 simulation, occur in the specific energy values. This can be attributed to the assumed pump and motor efficiencies of 0.85. While we take these as conventional values for well-known components, they are likely to be higher. These variables were not included in initialization because they are independent and only affect energy intensity.

Product water salinity presents consistently a relatively high error in the ROX simulations when compared to the rest of the parameters in the General hierarchy. This is likely due to the mass transfer correlations, which capture the concentration polarization phenomena and directly influence the trans-membrane salt passage. These correlations are membrane-specific and therefore implementing a correlation from the literature will inevitably result in a small error.

The potential discrepancy in the mass transfer coefficient is likely to be the cause for a large percent error in the system area and number of modules calculated in the ROX Plant 2 simulation. There are two reasons that suggest this is the case.

First, the ROX algorithm discretizes the membrane into small segments and keeps adding modules in parallel to preserve flow rate, and in series until the desired recovery is achieved or until the resulting osmotic pressure is larger than the maximum pressure tolerated by the membrane. The mass transfer coefficient determines the water flux through each differential membrane element. Therefore, it is likely to be underestimating the amount of permeated water and therefore, the model compensates by adding more differential membrane elements in series. The small percent error in the General Outputs, which is related to the mass flow rates, supports this justification. Furthermore, the mass transfer correlation used was developed from experimental data from commercially fabricated polyamide composite, Extra Low Energy (XLE) membranes (DOW-Filmtec) [127], which are the same material, but not the same manufacturer as the LG SW440 series membranes featured in the ROX Plant 2 system. Conversely, the membrane modules that correspond to the ROX Plant 1 are indeed DOW-Filmtec SW30 series membranes (from the XLE product line). It is likely that this results in a lower percent error in the calculated system area and number of modules for this case study.

4.4. Discussion

This section elaborates on the method limitations and important considerations for deploying it on other desalination systems in the field. The value of case study simulations is highlighted through a proposed theoretical efficiency parameter to quantify system performance with respect to achievable recovery.

4.4.1. Method Limitations

The main limitation of the proposed algorithm is that the uncertainty of the results is dependent on the number of known parameters available. Unless the full input and output sets are known, the algorithm will produce input sets that describe plausible operation that fits observed data. Increasing the number of available parameters from the case study imposes stricter constraints for valid simulations, and thus, more sampling iterations or simulations within each iteration could be required for two main reasons. First, the constrained search space is likely to result in more failed simulations as less sampled parameters would meet non-changing bounds from physical laws (e.g.: A known temperature imposes a fixed thermodynamic limit for heat transfer as opposed to a more flexible constraint if this temperature value is sampled in each iteration). Second, a larger number of known outputs to compute percent errors imposes a narrower valid input search space and thus a smaller probability of being sampled. On the other hand, using too few simulations in each iteration can negatively impact the performance of the method by not allowing sufficient exploration of the input ranges. Wider input range would naturally require a larger number of simulations to avoid constraining the sampling range too early and locking into local minima. One way to make this process more efficient would be to use an adaptive number of simulations that decreases as the sampling range gets narrower through each iteration.

The minimum requirements for inputs are M_d, C_f, and T_{in}, as these are the most fundamental independent variables with the greatest impact on simulated operation. Outputs are more critical than inputs as they guide the sampling space

for the inputs. General outputs, which are usually easily obtained or measured, provide a validation point for mass transfer modeling accuracy. Specific energy would provide a validation point for modeled system efficiency; however, this value is usually hard to obtain or measure. Additional parameters corresponding to the Specific hierarchy or Intermediate process parameters would help in faster convergence and greater accuracy.

4.4.2. Theoretically Possible Efficiency

The inputs estimated by the proposed algorithm describe plausible system operation that might not necessarily represent optimal operation. Figure 4-7 shows the simulated recovery ratios from this work in the optimized theoretical MED or RO system recovery curves disseminated from our previous study [186]. This comparison is appropriate because the underlying separation process is the same, and the energy recovery device used in the two system affects primarily Family and Specific outputs. The difference in simulated recovery ratios caused by implementing energy recovery using the validation studies for MDT and ROX [95], [187], are only 2.3% and 0.1% for MED-MDT and RO-ROX, respectively. Thus, the difference between the achieved recovery calculated by the model and the ideal thermodynamic recovery, RR_{th}, can be quantified in a theoretical efficiency parameter as:

$$\eta_{th} = \frac{RR_{cs}}{RR_{th}}, \tag{4-9}$$

where RR_{cs} is the simulated case study recovery, and RR_{th} is the theoretical recovery described by the linear equations shown in Figure 4-7 corresponding to

RO and MED systems. The closer η_{th} is to 1, the closer the system is running to ideal operation.

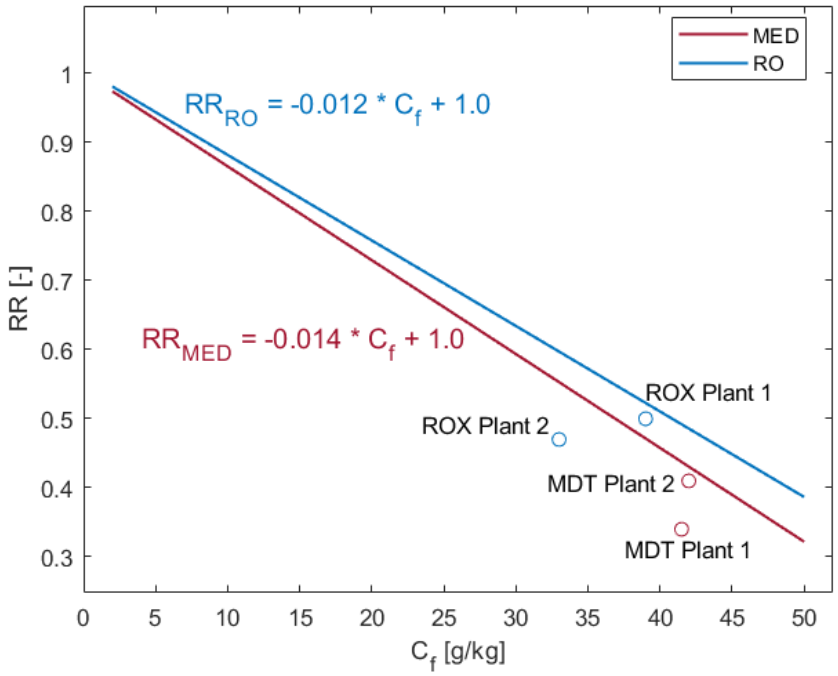

Figure 4-7: RR vs C_f operational curves with case study data.

The resulting theoretical efficiencies are 0.78, 0.95, 0.96, and 0.79 for MDT Plant 1, MDT Plant 2, ROX Plant 1, and ROX Plant 2, respectively. This implies that the MDT Plant 1 underperformed by not recovering as much desalinated water as it could from the feed, however, greater recovery can result in higher energy intensities. The MDT Plant 1 can afford to run at a much lower efficiency than MDT Plant 2 since thermal energy from liquified petroleum gas in Saudi Arabia has a low cost of 0.2 USD/L in comparison to the cost in India of 0.827 USD/L [194]. A similar relationship between theoretical efficiency and energy cost is demonstrated in the ROX case studies. The ROX Plant 1 has a theoretical efficiency of 0.96 while the ROX Plant 2 plant has a theoretical efficiency of 0.79. This demonstrates a sub optimal performance of the ROX Plant 2 as the operation

describes less recovery than the theoretical maximum. Without considering technical limitations such as fouling and treatment costs, it is likely that the electricity rates for Vietnam at 0.078 USD/kWh in comparison to the rates in the Bahamas at 0.253 USD/kWh [195], are a motivation for sub-optimal operation.

Energy prices might not be the only factor that discourages plant managers from running their plants at greater efficiencies becasue each facility might be limited by brine disposal regulations, operational expenses, or other financial constraints. Another possibility is that an existing desalination system does not operate as designed, or that baseline performance is simply unkown. Therefore, model validation should be completed using the proposed methodology before assessing the theoretical efficiency factor to avoid judging a system as underperforming while the inefficency might be related to a sub-optimal modeling of the system.

4.5. Conclusion

In this study, we propose a methodology to infer unknown operational parameters in actual desalination plants. This method relies on low-runtime, reduced-order desalination models, and a data-driven iterative procedure for initializing and adjusting input variables through sampling schemes. By implementing this algorithm, one can close the information gap in desalination operation and modeling to accurately simulate performance of desalination plants. Once the most plausible simulation is constructed, the plant's operation can be analyzed to address how well it is designed and/or maintained. Importantly, this study analyzed four desalination plants to demonstrate performance of the

developed methodology. The analysis results have a global minimum for the error expressing a difference between simulation results and available data. Specifically, the maximum percent error between simulated and collected operational data is 5.5% and 2.5% for the two MDT plants, and 6.4% and 9.3% for the two ROX plants. Therefore, this study successfully demonstrated that it is possible to recover unknown operational parameters and use them for evaluating desalination system performance with prediction errors for all operation performance parameters being lower than 10%.

The desalination system performance can be further evaluated with successfully recovered operational parameters. Specifically, this study proposes a theoretical efficiency factor that quantifies the difference in ideal recovery of the specified feed salinity desalination system and the actual recovery based on system operation. Using this approach, suboptimal performance is identified for MDT Plant 1 and ROX Plant 2 with theoretical efficiencies of 0.78 and 0.79, respectively. Furthermore, MDT Plant 2 and ROX Plant 1 display high theoretical efficiencies of 0.95 and 0.96, respectively. Therefore, two of the analyzed plants operate around 20% below their theoretically achievable recovery rates. The local utility costs at each plant site suggest that underperforming desalination systems can afford to do so because thermal and electrical energy costs are about 18% and 69% lower, respectively, then the utility costs at their high-performing counterpart sites. The calculation of the efficiency parameter could be used by desalination plant managers for evaluating performance of their plant systems as well as establishing a baseline for benchmarking new or retrofitted systems. Overall, the methods and

results presented in this paper can be applied to other MDT and ROX desalination plants to establish theoretically possible recovery targets.

Chapter 5: Mapping A Novel Desalination Technology Within Existing Operational Space

This chapter is reproduced from the following journal paper:

> S. A. Romo, M. A. Elhashimi Khalifa, B. Abbasi, and J. Srebric, "Mapping of a Novel Zero Liquid Discharge Desalination System based on Humidification-Dehumidification onto the Field of Existing Desalination Technologies," *Water*, Special Issue: Advanced Technologies for Seawater Desalination, 2022, Manuscript Number: water-1707191. Under peer-review. [Journal Impact Factor: 3.103].

5.1. Introduction

Desalination systems as a vital infrastructure need innovations focused on their production capabilities, adaptation to site-specific factors like feed water characteristics or available energy type, and operation issues that compromise performance [5], [166]. Within the latter, fouling and brine discharge are two serious and recurrent problems in the operation of both membrane-based and thermal desalination systems that reduce performance and incur in significant costs [85], [196], [197]. Reverse Osmosis (RO) is the most important membrane-based technology that consumes relatively small amount of energy per product flow rate [23], [198], but it is consistently challenged by fouling problems [199], [200]. Fouling can be organic, inorganic (scaling), biological, oxidization, or other types [201]. Fouling leads to increases in the required pumping power [202], [203], and can account for 11-24% of the total operating expenses [204]. This generally limits the membrane-based technologies to an average threshold of feed salinity and

recovery to stay competitive [12]. Although still present, fouling is less impactful in thermal desalination processes [50], [205]. Thermal methods, such as Multi-Effect Distillation (MED) and Multi-Stage Flash, consume larger amounts of energy per product flow rate compared to the RO consumption. Therefore, the thermal desalination methods are associated with higher production costs than the membrane-based molecular transport methods [23]. Scaling limits feed water quality to brackish and seawater salinities and unsuitable to treat local high-salinity water [12]. Therefore, the treatment of high-concentration brines remains an unviable investment in many cases.

In desalination, the water product is usually separated from the feed stream and the remaining water is discharged as brine. Brine disposal can be problematic due to high salinity and in the case of thermal desalination, elevated temperatures. This can have a severe impacts on both ground and marine environments due to pollution and sometimes toxicity [206]. Therefore, strict environmental regulations govern and limit brine discharges in many different locations around the world [18]. Zero-Liquid Discharge (ZLD) is an attractive alternative to brine disposal as the only process byproduct is solid salt. However, the only practical and scalable implementations of ZLD consist of brine post-treatment through mechanical crystallizers and evaporation ponds [12]. In the first option, a brine crystallizer is an additional device that further desalinates the brine stream by gradually flashing vapor until salt crystals form. Besides an additional capital expense of brine crystallizer systems, pumping the viscous sludge can incur in high operation costs that this option economically unviable [12], [20]. Evaporation ponds, while having

small operation expenses, require large land areas and time for brine processing [22].

A novel humidification-dehumidification (HDH) water desalination technology with ZLD has a potential to solve problems associated with fouling, brine discharge and decentralization, so it was conceptually embodied in a Solar Thermal Extraction of Water by Atomization and Recuperative Desalination (STEWARD) system [207]. The use of humidification-dehumidification should make the STEWARD system less sensitive to fouling and should also allow the potential use of low-grade energy, such as solar energy and industrial waste heat [115]. The HDH-ZLD process within the STEWARD system currently has ongoing research efforts focused on component-based investigations of the rates of humidification [208], atomizer design [9], and centrifugal salt separation [209]. Therefore, the present study focused on first principles analyses of these system components and further modeled performance of a complete system to enable mapping of potential operational ranges onto the operational field of existing desalination technologies. Specifically, the contributions of this study are:

- A mathematical model for the proposed STEWARD system used to bound operational space through physical conservation laws and to estimate the thermodynamic states at each point of the desalination process;
- A sensitivity analysis highlighting the engineering tradeoffs associated with variations in product flow rate and feed salinity;

- An evaluation of the practical implications related to deploying the STEWARD system to potentially replace existing desalination plants or complement brine processing;
- Identification of deployment opportunities for STEWARD within the current operational space of existing desalination technologies;

The paper first presents a description of the STEWARD system, associated modeling equations, and simulation algorithm. Afterwards, the paper presents the simulation results of baseline operation and sensitivity analysis. Furthermore, the paper discusses practical implications of deploying the STEWARD system to potentially replace existing systems or supplement brine processing in actual desalination facilities. Finally, this HDH-ZLD system is mapped onto the operational space of existing desalination technologies to potentially identify the technical niche for the proposed system.

5.2. Methodology

This section explains the underlying thermodynamic process of the STEWARD system and disseminates the key equations that describe its operation. The simulation challenges related to calculating the thermodynamic state after atomization are explained as well as the modeling constraints and algorithm employed by the proposed model.

5.2.1. Overall System Description

Figure 5-1 shows a schematic of the novel desalination system modeled in this work. At point (1) near-stagnant air enters a compressor where it is compressed.

The stream leaves leaving as hot air jets (2) used to atomize a thin saline water film. Atomizing a saline water with salinity higher than 100,000 ppm (typical RO discharge salinity) using conventional atomizers is a challenge as scaling can clog any orifices in very short time periods [208]. A novel atomizer design (3) is implemented to suppress the fouling and sustain the cycle [9]. The next stage is the heat exchange, which is a double phase heat exchanger (evaporator/condenser) and a first heat recuperation stage. The fine spray generated by the atomizer is fully evaporated and absorbed by the carrier dry air. To stay economically viable, the maximum energy needs to be recuperated in this heat exchanger. For that, the boundary conditions need to be accurately pinpointed. Before entering the evaporator, the dry air is slightly humidified by the partial evaporation of the saline water. Conventional analytical models fail to pinpoint the thermodynamic state at this point as it is a multi-constraint optimization problem. The constraints of mass and energy continuities and maximization of entropy are not sufficient to solve the problem. Additional constraints from the working cycle need to be introduced.

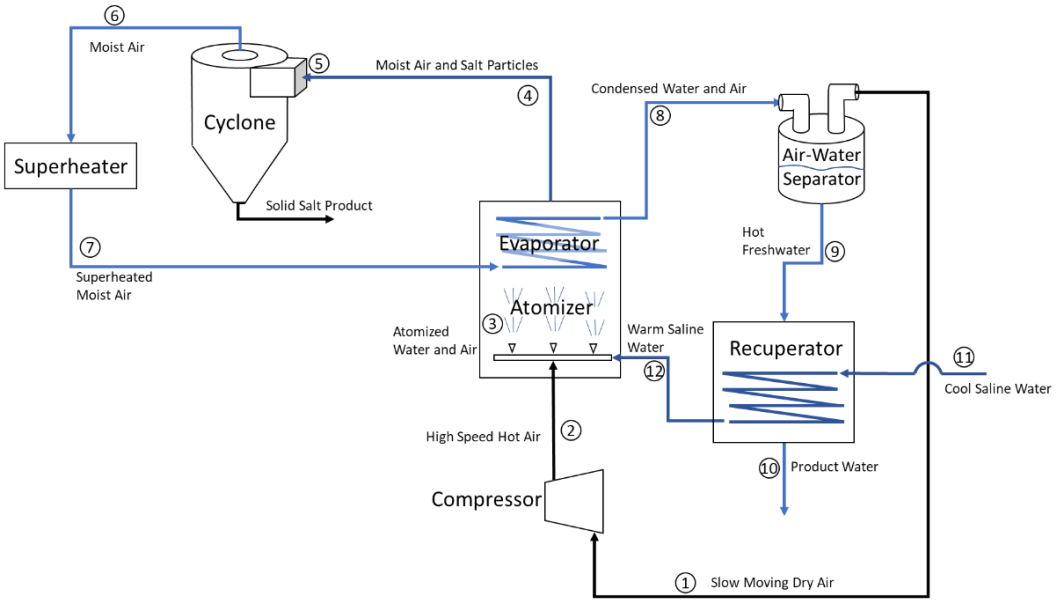

Figure 5-1: Diagram schematic of the proposed system.

After the heat exchanger (4), a homogenous mixture of moist air and salt crystals enters a cyclone separator (5), which is another potential choking point in the cycle. Analytical, numerical, and experimental investigations proved how the cyclone separator has a high resistant to fouling [209]. The continuous salt separation in the solid phase coupled with the nature of the HDH makes the technology resistant to fouling. The clean humid air (6) then enters a superheater which uses low-grade thermal energy to introduce additional energy to the system and prevents premature condensation prior to the condenser. The hot moist air then enters the condenser side where it recoups the sensible and latent heats to evaporate the sprays in the evaporator side. Then, a mixture of almost dry air (down to the thermodynamic limit) and liquid water exits the condenser (8). This mixture enters an air-water separator after which the air recirculates in the cycle. At some operating conditions, the warm freshwater could potentially be used to preheat the incoming streams of saline water.

5.2.2. Model Description

A significant challenge in the proposed design lies in bounding the thermodynamic state of the atomized water and air mixture for plausible operation. To achieve this, an iterative algorithm is employed that tests all the possible temperature-relative humidity combinations and eliminates non-physically viable options through checkpoints along the evaporator, cyclone, superheater, and condenser loop. The pressure loss of atomization is determined to be around 50 kPa at the operating flow rates [208], the possible temperature range is bounded by the water and air temperatures, T_{12} and T_2, respectively, and finally, the possible relative humidity range is between 0 and 100%. Each iteration, consists in setting a temperature value from the range and trying all possible relative humidity range values and eliminating the combinations that do not pass the following checkpoints:

The partial pressure of water ($P_{3,w}$) is defined by T_3 and ϕ_3, which must be lower than P_3 to result in a positive humidity ratio:

$$W_3 > 0 \tag{5-1}$$

State 4 is calculated through an iterative algorithm that finds T_4 such that the resulting humidity ratio W_4 matches that of full evaporation of the warm saline water stream (m_{12}/m_2). To guarantee heat transfer and full evaporation T_4 must be slightly greater than T_3 and thus the checkpoint follows that:

$$T_4 - 0.5 > T_3 \tag{5-2}$$

It has been determined that expansion cooling of the gas as well as cooling of the liquid through heat transfer are minimal during atomization processes, especially at fast discharges [210]. Therefore, the total enthalpy of the high-speed

hot air and warm saline water streams before and after atomization mixing must remain equal or slightly lower due to losses in local evaporation and breaking of water droplets. The implemented checkpoint therefore ensures that H_3 is between 0 and 8% lower than the addition of the enthalpies in the streams preceding the atomizer such that:

$$\frac{(H_2 + H_{12}) - H_3}{(H_2 + H_{12})} < 0.08 \tag{5-3}$$

The superheated moist air temperature is an input to the model and must be larger than the calculated temperature at the evaporator outlet per the second law of thermodynamics. Furthermore, the temperature at the evaporator outlet must be lower than the temperature of the condensed water and air stream leaving the condenser. Therefore, the implemented checkpoint verifies that:

$$T_4 < T_7 \tag{5-4}$$

and

$$T_8 < T_7 \tag{5-5}$$

The heat available on the condensing side of the evaporator Q_c must be greater than the heat required to complete evaporation Q_e. This condition checks that at minimum:

$$Q_c > Q_e \tag{5-6}$$

All possible atomized water and air (state 3) points that pass all the checkpoints are stored in an array. The most plausible state point is finally selected using the uniformly weighted ranking criteria based on three parameters: difference between available and required heat across the evaporator, entropy increase through atomization, and total enthalpy difference before and after atomization. At this

stage in the simulation, the identified thermodynamic state points following atomization have at the equal or greater heat available in the condensing side of the evaporator to achieve full evaporation of the atomized water stream. The model bounds the design space by selecting the point associated to the minimum difference between heat available and heat required in the evaporator. Furthermore, the model considers the atomized water and air state point that results in the largest entropy after atomization to implement a worst-case scenario design safety in thermodynamic performance. Finally, the design is bounded by considering the lowest difference in total enthalpy of the air and water streams before and the combined stream after atomization. This assumes an optimized atomizer design with high discharge, which uses the air velocity for atomizing the water stream without incurring in major thermodynamic losses [210].

The complete set of model equations for the desalination system are shown in Table 5-1. After determining the thermodynamic state point of the atomized water and air stream, the model continues calculations through the air-water separator and the recuperator. The state points at the recuperator inlets and outlets are calculated using the warm saline water state point 12, the temperatures of the cool saline water intake and hot freshwater streams at points 11 and 9, respectively, and a heat exchanger effectiveness of 0.8 as design constraints.

The cyclone effects are modeled through the pressure drop (dP_{cy}) it incurs in the moist air flow and the collection efficiency (η_{cy}), which dictates the percentage of salt particles that get removed from the stream. The modeling approaches for pressure drop and collection efficiency are detailed to great extent

in the literature [211], [212]. A model which considers cyclone dimensions, inlet thermodynamic state, flow velocity and salt particle characteristics was implemented initially to size the component. Nevertheless, preliminary design experiments for the desalination system showed that these modeling approaches generally overestimated the pressure drop, likely due to the small size of the required cyclone, and that the achieved collection efficiency was consistently 0.99 or higher [209]. Thus, the presented model assumes a constant dP_{cy} of 5 kPa and η_{cy} of 0.99.

The presented model has two major assumptions: a) constant cyclone separation efficiency and b) constant pressure drops across system components. The first major assumption consists of a constant cyclone efficiency of 0.99, this is a slightly conservative assumption justified by experimental results for intake salinities ranging from 25 g/kg to 147 g/kg where the separation efficiencies remained between 0.991 and 0.999 [213]. The second major assumption includes constant pressure drops across system components being: 50 kPa for atomization (process 2-3), 15% of the total pressure during evaporation (process 3-4), 5 kPa for the pressure drop across the cyclone (process 5-6), and 15% of the total pressure for condensation (process 7-8). These assumptions are justified by experimental data for each separate system component. Specifically, the atomizer air-side 50 kPa pressure drop is assumed as a design target for the ongoing atomizer development. Experimental results on a novel perforated plate airblast atomizer for saline water at the corresponding air flow rate show about 150 kPa pressure drops [214]. However, the pressure drop can be significantly reduced through different atomizer

design avenues. The pressure drop in effervescent atomization, for instance, at similar water flow rates can be as low as 25 kPa [215]. A combination of effervescent and airblast atomization can operate with air pressures ranging from 15 to 180 kPa [216]. Novel pneumatic atomizer designs can achieve atomization with less than 10 kPa pressure drop in the air stream, and 1.2 kPa in the water stream [217]. It must be noted that the water stream in the presented system serves two purposes: atomization, and a medium through which to transport water. Therefore, the energy required for atomization could further be reduced by assisting atomization with ultrasonic atomizers [218], [219], while bypassing the necessary air flow to maintain moisture absorption and release. The cyclone pressure drop is experimentally determined to be negligible compared to the other component pressure drops [213], therefore the assumption of a 5 kPa is a conservative assumption that at this stage in design can be regarded as a worst-case scenario. The assumptions for pressure drop for both the evaporator and condenser sides correspond to the maximum pressure drops required to achieve the humidification rates for the baseline product water flow rate. Although preliminary experiments on different heat exchanger design suggest lower pressure drops, we implement a conservative scenario for energy consumption calculations. Finally, the model assumes an air stream pressure of 48 kPa (state 1), and thus any excess pressure is released in the air-water separator. This is a conservative assumption as it has been determined that the pressure across the air-water separator pressure is within the ranges of 0.5 to 1.5 kPa [220], and thus leaves a safety margin for further optimization as the system is integrated into a pilot plant.

Moist air properties with temperature, pressure, and humidity dependence are calculated using the AirProperties MATLAB library [110], which is based on published correlations [63], [109]. Dry air thermodynamic properties are calculated using the IdealAir MATLAB package [221]. Most saline and pure water properties are calculated using the Thermophysical Properties of Seawater library [57], [58], and two-phase vapor-steam properties are calculated using the XSteam library [61]. Both XSteam and the Seawater libraries, however, could be used interchangeably at zero salinity.

Table 5-1: Model Key Equations.

Component	Equation		Variables	
Compressor	$W_{isen} = m_1 \left(\frac{\gamma_1}{\gamma_1 - 1}\right) P_1 \left(\frac{1}{\rho_1}\right) \left[\left(\frac{P_2}{P_1}\right)^{\left(\frac{\gamma_1 - 1}{\gamma_1}\right)} - 1\right]$	(5-7)	W_{isen}	Compressor power, isentropic
			m_1	Slow-moving dry air mass flowrate
			γ_1	Isentropic ratio
			P_1	Inlet pressure
	$W_{comp} = \frac{W_{isen}}{\eta_{c,isen}}$	(5-8)	P_2	Outlet pressure
			W_{comp}	Actual compressor power
			$\eta_{c,isen}$	Compressor isentropic efficiency
Evaporator	$Q_e = m_{3,sw}\lambda_{3,sw} + (m_{3,w} + m_{3,a})c_{p,ma}(T_4 - T_3)$	(5-9)	Q_e	Heat required for full evaporation
			$m_{3,sw}$	Saltwater flow rate
			$\lambda_{3,sw}$	Saltwater latent heat of vaporization
			$m_{3,w}$	Water vapor flow rate
			$m_{3,a}$	Air flow rate
			$c_{p,ma}$	Specific heat capacity of moist air
			T_4	Outlet temperature
			T_3	Inlet temperature
Superheater	$dH_{sup} = m_w(h_{7,w} - h_{6,w}) + m_a(h_{7,a} - h_{6,a}) + m_s(c_{p_{7s}}T_7 - c_{p_{6s}}T_6)$	(5-10)	dH_{sup}	Superheat enthalpy difference
			m_w	Water vapor mass flow rate
			$h_{7,w}$	Water vapor enthalpy at superheat temp.
			$h_{6,w}$	Water vapor enthalpy at vapor saturation

		$m_{7,a}$	Dry air mass flow rate
		$h_{7,a}$	Air enthalpy at superheat temp.
		$h_{6,a}$	Air enthalpy at saturation temp.
		$m_{7,s}$	Solid salt mass flow rate
		c_{p_s}	Specific heat capacity of solid salt
		T_7	Superheat temp.
		T_6	Saturation temp.
Condenser	$dH_{sat} = m_w(h_{6,w} - h_{8,w}) + m_a(h_{6,a} - h_{8,a})$ (5-11)	dH_{sat}	Condensation enthalpy difference
		$h_{8,w}$	Water vapor enthalpy at liquid saturation
		$h_{8,a}$	Air enthalpy at saturation temp.
	$Q_c = dH_{sup} + dH_{sat}$ (5-12)	Q_c	Condensation heat
Cyclone	$P_6 = P_5 - dP_{cy}$ (5-13)	P_6	Outlet pressure
		P_5	Inlet pressure
		dP_{cy}	Cyclone pressure drop
	$m_s = m_{5,s}\eta_{cy}$ (5-14)	m_s	System salt flow rate
		$m_{5,s}$	Inlet salt flow rate
		η_{cy}	Collection efficiency

5.3. Results

This section presents the simulation results at baseline operations and the underlying thermodynamic cycle of the system to find critical processes and components. A subsequent sensitivity analysis is presented by parametrizing product flow rate and feed salinities to understand the operational tradeoffs inhered to the system.

5.3.1. Baseline Operation

Table 5-2 shows the complete input set for simulation. The presented HDH-ZLD system employs a thermal process to drive desalination, however, it additionally features an air compressor driven by electric energy. In this analysis,

we assume a scenario in which the superheater is driven by motive steam at the saturation pressure (P_s) corresponding to the superheated temperature, and another scenario where we assume an electric superheater. The compressor is always considered in the total energy consumption as it incurs in significant energy requirements within the process.

Table 5-2: Model Inputs – Baseline.

General Inputs	
Product flow rate, M_d (kg/s)	0.0027
Intake salinity, C_f (g/kg)	100
Intake temp., T_{in} (°C)	18
Family Inputs	
Motive steam pressure, P_s (kPa)	200
Specific Inputs	
Superheat temp., T_{sup} (°C)	120
Slow moving dry air pressure, P_1 (kPa)	48
Slow moving dry air temp., T_1 (°C)	20
Slow moving dry air rel. hum., ϕ_1 (-)	0.63
Air flow rate, m_1 (kg/s)	0.0054
High speed hot air pressure, P_2 (kPa)	150
Warm saline water temperature, T_{12} (°C)	20

Table 5-3 shows the outputs of the simulation of the proposed system at baseline operation. The results show the most feasible operation point that follows the physical conservation laws. Thus, practically complete water recovery can be achieved from a considerably high feed water salinity through the proposed system. Although the total specific energy consumption is large, it must be noted that roughly 10% of the required heat for evaporation is an external thermal input through the superheater. This translates to a high gain ratio that might not be an accurate metric of thermal performance as it is with other thermal desalination systems driven by a single energy input. This is a considerable difference from

other thermal desalination systems such as conventional HDH and MED in which the heat required for desalination is completely supplied externally, or partially supplemented by recirculated product steam in the case of energy recovery devices [ref. submitted for peer-review]. Instead, the proposed STEWARD system offsets the evaporation load to the compressor which uses air to provide energy for increasing the surface area of evaporation of the water through atomization, absorbing moisture, and transferring heat through psychrometric processes.

Table 5-3: Model Outputs – Baseline.

General Outputs	
Product flow rate, M_d (kg/s)	0.0029
Feed water flow rate, M_f (kg/s)	0.003
Brine flow rate, M_b (kg/s)	n/a
Product water salinity, C_p (g/kg)	1
Feed water salinity, C_f (g/kg)	100
Brine salinity, C_b (g/kg)	n/a
Actual Recovery Ratio, R	0.99
Family Outputs	
Specific energy, E_{des} (kWh/m^3)	Scenario 1: 905_{el}, 49_{th} Scenario 2: 954_{el}
Motive steam flow rate, M_p (kg/s)	2.37e-04 / n/a
Gain ratio, GR	12 / n/a
Sp. cooling water flow rate, sM_{cw} (kg/kg)	n/a
Specific Outputs	
Atomized water and air temp., T_3 (°C)	75
Atomized water and air rel. hum., ϕ_3 (-)	0.29
Solid salt product flow rate., m_s (kg/s)	2.94e-04
Compressor power, W_{comp} (kW)	9.6
Evaporator heat required, Q_e (kW)	5.1
Condenser heat available, Q_c (kW)	7.2
Superheater heat, dH_{sup} (kW)	0.5

Some conventional performance indicators such as gain ratio or specific cooling water flow rate do not completely apply in the proposed STEWARD system. Therefore, analyzing each of the cross-comparison hierarchies can provide

a systematized method to assess its operation space and cycle characteristics through both energy supply scenarios. At the General Outputs level, the STEWARD system does not have a brine flow rate or salinity. Instead, almost 100% of the salt content is separated in the cyclone and rejected as a solid salt product. The baseline recovery ratio is close to 1, which is usually achievable only at low salinities with conventional desalination systems like MED or RO [186]. The results show viability for hypersaline water with a feed concentration of 100 g/kg which is generally out of range for conventional desalination applications.

The Family Outputs highlight a discrepancy in operation between conventional thermal desalination and the proposed method. The system does not have a cooling water to reject excess heat from the warm freshwater product. Heat losses in the air-water separator and the similar mass flows of hot and cold streams across the heat exchangers can make the need for a rejected cooling water stream redundant. The motive steam flow rate is considerably low in comparison to conventional Humidification-Dehumidification systems [32], [65], [111], which leads to a much higher gain ratio as the external heat input is only required for the superheat portion of the evaporation curve. The specific energy required by the outlined process is fairly high but roughly within the order of magnitude of the energy intensity reported in across the literature [186]. Although the separation phenomena in this system is driven by a thermal process, the superheat input can be electric and thus, the system can be compared to the molecular transport desalination methods at an energy source level. The total electric input including superheater and compressor loads of baseline operation is 954 kWh/m^3. The total

thermal load of ~50 kWh/m^3 is similar to that reported in other hypersaline brine desalination systems [26].

The parameters within the Specific Outputs category emphasize the importance of the evaporator design given the important constraints of the required flow and heat exchange. The superheat portion of the cooling-dehumidification process that takes place in the heat exchanger accounts for roughly 7% of the heat available. Superheat temperature, nevertheless, is required in the system as it provides important control of the heat exchange pinch point and thus, overall system performance. One of the checkpoints to evaluate the atomized water and air state before the evaporator (state point 3) checks that the heat available through the condensation of the superheated stream exceeds the heat required to achieve full evaporation. The results show that the heat available in the condenser side exceeds the required heat by the evaporator by about 28%. While some improvements could occur to minimize this difference, a small excess available heat could make the system robust to changes in M_d and C_f.

Figure 5-2 shows the T-P diagram for baseline operation. The greatest temperature-pressure differential takes place in compression which is the greatest energy input to the system. The conditions for state point 2 are defined by the minimum flow velocity required for atomization considering the dynamic pressure losses in the atomizer and heat exchanger such that the target 21 m/s at the cyclone inlet is met to achieve >99% separation. An advantage of the presented system is that the air-absorbing capabilities of air are accentuated through the temperature increase of the air stream as a side effect of the compressor. This would favor the

saline water preheating through the recuperator and eliminate the need for cooling water that is discarded after preheating like it occurs in Thermovapor Compression (TVC), MED, and conventional HDH methods. Atomization is accountable for roughly half of the total pressure loss, followed by condensation and air-water separation that are responsible roughly one third each. In the case of temperature, the differential incurred in the air stream through compression and atomization are the largest, followed by the temperature drop after removing water from the condensed mixture stream.

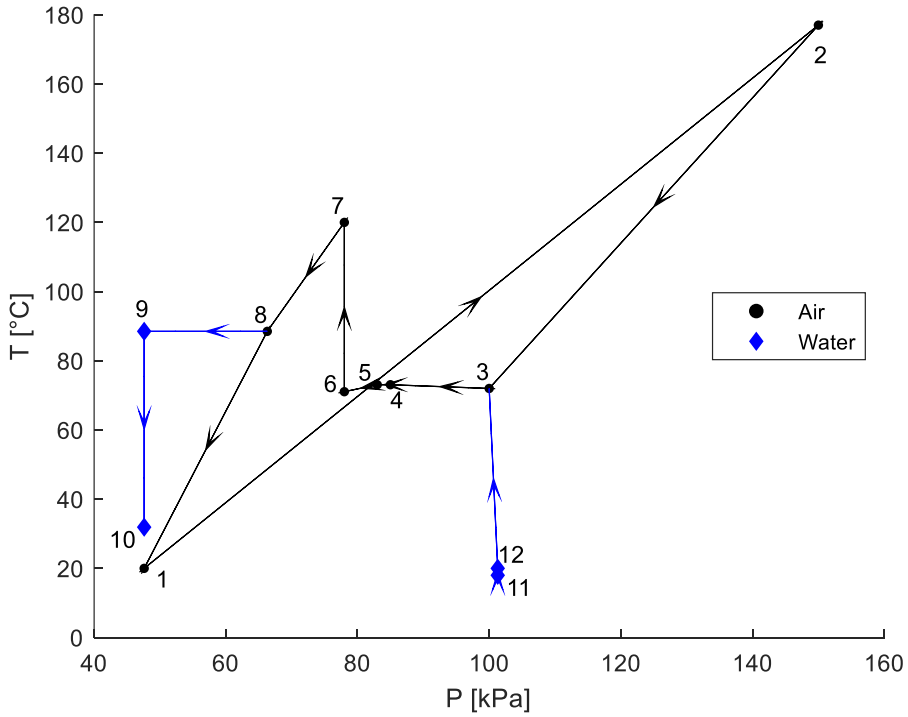

Figure 5-2: T-P diagram for the baseline cycle.

Figure 5-3 shows the humidity ratio and pressure changes in the air cycle within the system. Atomization alone accounts for almost half of the total air humidification in concurrence with the highest pressure drop. This is a unique characteristic in thermodynamic operation as the thermal load conventionally used

in driving distillation is offset by atomization. Atomization, by contrast incurs in a significant energy loss through a pressure drop, however, this also acts as a facilitator for evaporation by substantially increasing available surface area for heat transfer. Moisture removal from the air, in contrast, occurs in a single step through cooling and dehumidification at the other side of the heat exchanger. For baseline simulation, we assume slight humidification of the air stream occurs in the air-water separator as the streams remain in contact. The moisture content of the air stream after the separator must be controlled through the superheater temperature and separator design as it could lead to corrosion in the compressor and losses in potentially recoverable product freshwater. Depending on ambient air conditions, implementing an open-air could be a possibility that requires investigation for optimizing water recovery.

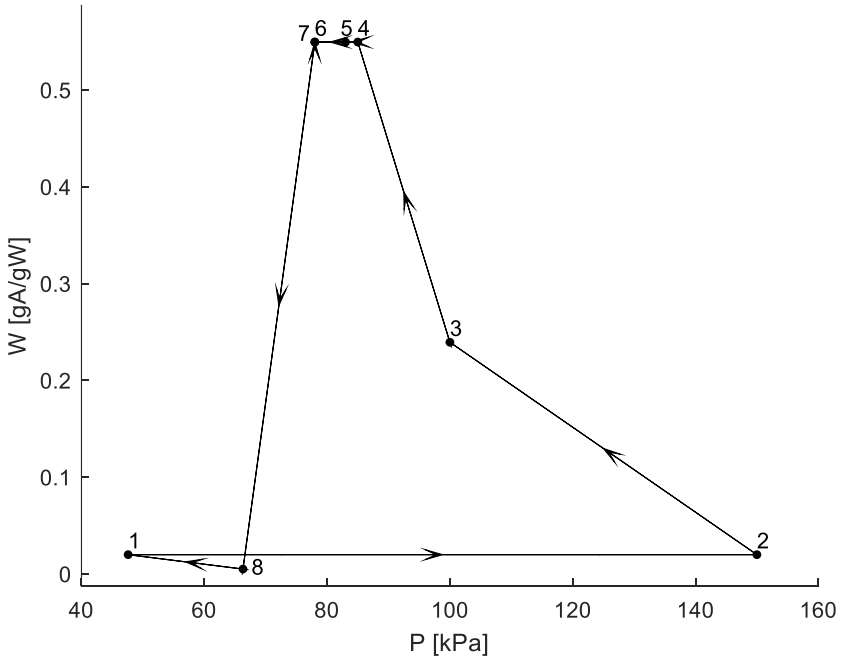

Figure 5-3: W-P diagram for the baseline cycle.

Figure 5-4 shows the enthalpy-pressure diagram for baseline operation. The greatest enthalpy changes occur between state points 3 and 4, and state points 7 and 8, which correspond to the evaporation and cooling-dehumidification processes. This is consistent with the energy increase in the system through the latent heat addition and removal of water in the air flow. Appropriate operation, therefore, is dependent on an effective heat exchanger as it is the most critical component of the system. This contrasts the external energy inputs which are associated to the smaller enthalpy changes through compression (state points 1-2) and superheating (state points 6-7).

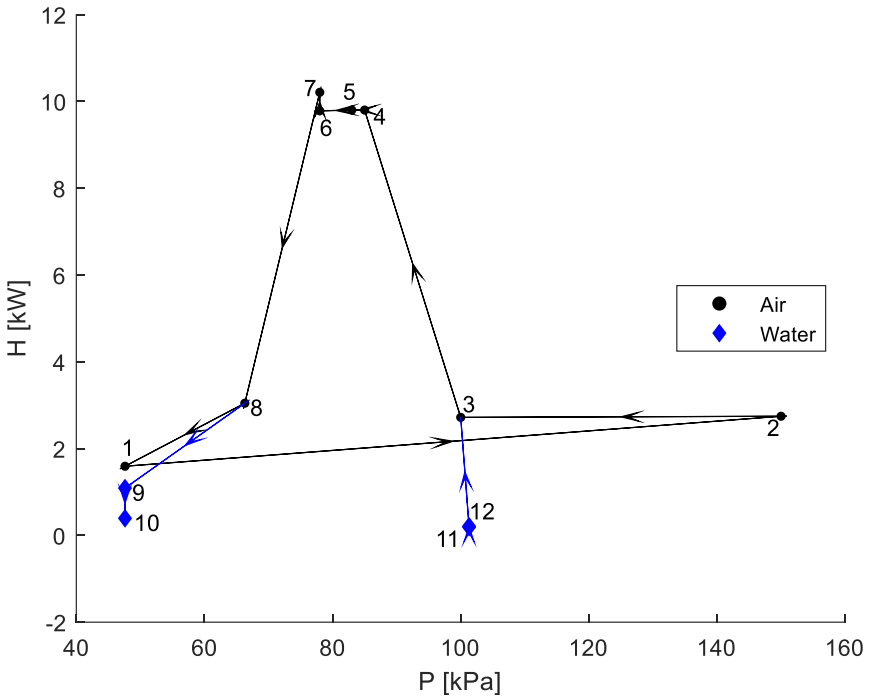

Figure 5-4: H-P diagram for baseline operation.

5.3.2. Sensitivity Analysis

In this section the system model is used to conduct a sensitivity analysis to establish operation tradeoffs. A simple simulation engine is presented, which

adjusts parameters in accordance with conservation and thermodynamic laws and bounds the simulation space by keeping the baseline parameters constant. The atomized water and air state (state point 3 in the cycle) is inferred by iterating through all possible temperatures between T_2 and T_{12} with $dT = 0.1$ °C and all possible air relative humidity values from 0 to 1 with a $d\phi$ = 0.01. Deviating from baseline M_d or C_f usually results in mismatch in energy across the evaporator either due to a different latent load or boiling point elevation, or a violation in conservation laws across the atomizer as the amount of air required in atomization and moisture transport would vary. When this occurs, the simulation engine adjusts the air flow by ± 0.001 kg/s to approach the baseline air to water ratio of 1.8.

Figure 5-5 shows the system response for variations of ±25% and ±75% with respect to baseline M_d and C_f, respectively. The results highlight a safety overdesign in the air flow rate for maintaining a recovery rate of at least 99%. Decreasing product flow rate implies a lower latent load at the evaporator which can be met by decreasing air flow rate if the baseline superheat temperature is kept constant. Decreasing M_d increases the contribution of the air stream in the total enthalpy during atomization as described by equation (5-3). Since the state point at the compressor outlet is fixed, after around 20% decrease in water flow rate the model must compensate the enthalpy contribution of water by decreasing the air flow. Thus, the air flow rate is directly proportional to decreasing M_d and this is reflected in the linear compressor power change in the same direction. At higher water production rates however, W_{comp} remains constant as there is no need for the simulation engine to vary the air flow rate as the heat available after the superheater

exceeds the heat required for evaporation and the increased contribution of water to enthalpy mixture before and after atomization follows energy conservation. The heat required for evaporation (Q_{req}), conversely, is directly proportional to M_d as higher water production increases the latent load in the evaporation process.

Increasing feed salinity, on the other hand, indirectly increases feed water as removing salt from higher concentrations result in less available water product. Furthermore, water transport increases since the operation must occur at higher temperatures which are more favorable for moisture absorption. This makes targeting higher feed salinities plausible as it also increases the product water output without changing the compressor power. Furthermore, the available heat in the stream after superheater, consisting of the superheat path and the latent load at saturation, is consistently greater than the heat required for full evaporation at the other side of the heat exchanger by about 54% at baseline operation and at least 29% at higher energy demand scenarios caused by greater M_d or C_f. Thus, although higher salt content generally leads to boiling point elevation and greater heat required for evaporation, the excess heat input at baseline operation to the superheat portion overcome the need for altering external heat inputs to the system. Therefore, Q_{req} and W_{comp} are practically independent from C_f if the rest of the parameters remain constant.

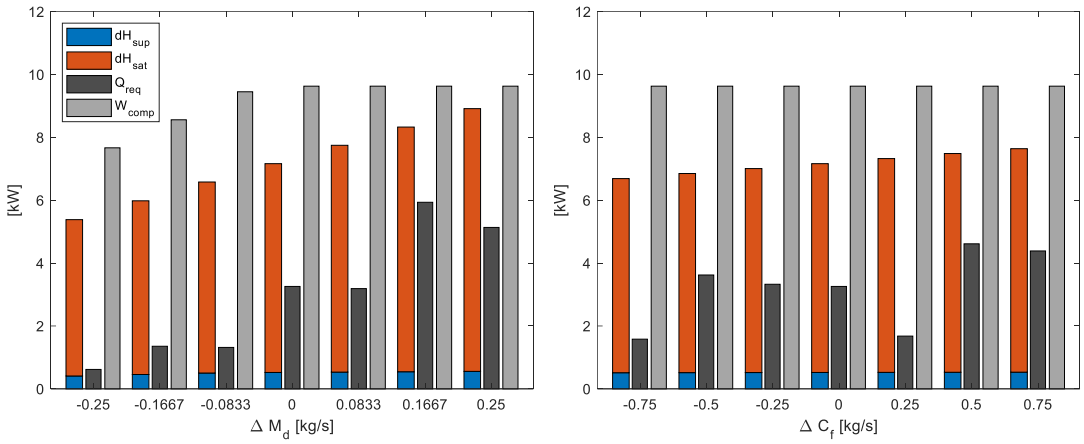

Figure 5-5: Sensitivity analysis for M_d (left) and C_f (right).

5.4. Discussion

While the thermodynamic analysis corroborates the physical viability of the STEWARD system, further simulations are conducted to investigate the possibility to replace conventional desalination systems in actual plants or supplement brine post-treatment. In this section, the implications of these deployment strategies are discussed, establishing the opportunities for STEWARD within the existing operational space of desalination methods.

5.4.1. Practical Operation

We assume multiple STEWARD units in parallel to fulfill large M_d values because adapting operation to a system whose target M_d exceeds the baseline by a factor of at least 10^3 is impractical. Obtaining an estimate of the number of units in parallel operation and the associated energy intensities, nonetheless, can help establish operational bounds that could guide further design iterations. Table 5-4 shows the operational costs assuming the implementation of enough STEWARD units in parallel to fulfill existing plant production requirements or process their corresponding brine product [222].

Table 5-4: STEWARD performance using case study simulation data.

System Type	**MDT**	**MDT**	**ROX**	**ROX**
Plant Location	Jeddah, KSA	Jamnagar, IN	Bimini, BS	Cát Bà, VT
M_d (kg/s)	55	284	12	17
C_f (g/kg)	41.5	42	39	33
T_{in} (°C)	30	26	29	32
M_b (kg/s)	109	409	12	20
C_b (g/kg)	62.5	70	78.9	62.9
T_b (°C)	46	43	39	33
E_{des} (kWh/m^3)	132$_{th}$	76$_{th}$	2.7$_{el}$	2.4$_{el}$
Q_{req} (kW)	26132	77619	n/a	n/a
W_{pump} (kW)	n/a	n/a	110	149
RR (-)	0.34	0.41	0.50	0.47
STEWARD Replacement				
Total M_d (kg/s)	55	284	12	17
Units in Parallel	19788	101740	4140	6314
$E_{des}/unit$ (kWh/m^3)	953	1004	1006	1012
$W_{comp}/unit$ (kW)	9.6	9.6	9.6	9.6
$dH_{sup}/unit$ (kW)	0.5	0.5	0.5	0.5
$Q_{req}/unit$ (kW)	3.0	2.9	1.6	2.1
$RR/unit$ (-)	0.99	0.99	0.99	0.99
STEWARD Complement				
Total M_d (kg/s)	109	409	12	20
Units in Parallel	38893	146071	4250	7150
$E_{des}/unit$ (kWh/m^3)	10142	1008	1023	1019
$W_{comp}/unit$ (kW)	9.98	9.98	10.0	10.0
$dH_{sup}/unit$ (kW)	0.5	0.5	0.5	0.5
$Q_{req}/unit$ (kW)	1.3	1.7	1.1	1.4
$RR/unit$ (-)	0.99	0.99	0.99	0.99

The high number of STEWARD units required to fulfill production rates and elevated energy intensity suggest that the proposed system might not replace existing desalination facilities but rather be a good supplement for brine processing. The latter scenario could be further supported if the brine is further concentrated into a hypersaline stream, or the STEWARD product water flow rate is augmented such that less units in parallel are required. Current practices for brine disposal in the fracking industry range from \$18/m^3 and \$174/m^3 for surface disposal and

existing deep injection well techniques, respectively, up to \$7,280/m^3 for lined evaporative pond methods [223]. Considering electricity rates in fracking states like Texas (\$0.086/kWh), West Virginia (\$0.1066/kWh), and Pennsylvania (\$0.0981/kWh), for cost comparison with STEWARD assuming electric heating, the baseline operation cost would range between \$81/m^3 and \$93/m^3 [224].

5.4.2. Operational Map

The most relevant desalination methods include thermal processes such as TVC, MED, and HDH, as well as molecular transport processes including RO, Electrodialysis (EDS), and Capacitive Deionization (CDI). Figure 5-6 shows the operational space of existing desalination technologies compiled from plant data, bench scale systems and models available in the literature [186]. The recovery achieved through HDH-ZLD is vastly different than conventional HDH methods and therefore it is considered as a standalone method. Thermal methods are usually associated to a higher energy intensity and low recovery ratios when compared to molecular transport methods. Furthermore, molecular transport methods are generally related to lower feed salinities due to high fouling tendencies [201], [202].

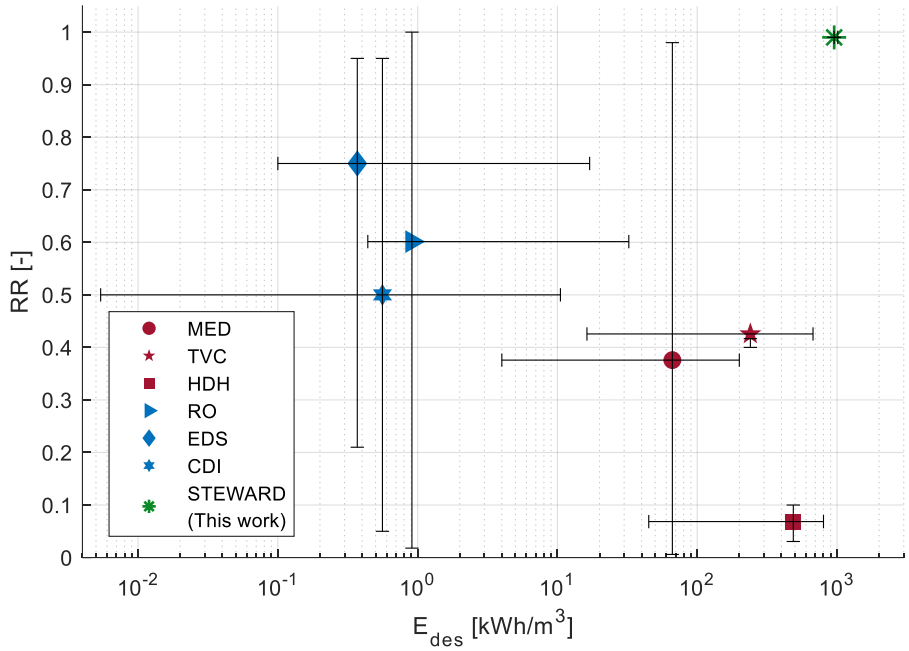

Figure 5-6: Operational map for different desalination technologies.

The achievable recovery rates of STEWARD are about 10 times larger than those achieved by conventional HDH processes, double the recovery reported in TVC methods, and comparable only to the high end of the recovery reported for MED. The practically full recovery ratio offered by STEWARD at baseline conditions could fulfill operation reported in the high recovery rate extremes within the molecular transport methods. Therefore, there is a niche in the operational space of desalination technologies characterized by high recovery rates and high feed salinities that are generally unfulfilled by conventional desalination methods.

The map represents potential operation ranges based on first principles, including mass balance of water, salt, and air, as well as conservation of energy. The actual operational ranges would depend on system component performance and could require more energy than predicted in this analysis due to system inefficiencies. Nevertheless, if an inexpensive energy source is available, the

STEWARD system could process high salinity brines with almost complete water recovery.

The total energy intensity associated to STEWARD is comparable to the higher end of the energy intensity reported in other thermal methods. About 49 kWh/m^3 correspond to thermal energy input to the superheater which is matches the midrange point of the thermal energy intensity of MED desalination and lies at the lower ranges of TVC and HDH desalination. This implies that most energy is required in atomization (about 95%), that facilitates and integrates ZLD within the desalination process, in contrast with the energy intensity associated to the conventional desalination methods presented in Figure 5-6 that represent the desalination process alone at lower feed salinities. The energy loss in atomization is reflected in the pressure drop across the component, therefore, the competitiveness of the STEWARD system in the marketplace is contingent upon efficient atomizer design and performance. The presence of the compressor implies that the current STEWARD concept must depend on electricity alone, or electricity and heat, to operate. This could potentially be an important factor when considering locations for deployment. From an operational perspective, adoption of the STEWARD system would ultimately be associated to the costs of energy available and brine management at the desalination site.

5.5. Conclusion

In this paper we present a thermodynamic model for a novel HDH-based process with ZLD capabilities embodied in a Solar Thermal Extraction of Water by Atomization and Recuperative Desalination (STEWARD) system. Modeling can

bound system operation based on conservation laws and find plausible operation states. A sensitivity analysis is conducted to identify the tradeoffs associated to changes in feed salinity and freshwater production to map out the operational space in which the technology could be deployed. Unlike conventional technologies like RO and MED, the energy intensity in the STEWARD system is minimally sensitive to changes in C_f. And its configuration allows for variation in M_d without incurring in additional external energy inputs. The resulting energy intensity is slightly higher than conventional desalination methods. However, the system can achieve almost complete recovery from hypersaline feeds, which is an area of operation that is not traditionally served by other well-established desalination processes. The total operation utility cost associated with the energy intensity is comparable with current brine management and disposal practices. The crux of the proposed STEWARD system lies at the achievable product flow rates which could challenge scalability. Overall, the proposed system shows great potential for off-grid hypersaline brine treatment. Future physics based and data driven predictive models can be developed as further research efforts bring STEWARD into a pilot plant deployment.

Chapter 6: Lessons Learned – Designing the Ideal Desalination System

A doctorate thesis is an exploration of the boundaries of scientific knowledge as well as a proxy for personal discovery. I would like to steer this chapter to a discussion of the lessons learned and express, in my opinion, efficient ways to overcome the challenges I faced. Paradigm shifts I developed during this journey are equally worthy of discussion as the developed technical concepts. A desalination system faces technical and operational challenges throughout its lifetime that are subject of research and development. New research will eventually produce upgraded and novel systems that will result in better performance and smoother operation. For those that find this thesis helpful and would use it as part of the foundation of further advances in the state of the art, I hope these "desalination system guidelines" are of personal help in your own research endeavors.

6.1. A lot of "salt" out there

Just like desalination has the objective of extracting the useful water out of the vast saline water supply, a recurrent objective through graduate research is extracting the useful information, methodologies, and insights out of the ocean of scientific publications. Unfortunately, there is an extremely large body of publications that could be considered salt in a desalination system. This first realization was heartbreaking as I always thought of scientists as the group of people to which society turns to for comprehension in the face of uncertainty. This mental image started to fall apart as I noticed how I could not reproduce published

work because of a missing equation, coefficients whose definition or values were not disclosed, or cited correlations whose coefficients were altered without explanation. When I noticed this was present across the literature including conference papers, low-impact journals, and even the most respected journals in the field my esteem to science crumbled. At some point I even questioned the purpose of science if researchers are actively suppressing key parts that would enable other to reproduce their work.

I am grateful with my advisor, from whom I was able to distillate a coffee-break course on scientific ethics and publishing responsibilities that otherwise I might not have come across through my academic path. The truth is that no system is perfect, and politics, unpaid bills, and tenure pursuit can force authors to publish loads of salt that could be overlooked by the peer-review process. Therefore, it is the author's responsibility throughout research and publication, to not only desalinate aggressively from the sea of publications, but also to make sure to not contribute towards increasing salinity levels. I could recommend two guidelines for publication: (1) ask yourself if you are making it hard for others to reproduce published work and use it as a foundation for advancing the state of the art, (2) remain open for critique and inquiries post-publication, you might inspire a few people by doing so. I recall the encouragement I felt during the first years of my graduate work in 2018 when an professor in an Italian university thoroughly replied to my inquiries about his publication from 1985 [225].

Desalination methods do not discriminate among water sources. Membranes, evaporation processes, or electrokinetic phenomena systematically

filter out materials that do not belong with pure water. Similarly, one must be critical of publications and identify those that take a collaborative approach to science. This, in the long run would not only set a high standard for what a researcher communicates to the world, but I hope it puts the scientific community in track of an openly, collaborative and therefore faster progress towards solving the great challenges of our time.

6.2. Design a Reliable System

Desalination will become a fundamental agent for water security in many countries around the world. Eke et al. have established that cumulative capacity of desalination plants worldwide has increased from 27,252 m^3/d in 1969 to 97.2 million m3/d in 2020, with increases of over 1600% and 1700% in desalination capacity in Europe and Africa, respectively, over the past 20 years [4]. Years of research and development have enabled the production of reliable systems that produce water consistently at a desired concentration. Similarly, to how nations and industries build confidence on desalination through increased adoption, a graduate student must build confidence on the quality of the work produced.

My graduate studies have not just been an opportunity for developing skills and knowledge but also building up confidence as a researcher. I remember sitting in the first quarterly review meeting in front of our program manager at the US Department of Energy (US DOE), their technical panel, and other senior researchers from other universities serving as co-investigators while feeling tiny in my conference chair and fighting the impostor syndrome as I presented. I kept thinking “Who would want to listen to a 22-year-old talk about desalination

systems?" After this repeated through the first year of report presentations to the US DOE, my advisor took time to debrief me after a meeting and stressed the importance of standing up for my work. "In a sense it is good you doubt your work because it keeps you humble and pushes you to maintain a high quality, "my advisor said, "but if you do not stand up and own it as you present it, people will not pay attention and even worse, will lose faith in what you are working on."

I have come to understand that the impostor syndrome is normal, because the moment you climb up to the next level within a field, such as moving from an undergraduate to a doctoral program, you are indeed out of your own place. This is actually a great opportunity to leverage that feeling to motivate learning in both the technical as well as soft skills realms. You must trust your mentor and trust the process that will slowly equip you with skills and knowledge towards expertise.

As graduate students we work on a very specific niche at the forefront of knowledge, and it is easy to lose perspective on how far ahead from the state of the art one has pushed through, and the important repercussions of the breakthroughs made. Part of enjoying the journey of graduate education is taking a step back and appreciating how far you have come from the place you started. One of the most wonderful ways to realize this, in my opinion, is through teaching and mentoring activities. Introspection can be very challenging due to a biased mindset that is present when doubting your own capabilities. But the moment younger students ask for help, perhaps you will remember an earlier version of yourself asking similar questions and realize how much you have learned throughout the process and your potential to make a valuable contribution.

I believe science is useless without dissemination, and to do this effectively you must stand up for your work. Graduate programs are filled with such opportunities: you will take the risk and defend a research proposal, have the courage to communicate findings through peer-reviewed publications and reports, and finally, establish competences through the dissertation defense. Over these experiences I have learned a key lesson: it is impossible to get other people excited about your work unless you are excited yourself in the first place.

Maintain humility and produce high quality work that you are not ashamed of standing up for. Remain skeptic and humble about your work so you are open to criticism and improvement but keep it in check so that it does not hurt the quality or your ability to defend your work. Overall, trust the process as it will naturally expose you to events that will strengthen your confidence and make you a competent researcher within your field.

6.3. Conduct Strategic Maintenance

The Addur plant in the Kingdom of Bahrain was commissioned in 1990 as one of the largest RO deployments of the time with a capacity of producing 10 mIgd of water at <500 g/kg, however, design shortcomings and improper maintenance led to an appalling performance as summarized [226], [227]:

> Within a year of operation, a fast flux decline was noticed requiring preventive measures. By 1993 product flow rate declined by more than 50% of the design value with a product concentration of about 1300 g/kg, and most of the 3696 membrane modules presenting severe fouling. It was not until 1995, with the plant struggling to run at more than 50% capacity while

incurring more than twice the production costs in comparison to 1993 (which were already higher than at time of commission) that less than half of the membranes were replaced. Finally, in 1996 the remaining old membranes were retired, forcing a major plant shutdown that allowed major essential system modifications before implementing strategies to recuperate plant operation.

The studies attribute the poor plant performance to errors in construction, design, and maintenance. And while causes and responses can be contested, it is important to note an urgent operational shut down did not occur due to pressures of rising local water demands. Evidently, those demands were not met optimally, and poor operation cascaded into further degeneration of the system's condition. Van Rooij et al. propose a modern data-driven strategy to schedule maintenance before actual damage occurs and therefore, with enough time to optimize the tradeoff between risk, cost and downtime [228]. The malfunctioning Addur plant would likely have had a different fate if such strategies were available and implemented at the time.

A doctoral program has its own share of requirements: courses, qualifier exams, thesis proposal, dissertations, and on top of that research proposal, responses to journal reviewers and sponsoring agency presentations that demand time and effort. In my own case, I followed an intense program by completing all course requirements and qualifier exam within the first two years, and advancing to candidacy, publishing 3 papers in peer-reviewed journals, writing, and defending my thesis in the subsequent two years. Along the way I had to present research

reports to the US DOE, teach a few classes, collaborate in three additional research projects (one as a team leader), supervise undergraduate students, and submit two proposals.

Did I feel overwhelmed? Yes, many times. Did I crash? Certainly, until I learned to take breaks.

Graduate school is an environment where you will be pushing to the peak of physical and cognitive capabilities, and if sustained for too long, in my experience, burnout is inevitable. Make sure to schedule breaks and pauses in advance because it is hard to judge when does one need to rest while immersed in work and research tasks. More importantly, if you do not schedule a break your body will do it for you by falling ill. Breaks are crucial not just to recharge and maintain peak performance, but rather enjoy the wonderful things that come along with the graduate experience. I hold that the friendships, adventures, and cherished moments with others are equally important as the academic pursuit throughout graduate education. And further, I hypothesize these moments are the ones I will forever remember about when I look back upon these years.

6.4. Schedule Operation

Just like desalination systems need their downtime to perform scheduled preventive maintenance, it is imperative to schedule optimized running time to maximize productivity. One way to optimize overall performance consists in implementing cogeneration schemes, coupling power and desalination plants, to produce electricity and water simultaneously [53], [170]. Xiao et al. expanded on this implementation by proposing a scheduling model to control water production

of RO and multi-stage flash systems that use heat and electricity produced from a power plant during different demand hours and seasons [229]. Their results show a promising opportunity to optimize utility cost and operation variability by implementing a robust schedule.

Similarly, in keeping up with the requirements of the doctoral program I have come to find how critical scheduling work is. This was first conveyed by my advisor who advocates for a semester research plan created by each student. As I started falling behind my own developed schedule, I realized how much I had underestimated the complexity of research and how the progress is non-linear with respect to time. I realized that if this is the nature of research, then the research plan should follow progress accordingly. Later, my advisor confirmed that the research plan is a dynamic tool that must sit next to your desk and be revised and edited every week. Once the bigger picture goals are well-established and revised, we can come up with a lower-level day-to-day plan.

I have found that the proposed strategy of Chris Bailey's *Hyperfocus* fitted my needs extremely well: alternating tasks that require complete attention (hyperfocus), such as coding, writing, or analyzing data, with those that would benefit or not suffer from a dispersed cognitive effort (scatterfocus), such as meetings and creative design sessions [230]. This was complemented by implementing concepts from Cal Newport's *Deep Work*: work deeply, embrace boredom, quit social media, and drain the shallows [231]. These two books have had a profound impact on my work, and I strongly recommend them to new students. Furthermore, I discovered the benefit of incorporating time management

applications such as Google Calendar and Keep for offsetting the information load in my mind.

Scheduling work time according to the nature of the task, in my experience, optimizes output in a sustainable manner. I strongly encourage new students to pay close attention to scheduling and implementing a strategy to guide their focus. Not only this will help them stay on track and meet the stringent requirements of a graduate degree, but also allow for scheduling of breaks and leisure time.

6.5. Disrupting the Desalination Map

Desalination technologies as we know today have undergone a remarkable process of innovation and research starting with one of the first documented scientific observations on desalination dating to the 4th century BC in Aristotle's *Meteorology*, followed by distillation processes employed in the 1500's for equipping ships with potable water [5]. In 1928, Aiton Ltd. built one of the first land-based mechanical desalination systems in Curacao with a 50-60 m^3/day production capacity [232]. Since then, relentless research pursuits have continued to create larger, efficient, advances occurred within the field which eventually culminated in the deployment of modern technologies, namely, in 1930 the first MED plant is built in Saudi Arabia, in 1957, Multi-stage flash desalination appears as a market competitor, and in 1965, reverse osmosis is introduced and disrupts the desalination map of technologies [4]. Additional technologies that have recently started to gain traction in the modern desalination market appear around this time as well. In the 1950's EDS was first deployed in an industrial process for separating electrolyte solutions after the advances in polymer-based ion exchange materials began to be

produced in the 1930's [233]. In the case of CDI, substantial developments starting in the 1970's have allowed the technology to emerge at bench or pilot scale in the present [151]. Currently, exciting new advances push the frontier of desalination even further through the developments of novel methods such as forward osmosis, membrane distillation, hybrid desalination technologies and methods that incorporate renewable energy sources [5].

Desalination technologies as we know today are a product of daring feats of experimentation, research, and engineering. Both the small contributions and disruptive advances made by graduate students, people like you, have contributed to the developments that we might depend on in the future.

Graduate students are in a fantastic situation for exploration at the frontiers of knowledge. You would already be working in a novel field with many opportunities for collaboration, discussion, and learning. So perhaps one of my best suggestions is to take action.

In my experience, it is hard to implement ideas because in a way or another I feared failure and exploration. Graduate research can be uncomfortable as it shines a light on how little we actually understand. It is easy to get paralyzed, intimidated by the complex theory, and feel reluctant to kickstart the trial-and-error process through which learning, and progress occurs. While developing the metamodels for desalination I delayed the code implementation with the excuse that I did not yet fully understand the process. Unconsciously, I dug deeper into the theory and preparations as a way to prolong taking action. This was very evident in the first pair of metamodels I produced. Eventually, I realized that there is a limited amount

of time and if I was going to produce four additional metamodels (it the end it was six more), I had to face the uncertainty and just give it a try and fail fast. After all, in research, failure is indeed progress.

Let your curiosity guide you. Venture into the unknown, do not be afraid of experimenting.

By failing fast, you will make the fastest progress, which might lead across something disruptive. And in the worst case, the risk of serious consequences is low because your advisor will steer you in the right direction. You are an action away of making significant progress in research. And realize that through your work you contribute to the state of the art that factors into the tremendous advances, such as those expressed in the development of desalination systems.

Chapter 7: Conclusions

Desalination is rapidly becoming a viable alternative for increasing water security for sustaining human activities as well as managing and disposing hypersaline brines. There is an ample variety of desalination systems available in the existing markets and in under research and development. Furthermore, there are many interdependent factors in the desalination process that affect system performance. This makes the decision-making process cumbersome and arbitrary when it comes to choosing an appropriate desalination system, evaluating the performance of existing plants, or guiding new technological developments. The present work addresses these problems through three numerical research objectives aiming to investigate the proposed hypotheses.

7.1. Hypothesis-driven Findings

Per **Hypothesis 1**, the first research objective is accomplished through the development, validation, and integration of metamodels for six relevant desalination methods including TVC, MED and HDH corresponding to the thermal processes, and RO, EDS and CDI corresponding to the molecular transport processes. The models are successfully validated using simulation data from different published studies showing that there is a generalizable underlying system of equations and correlations that accurately describe each studied desalination method under different operation conditions. These models are then integrated into a framework that establishes common input-output structures based on analytical hierarchies. Namely, the General Hierarchy, including parameters that are numerically equivalent across all desalination methods, Family Hierarchy, for

parameters that are numerically equivalent only across the thermal or molecular transport families of desalination methods, and the Specific Hierarchy which includes parameters applicable only within a single desalination method. Numerical investigations show that the models present similar responses for changes in the General Hierarchy and thus, if the parameters are compared across the same analytical hierarchy, cross-comparison is possible. This supports the first hypothesis as there is a common framework that can integrate different desalination models and enable simulation-based cross-comparisons.

Within each family of desalination processes, namely, the thermal and molecular transport, there are two methods that outperform the others. MED and RO, respectively, are the most scalable technologies that currently dominate the market. The literature generally reports performance metrics of these desalination methods in isolation without highlighting intrinsic operation tradeoffs. The developed simulation framework finally enabled an integral cross-comparison of these two methods across continuous product flow rate and feed salinity ranges. The analysis suggests that energy intensity for MED is an order of magnitude greater than RO for the same operational conditions, but actual operational costs are comparable across different feed salinity levels. Therefore, the simulation framework aids decision-making by highlighting the best desalination system that fulfills specific requirements and available energy type at the deployment site.

Per **Hypothesis 2**, after establishing the generalizability of the developed framework with respect to desalination methods and operation conditions, the next research objective aims to validate it using field data. This is achieved by adapting

the MED and RO metamodels to incorporate energy recovery devices commonly used in plants in the field. The resulting MDT and ROX models are validated with literature data before deploying them to simulate actual plants in the field. A recurrent problem in the desalination industry and literature is that not all the parameters required for simulation are usually available. Therefore, a novel semi-supervised methodology that employs the MDT and ROX models along with iterative sampling schemes is proposed to infer the most plausible operation conditions using sparse data. The methodology is deployed in four case studies formed consisting of two MDT and two ROX plants in the field. The resulting simulations show excellent agreement with field data, specifically, the highest percent errors are 5.5% and 2.5% for the MDT plants as well as 6.4% and 9.3% for the ROX plants. Therefore, the results support the second hypotheses as the developed simulation framework meets rigorous validations with data from different desalination plants in the field. Furthermore, the simulation framework can also be used to identify underperforming plants through a novel metric that quantifies how close to ideal recovery a system is.

Per **Hypothesis 3**, the curated and systematized knowledge in desalination modeling incorporated in the simulation framework provides an opportunity for identifying technical gaps within the existing operation field of desalination technologies. The final research objective is achieved by modeling a novel HDH-based system with ZLD capabilities and implementing a simulation-based approach for bounding its performance and identifying a technical niche for operation. First, the operation map of existing desalination technologies is established using the six

metamodels from the first research objective. Such map is constructed by published operation datapoints of plants, models, and bench scale systems in the literature. Then, the developed framework complements this map by establishing optimized operation points within the mapped clusters. The operation bounds of the HDH-ZLD technology are identified through a numerical analysis and the operation ranges are included within the operation map of existing desalination technologies. This shows that the simulation framework is also compatible with first-principles models of developing systems. The results show that the novel system can cater to desalination operation characterized by high recovery rates, high feed salinity, and high energy intensity, that is not completely fulfilled by existing methods. This operation profile is usually encountered in hypersaline brine processing facilities from the fracking industries or specific desalination deployments in remote locations. The results support the third research hypothesis as the results show that the validated framework can enable introduction of novel desalination technologies through numerical analyses to map their operation onto the existing operational space of established desalination systems.

7.2. Summary of Contributions

The complexion of the conducted research demands that the efforts take place in two interrelated fronts. One side relates to the development of the comprehensive analytical framework including the desalination models, underlying computational structure and simulation engine. The other end relates to the validation of the developed framework with actual facility data. The progression of

research through these fronts is not separate, but rather an iterative process that involves going back and forth due to the challenges presented along the way.

The first challenge was encountered during throughout the development of desalination models. Not only the approaches to modeling desalination systems were dissimilar and initially incompatible, but the modeling equations and required parameters were for the most part unavailable. This chaos was resolved by distilling useful equations and curating data from more than 230 references and developing a classification system for desalination methods and process variables. This development made cross-comparison possible across similar analytical hierarchy levels. The next challenge consisted in validating the developed models with the literature because published models are usually tested at a single operation point and the complete set of parameters is undisclosed. Therefore, another iteration in model development was required to incorporate temperature, pressure, and salinity based thermophysical property correlations as well as a broad range of empirical correlations for system components to make their application generalizable. Additional work involved supplementing incomplete input parameters with values available in other studies that simulated plants with similar operation conditions.

The next iteration in the validation front consisted in using actual facility data to further validate the developed models. As foreshadowed by data secrecy in the literature, recruiting desalination plants in the field was extremely challenging. After cold-contacting more than 40 desalination plant manufacturers and users, 4 agreed to serve as case studies and share some data. The obtained data brought along two more challenges to the research, first, the actual desalination systems in

the field employ energy recovery devices and second, the available data was not enough to construct a simulation. Solving this required another major iteration in the development process. Specifically, the developed models for MED and RO had to be modified to include a thermoejector and pressure exchanger, respectively. This resulted in two new models, MDT and ROX, involving new variables for which the simulation framework had to be further adapted. Major developments in optimization algorithms and sampling schemes were undertaken to make the models work with the scarce data from the field. This resulted in a novel semi-supervised algorithm for discovering plausible simulation conditions to reproduce available data.

Extensive validation in the presented research involved compiling and curating a database of operation conditions for the studied desalination systems. These ranges, along with optimized simulations for conventional operation were integrated into an operational map of desalination methods. This is one of the only instances in the literature that defines operational spaces corresponding to each desalination process. In the third research objective, the map was leveraged to introduce a new desalination system that incorporates ZLD and HDH desalination. However, model development of a concept system at early stages in development is difficult since there is no data for appropriate or optimized operation. Solving this involved implementing a model using only first principles such as mass balance of water, air, and salt as well as energy conservation. The resulting model, while not reflecting actual operation of the system, can be used to bound its performance and include it in the map of existing desalination technologies.

The main contributions of the present work are as the following:

Development of the Comprehensive Analytical Framework

- Organizing and systematizing the knowledge in desalination modeling by developing six reduced-order metamodels for different desalination methods including TVC, MED, HDH, RO, EDS, and CDI. The metamodels are validated within 10% error with respect to data from the literature.
- Developing a novel simulation framework that allows for cross-comparative simulations between different desalination methods and/or different operation conditions within a single method. The framework employs a systematic comparison through parameter hierarchies reflected in the input-output structures of the desalination metamodels. The framework is demonstrated through a fully developed cross-comparative analysis between MED and RO desalination.
- Constructing fully deployable models for MDT and ROX desalination systems. These systems incorporate energy recover devices that are common in the field. The models are validated with maximum errors of 8% and 10% with respect to data form the literature.
- Developing mathematical model for a novel HDH-based ZLD system used to bound operational space through physical conservation laws and estimate the thermodynamic states at each point of the process. Additionally, the model is used in conducting a sensitivity analysis for understanding the engineering tradeoffs involved in the new system.

Validation of the Framework with Actual Facility Data

- Introducing a pioneering semi-supervised method that employs the developed MDT and ROX models to simulate operation of actual desalination systems in the field with incomplete input and output datasets. The method makes use of low model runtime and iterative sampling for finding the most plausible operating conditions given the available system data and recovering unknown operation parameters.
- Validating the proposed method using data from four actual desalination plants from the field. Specifically, plant operation can be reproduced within 5.5% and 2.5% for the two MDT plants and 6.4% and 9.3% for the two ROX plants, respectively.
- Introducing a new theoretical efficiency metric used to identify underperforming systems. This efficiency calculation could help plant managers identify underperforming systems and evaluate the need for potential retrofits.
- Proposing deployment opportunities for the novel system within the current operational map of existing desalination technologies. By establishing the operational limits of existing technologies, additional technical niches can be identified to guide new developments.

7.3. Summary of Published Work

This presented work resulted in the following publications available in the public domain:

Journal Papers

- S. A. Romo, N. Mattise, and J. Srebric, "Desalination metamodels and a framework for cross-comparative performance simulations," *Desalination*, vol. 525, no. 1 March 2022, p. 115474, Mar. 2022, doi: 10.1016/j.desal.2021.115474.
- S. A. Romo, M. Storch Jr., and J. Srebric, "Operation Modeling of Actual Desalination Plants," *Desalination,* 2022. Under peer-review.
- S. A. Romo, M. A. Elhashimi Khalifa, B. Abbasi, and J. Srebric, "Mapping of a Novel Zero Liquid Discharge Desalination System based on Humidification-Dehumidification onto the Field of Existing Desalination Technologies," *Water,* Special Issue: Advanced Technologies for Seawater Desalination, 2022, Manuscript Number: water-1707191. Under peer review.

US Department of Energy Report Publications (Contract Number: DE-EE0008402)

- Budget Period 1: Quarterly Reports 1-4
- Budget Period 2: Quarterly Reports 5-8
- Budget Period 3: Quarterly Reports 9-14

Software

- S. A. Romo, N. Mattise, M. Storch, and J. Srebric. (2021). DESAL. PS-2022-017. College Park, MD: UMDCP Office of Technology and Commercialization. Web application available at https://desal.city.umd.edu. Source code available at https://github.com/CITY-at-UMD/Desalination.

Web-Based Publications

- S. A. Romo, N. Mattise, and J. Srebric, "DESAL Program Documentation Version 1.3," *CITY@UMD*, Sep. 2020, url: https://desal.city.umd.edu.

7.4. Future Work

This work pioneers a generalizable approach to desalination modeling that helps bridge gaps in data availability for existing systems, both experimental and well-established ones, and supports future technology developments. The proposed framework lays the foundation for organizing models that were seemingly disconnected and allows numerical evaluations of desalination systems. This section proposes future work for enhancing the current modeling and analytical capabilities of the simulation suite. Specifically, this future work proposal covers:

- Updating Current Models and Including Other Desalination Methods
- Developing Additional Tools
- Leveraging Simulation Data

Updating Current Models and Including Other Desalination Methods

The first avenue for future work consists in updating the existing desalination models according to advances within desalination modeling research. Many of the current metamodels rely on mass and energy transfer coefficients that are calculated through empirical correlations. These include heat transfer coefficients in heat exchangers for thermal based processes, mass transfer coefficients for the thermoejector in TVC and MDT, humidification constants in HDH, concentration polarization in RO and ROX, and limiting current density

calculations in EDS. The developed metamodels compile all the appropriate correlations for each desalination model available in the literature. However, it would be interesting to move away from operation-specific correlations to more generalizable, physics-based expressions. These updates would be particularly important for EDS and CDI metamodels whose current correlations are only valid for single validation points with literature data. Furthermore, the model for the HDH-based ZLD process can be updated as the STEWARD system is developed into a pilot desalination plant.

Additional models for other desalination methods can also be added to the developed framework to increase the impact and applicability of the presented research. These can include mechanical vapor compression, multi-stage flash, forward osmosis, and other important desalination processes. Specifically, multi-stage flash is a well-established desalination process within the thermal family that, although it is being displaced by MED and MDT, has still a considerable market share. Forward osmosis on the other hand is a prominent novel technology that is still in early development stages but shows great potential.

Finally, the modeling methodology disseminated in Chapter 4 focuses on MDT and ROX desalination systems. It is important to highlight that only four facilities agreed to share data out of more than 40 that were contacted. Furthermore, MDT and ROX have the largest market share, so finding any other facility with a different desalination method is difficult and the impact of the research outcomes, therefore, smaller. Although operational data for MDT and ROX was the only data available from desalination plants in the field, it would be interesting to expand the

proposed methodology to the other desalination methods studied in this work. Systems like HDH, EDS and CDI, are not as scalable as MED based and RO based technologies. Nevertheless, having easily deployable simulation tools could facilitate their adoption, particularly with small-scale, decentralized operation requirements.

Developing Additional Tools

Another path for future work consists in constructing new simulation tools over the presented framework. These tasks would take significant development of existing and additional model capabilities. One interesting possibility is to explore options for upgrading the existing case study replication methodology into a fully unsupervised algorithm and calculating a confidence value for the most plausible inferred operation conditions. This would be very valuable as it eliminates the human input and makes the tools more accessible to the broader desalination community.

Most of the existing literature on desalination system modeling assumes steady state operation. Further research towards higher fidelity simulations could involve transient modeling by incorporating time effects the developed steady state metamodels. Data availability for validation currently hampers this possibility. However, dynamic simulations can open new modeling possibilities such as including renewable energy sources, downtime scheduling, and control strategies, which are essential in the deployment of decentralized desalination technologies. One option is integrating transient desalination models into existing software such as the System Advisory Model (SAM) software which provides opportunities for

integration with existing photovoltaic and wind turbine generation, solar collectors, and cash flow models. Another interesting application of transient models is compatibility with existing energy simulation software such as EnergyPlus, which incorporates information from weather data, operation schedules, and cogeneration schemes (power, heating/cooling, water) for incorporating desalination systems in building environments.

Leveraging Simulation Data

The simulation framework, models, and case study replicating algorithms are openly available online as a web-application named DESAL. A final avenue for future work consists in leveraging the data capabilities of the existing simulation suite to build new tools for simulation and guiding new desalination developments. Successful simulations can be saved in the web-application to compile a database of physically and thermodynamically viable operation. Such database could be used to investigate data-driven models and optimization schemes. Data accessibility limits data-driven applications, openly available simulated data can be a starting point for such endeavors. In another application, the operational map of existing desalination technologies developed in Chapter 5 can be disseminated as a live feed that compiles data from successful simulations. This could help establish high value targets or operational niches to direct the development of existing and new desalination technologies.

Appendix A: Supplementary Material for Chapter 3

A1. Model Results and Validation

Table A-1: Thermovapor compression model results and validation.

TVC	Ji et al. [43]*	El-Dessouky [75], [82] Case A: $CR = 2.68$	El-Dessouky [75], [82] Case B: $CR = 1.895$
General Inputs			
Product flow rate, M_d (kg/s)	0.5787 [0%]	1.5	1.5
Intake salinity, C_f (g/kg)	35 [0%]	42 [0%]	42 [0%]
Intake temp. T_{in} (°C)	25 [0%]	25 [0%]	25 [0%]
Family Inputs			
Motive steam pressure, P_s (kPa)	530	1002 [0%]	1002 [0%]
Specific Inputs			
Operating temperature, T_v (°C)	49.61 [1%]	55 [0%]	55 [0%]
Cond. area, A_c (m^2)	30 [0%]	90.66	75.08
Compression ratio, CR	1.85 [0%]	2.68 [0%]	1.895 [0%]
Condenser effectiveness, η_c	1	0.9 [0%]	0.9 [0%]
General Outputs			
Feed water flow rate, M_f (kg/s)	1.3598 [2%]	3.3213	3.4045
Brine flow rate, M_b (kg/s)	0.7811	1.8213	1.9045
Product water salinity, C_p (g/kg)	0 [0%]	0 [0%]	0 [0%]
Brine salinity, C_b (g/kg)	60.93 [2%]	76.59 [9%]	75.08 [7%]
Recovery Ratio, RR	0.4256	0.4516	0.4406
Family Outputs			
Specific energy, E_{des} (kWh/m^3)	239.9	313.33	240.88
Motive steam flow rate, M_p (kg/s)	0.2810 [6%]	0.8845	0.7264
Gain ratio, GOR	2.06 [7%]	1.70 [14%]**	2.07 [13%]**
Sp. cooling water flow rate, sM_{cw} (kg/kg)	11.844 [7%]	11.2967 [43%]**	8.9194 [9%]**
Specific Outputs			
Evap. area, A_e (m^2)	48.16 [3%]	69.95	113.10
Specific area, sA (m^2/kg/s)	135.07	107 [14%]	125.4 [0%]
Intermediate Parameters			
Cooling water flow rate, M_{cw} (kg/s)	6.8539 [7%]	16.95	13.38
Cond. HT Coeff. U_c (kW/m^2°C)	1.8924	1.9101 [3%]	1.9101 [3%]
Evap. HT Coeff. U_e (kW/m^2°C)	2.3893	2.4175 [1%]	2.4175 [1%]

*: Most representative model (code structure and validation)
**: Obtained from figure in the reference

: Parameter value available in the study
[%]: Percent difference

Table A-2 Parallel feed multi-effect distillation model results and validation.

MED	Darwish et al. [64], [101]*, **	El-Dessouky et al. [62] Case A: $N_{eff} = 4$	El-Dessouky et al. [62] Case B: $N_{eff} = 12$	Sharaf et al. [100] Case A: 1st Technique	Sharaf et al. [100] Case B: 2nd Technique	Darwish et al. [86]
General Inputs						
Product flow rate, M_d (kg/s)	137.86 [0%]	60.00	60.00	1.16 [0%]	1.1570 [0%]	52.62 [0%]
Intake salinity, C_f (g/kg)	46 [0%]	42 [0%]	42 [0%]	42 [0%]	42 [0%]	46 [0%]
Intake temp. T_{in} (°C)	28 [0%]	25 [0%]	25 [0%]	25 [0%]	25 [0%]	28 [0%]
Family Inputs						
Motive steam pressure, P_s (kPa)	31.198	19.94 [0%]	143.38 [0%]	38.6 [0%]	1555.1 [0%]	24
Specific Inputs						
Top brine temp. Tbt (°C)	65 [0%]	55	64	73.53 [0%]	88.23 [0%]	64 [0%]
Last effect brine temp. T_b (°C)	38 [0%]	40 [0%]	40 [0%]	40	55	36 [0%]
Feed water temp. T_f (°C)	35 [0%]	35 [0%]	35 [0%]	36.38 [0%]	36.38 [0%]	32.3 [0%]
Brine salinity, C_b (g/kg)	72 [0%]	70 [0%]	70 [0%]	70 [0%]	70 [0%]	69 [0%]
No. effects, N_{eff}	12 [0%]	4 [0%]	12 [0%]	16 [0%]	16 [0%]	4 [0%]
Motive steam flow rate, M_p (kg/s)	14.293 [3%]	17.102	7.848	0.130 [71%]	0.219 [54%]	16.026 [2%]
General Outputs						
Feed water flow rate, M_f (kg/s)	366.85 [4%]	147.26	145.45	2.77 [4%]	2.75 [0%]	150.84 [4%]
Brine flow rate, M_b (kg/s)	234.37 [4%]	88.36	87.27	1.66 [4%]	1.65 [5%]	100.56 [4%]
Product water salinity, C_p (g/kg)	0 [0%]	0 [0%]	0 [0%]	0 [0%]	0 [0%]	0 [0%]
Brine salinity, C_b (g/kg)	72 [0%]	70 [0%]	70 [0%]	70 [0%]	70 [0%]	69 [0%]
Recovery Ratio, RR	0.3758 [4%]	0.4074	0.4125	0.4179 [5%]	0.4204 [5%]	0.3488
Family Outputs						
Specific energy, E_{des} (kWh/m^3)	66.37	184.76	79.99	71.33	99.40	196.4
Motive steam flow rate, M_p (kg/s)	14.293 [3%]	17.102	7.848	0.130 [71%]	0.219 [54%]	16.026 [1%]
Gain ratio, GOR	9.65 [4%]	3.51 [5%]	7.65 [34%]	8.9 [41%]	5.28 [116%]	3.28 [2%]
Sp. cooling water flow rate, sM_{cw} (kg/kg)	4.89	12.52 [4%]	2.46	1.042 [72%]	0.081 [86%]	33.55
Specific Outputs						
Cond. area, A_c (m^2)	4435	2691	877	17 [27%]	3 [77%]	5151.6
Specific area, sA (m^2/kg/s)	280	173 [50%]	222.11 [2%]	214.26 [71%]	97 [78%]	210.38
Intermediate Parameters						
Vapor temp. 1st effect (°C)	64.44 [1%]	54.53	63.50	72.99 [0%]	87.64 [0%]	63.44
Distillate by boiling, M_{sb} (kg/s)	132.47 [1%]	58.91	58.18	1.11	1.10	50.28 [0%]
Distillate by flashing, M_{sf} (kg/s)	5.38 [12%]	1.09	1.82	0.05	0.06	2.33[3%]
Cond. HT coeff. U_c (kW/m^2°C)	1.85	1.85	1.85	1.85	1.91	1.83 [22%]
Mean evap. HT coeff. U_e (kW/m^2°C)	2.40	2.35	2.33	2.33	2.42	2.35 [23%]

*: Most representative model (code structure and validation)
**: Thermophysical properties calculated with salinity, temperature, and pressure dependence. Energy for feed preheating is neglected.

: Parameter value available in the study
[%]: Percent difference

Table A-3: Humidification-dehumidification model results and validation.

HDH	Ettouney [65]*	Sharaqawy [32]	Farsad et al. [111]**
General Inputs			
Product Flow rate, M_d (kg/s)	1.1562 [0%]	0.0028 [0%]	0.0306 [0%]
Intake Salinity, C_f (g/kg)	35	35 [0%]	25
Intake Temp. T_{in} (C)	25 [0%]	30 [0%]	20 [0%]
Family Inputs			
Motive steam pressure, P_s (kPa)	101.4187 [0%]	101.4	101.4
Specific Inputs			
Heater outlet air temperature, T_{high} (°C)	90 [0%]	60 [0%]	51 [0%]
Hum. air inlet temperature, T_{a1} (°C)	25 [0%]	20	25 [0%]
Humidifier outlet air temperature, T_{a2} (°C)	65 [0%]	59	41 [0%]
Condenser outlet air temperature, T_{a3} (°C)	35 [0%]	44.5	28 [0%]
Hum. air inlet rel. hum. φ_1	0.1 [0%]	0.1	0.4 [0%]
Humidifier outlet air rel. hum. φ_2	1 [0%]	0.9 [0%]	1 [0%]
Condenser outlet air rel. hum. φ_3	1 [0%]	0.9 [0%]	1 [0%]
Feed water flow rate, M_f (kg/s)	16.87 [0%]	0.086 [4%]	1 [0%]
Condenser outlet water temp. T_{w1} (°C)	60 [0%]	50	36 [0%]
Cond. HT coeff. U_c (kW/m^2°C)	0.1 [0%]	0.01 [0%]	0.1
Humidifier crossectional area, A_h (m^2)	6.4	0.06 [0%]	0.5
Vapor mass transfer coefficient, k (kg/(sm^3))	0.354 [0%]	0.354	0.0184

General Outputs			
Feed water flow rate, M_f (kg/s)	16.87 [0%]	0.086 [4%]	1.000 [0%]
Brine flow rate, M_b (kg/s)	15.5 [1%]	0.0810 [7%]	0.951 [2%]
Product water salinity, C_p (g/kg)	0 [0%]	0 [0%]	0 [0%]
Brine salinity, C_b (g/kg)	38.16	37.15	26.27
Recovery Ratio, RR	0.0685	0.0326 [0%]	0.0306
Family Outputs			
Specific energy, E_{des} (kWh/m^3)	486.5	339.5 [2%]	550.0
Motive steam flow rate, M_p (kg/s)	0.90 [4%]	0.0015	0.0270
Gain ratio, GOR	1.28 [4%]	1.83 [5%]	1.14
Sp. cooling water flow rate, sM_{cw} (kg/kg)	5.47 [27%]	4.75	14.91
Specific Outputs			
Cond. area, A_c (m^2)	4511 [2%]	69 [490%]	148
Hum. Height, L_h (m)	16.65 [0%]	0.0003 [100%]	4.74 [0%]
Air mass flow rate, M_a (kg/s)	6.90 [0%]	0.0399 [10%]	1.106 [38%]
Total intake water flow rate, M_w (kg/s)	23.19 [6%]	0.0993	1.456

Intermediate Parameters			
Brine temperature, T_{w3} (°C)	34.55 [14%]	19.40	16.70 [57%]
Cooling water flow rate, M_{cw} (kg/s)	6.33 [27%]	0.01	0.456
Heat rate input, Q_{in} (kW)	2037.3 [4%]	3.46 [3%]	60.87 [1%]

*: Most representative model (code structure and validation)

**: Literature values obtained by extracting data from the reference's figures using an open-source software

: Parameter value available in the study

[%]: Percent difference

Table A-4: Reverse osmosis model results and validation.

RO	Zhang [66]*	Mazlan et al. [129]	Altaee [126] Case A: $C_f = 35$	Altaee [126] Case B: $C_f = 38$	Kaghazchi [121] Case A: $M_f = 135$ kg/s	Kaghazchi [121] Case B: $M_f = 1.45$ kg/s
k_{cp} calculation method	[133] $\lambda = 0.47$	[133] $\lambda = 0.47$	[132]	[132]	[127]	[133] $\lambda = 0.47$
General Inputs						
Product flow rate, M_d (kg/s)	2.087 [0%]	1.7842 [0%]	0.3237 [3%]	0.3235 [3%]	38.54 [4%]	0.586 [3%]
Intake salinity, C_f (g/kg)	2 [0%]	35 [0%]	35 [0%]	38 [0%]	45 [0%]	37.76 [0%]
Intake temp. T_{in} (C)	20 [0%]	25	25 [0%]	25 [0%]	25	25
Family Inputs						
Target Recovery ratio, RR	0.6 [0%]	0.50 [0%]	0.3 [0%]	0.3 [0%]	0.3 [0%]	0.41 [0%]
Specific Inputs						
Feed pressure, P_f (bar)	14.2 [0%]	59.5 [0%]	43.58 [0%]	46.1 [0%]	67 [0%]	66 [0%]
Feed velocity, v_f (m/s)	0.7 [0%]	0.3469 [0%]	0.7	0.7	0.7	0.7
Permeate pressure, P_p (bar)	0.3 [0%]	0.3	0.3	0.3	0.3	0.3
Module length, l (m)	1 [0%]	1.01 [0%]	1.01 [0%]***	1.01 [0%]***	1.016 [0%]	1.016 [0%]
Channel width, h (mm)	0.125 [0%]	0.737 [0%]	0.125	0.125	0.593 [0%]	0.593 [0%]
Module area, a (m^2)	32.5 [0%]	35 [0%]	37.2	37.2	35 [0%]	35 [0%]
Module head loss, hl (bar)	0.2 [0%]	0.2	0.2	0.2	0.2	0.2
Module design velocity, v_0 (m/s)	0.5 [0%]	0.5	0.5	0.5	0.5	0.5
Membrane water permeability at 25°C, K_{w25} L/(m^2.h.bar)	7.56 [0%]	1.26 [0%]	1.056 [0%]	1.056 [0%]	1.08 [0%]	1.08 [0%]
Membrane salt permeability at 25°C, K_{s25} (m/h)	0.000614 [0%]	0.0000865 [0%]	0.00007875 [0%]	0.00007875 [0%]	0.0000612 [0%]	0.0000612 [0%]
Temperature coefficient for water transport, K_{wt} (K)	-2849 [0%]	-2849	-2849	-2849	-2849	-2849
Temperature coefficient for salt transport, K_{st} (K)	-3281 [0%]	-3281	-3281	-3281	-3281	-3281
General Outputs						
Feed water flow rate, M_f (kg/s)	3.472	3.5684 [0%]	1.1110 [0%]	1.1110 [0%]	133 [1%]	1.48 [2%]
Brine flow rate, M_b (kg/s)	1.383	1.8312 [3%]	0.7865 [1%]	0.7868 [1%]	95 [0%]	0.887 [5%]
Product water salinity, C_p (g/kg)	0.023	0.285	0.428	0.521	0.341 [4%]	0.149
Brine salinity, C_b (g/kg)	4.99 [0%]	69.696	49.798	54.075	64.119 [0%]	63.872 [1%]
Actual Recovery Ratio, RR	0.6 [0%]	0.50 [0%]	0.3 [0%]	0.3 [0%]	0.3 [0%]	0.41 [0%]
Family Outputs						
Specific energy, E_{des} (kWh/m^3)	0.909	6.7460 [2%]	4.0352	4.2685	6.2037	4.4715
Product salinity, C_p (g/kg)	0.023	0.2846	0.428	0.521	0.341 [4%]	0.149
Specific Outputs						
Number of stages, N_{stage}	2 [0%]	1	1 [0%]	1 [0%]	1 [0%]	1 [0%]
Number of modules, $N_{modules}$	4	12	4 [0%]	4 [0%]	306 [4%]	4 [100%]
System area**, $totalA$ (m^2)	105	399 [5%]	124.5 [7%]	132.4 [11%]	10688 [4%]	133.64 [100%]
Average water flux, J_w (L/(m^{2}h))	71 [1%]	18.18	8.50	7.62	12.20	22.93

*: Most representative model (code structure and validation)
**: Model calculates active area which can be different from the actual system area and is a discrete multiple of the number of modules
***: From actual product datasheet

: Parameter value available in the study
[%]: Percent difference

The limiting current density correlation coefficients in this model are only valid for the electordialysis system that the correlation is developed for. Unfortunately, other studies that could be used for further validation do not disclose the limiting current density correlation form or its corresponding coefficients.

Table A-5: Electrodialisys model results and validation.

ED	Lee et al. [67]*
General Inputs	
Product Flow rate, M_d (kg/s)	4.051 [0%]
Intake Salinity, C_f (g/kg)	3.5 [0%]
Intake Temp. T_{in} (°C)	20
Family Inputs	
Target recovery ratio, RR	0.75 [0%]
Specific Inputs	
Product Concentration, C_d (g/kg)	0.35 [0%]
Linear flow velocity, u (m/s)	0.075 [0%]
Cell thickness, del (m)	0.00065 [0%]
Cell width, w (m)	0.42 [0%]
Length per stack, L_{st} (m)	0.725 [0%]
Anion selective membrane resistance, ρ_a (Ohm.m^2)	0.0004
Cation selective membrane resistance, ρ_c (Ohm.m^2)	0.0003
LCD Constant, a (A.s^{b}m$^{(1-b)}$/keq)	25000 [0%]
LCD Constant, b	0.5 [0%]
Safety factor, s	0.7 [0%]
Volume factor, α	0.8 [0%]
Area factor, β	0.7 [0%]
Current utilization factor, ζ	0.9 [0%]

General Outputs	
Feed water flow rate, M_f (kg/s)	5.401
Brine flow rate, M_b (kg/s)	1.3601
Product water salinity, C_p (g/kg)	0.35 [0%]
Brine salinity, C_b (g/kg)	12.95 [3%]
Actual recovery ratio, RR	0.75 [0%]
Family Outputs	
Specific energy, E_{des} (kWh/m^3)	0.36877 [9%]
Product salinity, C_p (g/kg)	0.350 [0%]
Specific Outputs	
Concentrate feed mass flowrate, M_{fb} (kg/s)	5.4275
Concentrate feed concentration, C_{fb} (g/kg)	9.8 [3%]
Stack current, I_{st} (A)	94.723 [3%]
Stack voltage, U_{st} (V)	81.1 [1%]
Number of cell pairs, N_{cp}	247 [0%]
Number of Stacks, N_{st}	5 [0%]

Intermediate Parameters	
Limiting current density, I_{lim} (A/m^2)	28.703 [3%]
Flow path length, L (m)	3.625 [0%]
Membrane area, A (m2)	752.115 [0%]

*: Most representative model (code structure and validation)

: Parameter value available in the study

[%]: Percent difference

Desalination through capacitive deionization remains a novel but immature technology. Most studies available do not disclose the complete set of operation parameters. Those studies that do disseminate the data present such different channel or electrode designs that the underlying equations cannot be generalized to a reduced-order equation model. Therefore, the capacitive deionization model validated with the study from which the model was originally adapted from until complete data from independent investigations becomes available.

Table A-6: Capacitive deionization model validation.

CDI	Qin et al. [68], [155]* Case A: I_{norm} = 5 A/m^2	Qin et al. [68], [155]* Case B: I_{norm} = 15 A/m^2	Qin et al. [68], [155]* Case C: I_{norm} = 20 A/m^2
General Inputs			
Product Flow rate (per cycle), M_d (kg/s)	6.1385e-5	6.1385e-5	6.1385e-5
Intake Salinity, C_f (g/kg)	2 [0%]	2 [0%]	2 [0%]
Intake Temp. T_{in} (°C)	25	25	25
Family Inputs			
Target recovery ratio, RR	0.5 [0%]	0.5 [0%]	0.5 [0%]
Specific Inputs			
Normalized Current, I_{norm} (A/m^2)	5 [0%]	15 [0%]	20 [0%]
Normalized Capacitance, C_{norm} (F/g)	60 [0%]	60 [0%]	60 [0%]
Normalized Internal resistance, s_{norm} (Ohm.m^2)	0.02 [0%]	0.02 [0%]	0.02 [0%]
Normalized electrode resistance, $R_{2,norm}$ (Ohm.m^2)	0.09 [0%]	0.09 [0%]	0.09 [0%]
Electrode area density, m (g/m^2)	89 [0%]	89 [0%]	89 [0%]
Charging step time, t_charge (s)	300 [0%]	300 [0%]	300 [0%]
CDI Stack volume, V_{cdi} (L)	0.02 [0%]	0.02 [0%]	0.02 [0%]
Channel thickness, l (mm)	0.10 [0%]	0.10 [0%]	0.10 [0%]
Charge efficiency, η_{charge}	0.8 [0%]	0.8 [0%]	0.8 [0%]
Discharging efficiency, $\eta_{discharging}$	1 [0%]	1 [0%]	1 [0%]
Max. Salt adsorption capacity, SAC (mg/g)	30 [0%]	30 [0%]	30 [0%]
Electrode area, A_e (m^2)	0.011	0.011	0.011
Channel cross-sectional area, A_c (m^2)	0.022097	0.022097	0.022097
General Outputs			
Feed water flow rate, (per cycle) M_f (kg/s)	1.2277e-04	1.2277e-04	1.2277e-04
Brine flow rate (per cycle), M_b (kg/s)	6.1385e-05	6.1385e-05	6.1385e-05
Product water salinity, C_p (g/kg)	1.5664	0.69825	0.26375
Brine salinity, C_b (g/kg)	2.1764	2.535	2.7663
Actual recovery ratio, RR	0.5 [0%]	0.5 [0%]	0.5 [0%]
Family Outputs			
Specific energy, E_{des} (kWh/m^3)	0.06 [5%]	0.56 [8%]	1.21 [33%]
Product salinity, C_p (g/kg)	1.5664	0.6982	0.26375
Specific Outputs			
Peak Voltage, (V)	0.32 [0%]	1.029	1.6 [23%]
Intermediate Parameters			
Channel Water flux, (L/mh)	10.017 [2%]	10.017 [2%]	10.017 [2%]

*: Most representative model (code structure and validation)

: Disclosed in the study
[%]: Percent Difference

Appendix B: Supplementary Material for Chapter 4

B1. ERD Impact on MED and RO Systems

Table B-1: ERD Impact on MED (MDT)

Inputs	Validation Data [95]	MDT (with ERD) Model Outputs	MDT (with ERD) % Err	MED (no ERD) Model Outputs	MED (no ERD) % Err	% Diff
Product flow rate, (kg/s)	104.17	104.17	0.0	104.17	0.0	0.0
Intake salinity, (g/kg)	40	40	0.0	40	0.0	0.0
Intake temp. (°C)	[10, 22]	22		22		0.0
Motive steam pressure, (kPa)	4500.0	4500	0.0	4500	0.0	0.0
Top brine temp. (°C)		63		63		0.0
Last effect brine temp. (°C)		38		38		0.0
Feed water temp. (°C)	[35, 55]	36		36		0.0
Brine salinity, (g/kg)	59.9	59.9	0.0	59.9	0.0	0.0
No. effects,	12	12	0.0	12	0.0	0.0
Motive steam flow rate, (kg/s)	6.25	6.25	0.0	12.545	100.7	100.7
Mixed steam sat. temp, (°C)	64.5	64.5	0.0	64.5	0.0	0.0
Entrained vapor target flow rate, (kg/s)	0.4167	0.4167	0.0	0.4167	0.0	0.0
Condenser effectiveness		0.69		0.69		0.0
General Outputs						
Product flow rate, (kg/s)	104.17	105.6	1.4	104.2	0.0	1.4
Feed water flow rate, (kg/s)	314.0	298.6	4.9	301.5	4.0	0.9
Brine flow rate, (kg/s)	209.7	192.6	8.2	201.3	4.0	4.5
Product water salinity, (g/kg)	< 0.1	0		0		
Feed water salinity, (g/kg)	40	40	0.0	40	0.0	0.0
Brine salinity, (g/kg)	59.9	59.9	0.0	59.9	0.0	0.0
Specific energy, (kWh/m^3)		43.6		55.5		27.4
Recovery ratio,	0.3317	0.3536	6.6	0.3456	4.2	2.3
Family Outputs						
Motive steam flow rate, (kg/s)	6.250	6.25	0.0	12.545	100.7	100.7
Gain ratio,	16.7	16.9	1.4	8.3	50.2	50.9
Sp. cooling water flow rate, (kg/kg)	0.40	0.41	1.7	1.60	301.3	294.5
Specific Outputs						
Cond. area, (m^2)		2070		2454		18.6
Specific area, (m^2/kg/s)		312		372		19.2
Intermediate Parameters						
Vapor temp. 1st effect (°C)	62.2	62.5	0.5	62.5	0.5	0.0

Vapor temp. last effect (°C)	37	38	1.6	38	1.6	0.0
Distillate by boiling, (kg/s)		99.2		100.1		0.9
Distillate by flashing, (kg/s)		6.8		4.0		41.0
Cooling water flow rate (kg/s)	41.56	42.86	3.1	166.78	301.3	289.1
Cond. HT coeff. ($kW/m^2°C$)		1.9		1.8		0.2
Mean evap. HT Coeff. ($kW/m^2°C$)		2.3		2.5		7.5

Table B-2: ERD Impact on RO (ROX)

Inputs	Validation Data [187]	ROX (with ERD) Model Outputs	ROX (with ERD) % Err	RO (no ERD) Model Outputs	RO (no ERD) % Err	% Diff
Product flow rate, (kg/s)	56.11	56.11	0.0	56.11	0.0	0.0
Intake salinity, (g/kg)	[13, 35]	29.5		29.5		0.0
Intake temp. (°C)	25	25	0.0	25	0.0	0.0
Recovery ratio	0.473382266	0.47	0.7	0.47	0.7	0.0
Feed pressure (bar)	60.3	60.3	0.0	60.3	0.0	0.0
Feed velocity (m/s)		0.25		0.25		0.0
Permeate pressure (bar)		0.3		0.3		0.0
Max pressure (bar)		83		83		0.0
Max temperature (°C)		45		45		0.0
Module length (m)		1.01		1.01		0.0
Channel thickness (mm)		0.8		0.8		0.0
Module area (m^2)		37.2		37.2		0.0
Module head loss (bar)		0.15		0.15		0.0
Design velocity (m/s)		0.5		0.5		0.0
Water permeability at 25°C ($L/(m^2.h.bar)$)		1.056		1.056		0.0
Salt permeability at 25°C (m/h)		0.00007875		0.00007875		0.0
Water permeability correction constant (K)		-2849		-2849		0.0
Salt permeability correction constant (K)		-3281		-3281		0.0
Pump efficiency		1		1		0.0
Motor efficiency		1		1		0.0
PX efficiency	0.966	0.966	0.0	0.966	0.0	0.0
PX fraction	0.5257	0.5257	0.0	0.5257	0.0	0.0
General Outputs						
Product flow rate, (kg/s)	56.11	54.74	2.4	54.79	2.3	0.1
Feed water flow rate, (kg/s)	118.53	119.42	0.8	119.38	0.7	0.0
Brine flow rate, (kg/s)	62.42	64.53	3.4	64.44	3.2	0.1
Product water salinity, (g/kg)	0.341	0.307	10.0	0.297	12.9	3.2
Feed water salinity, (g/kg)	30.6	29.5	3.6	29.5	3.6	0.0
Brine salinity, (g/kg)	57.8	56.2	2.7	55.4	4.1	1.4
Specific energy, (kWh/m3)		1.67		3.56		112.8
Family Outputs						
Actual Recovery Ratio	0.473	0.470	0.7	0.470	0.6	0.1
Specific Outputs						

Number of Stages		1		1		0.0
Number of Modules	308	337	9.4	329	6.8	2.4
Total system area (m^2)		12500		12208		2.3
Average Flux ($L/m^2.h$)		15.78		16.20		2.7
Brine Pressure (bar)	59.4	59.9	0.8	59.9	0.8	0.0
Feed Stream PX Salinity (g/kg)	30.15	30.35	0.7	n/a		

References

[1] N. C. Darre and G. S. Toor, "Desalination of Water: a Review," *Curr. Pollut. Reports*, vol. 4, no. 2, pp. 104–111, Jun. 2018, doi: 10.1007/s40726-018-0085-9.

[2] E. Jones, M. Qadir, M. T. H. van Vliet, V. Smakhtin, and S. Kang, "The state of desalination and brine production: A global outlook," *Sci. Total Environ.*, vol. 657, pp. 1343–1356, Mar. 2019, doi: 10.1016/j.scitotenv.2018.12.076.

[3] EPA, "Water Conservation at EPA," *Greening EPA*, 2020. https://www.epa.gov/greeningepa/water-conservation-epa (accessed Jan. 20, 2021).

[4] J. Eke, A. Yusuf, A. Giwa, and A. Sodiq, "The global status of desalination: An assessment of current desalination technologies, plants and capacity," *Desalination*, vol. 495, no. March, p. 114633, Dec. 2020, doi: 10.1016/j.desal.2020.114633.

[5] F. E. Ahmed, A. Khalil, and N. Hilal, "Emerging desalination technologies: Current status, challenges and future trends," *Desalination*, vol. 517, no. July, p. 115183, 2021, doi: 10.1016/j.desal.2021.115183.

[6] L. Nthunya, S. Maifadi, B. Mamba, A. Verliefde, and S. Mhlanga, "Spectroscopic Determination of Water Salinity in Brackish Surface Water in Nandoni Dam, at Vhembe District, Limpopo Province, South Africa," *Water*, vol. 10, no. 8, p. 990, Jul. 2018, doi: 10.3390/w10080990.

[7] Y. Xia *et al.*, "A self-rotating solar evaporator for continuous and efficient desalination of hypersaline brine," *J. Mater. Chem. A*, vol. 8, no. 32, pp. 16212–16217, 2020, doi: 10.1039/d0ta04677a.

[8] D. M. Davenport, A. Deshmukh, J. R. Werber, and M. Elimelech, "High-Pressure Reverse Osmosis for Energy-Efficient Hypersaline Brine Desalination: Current Status, Design Considerations, and Research Needs," *Environ. Sci. Technol. Lett.*, vol. 5, no. 8, pp. 467–475, Aug. 2018, doi: 10.1021/acs.estlett.8b00274.

[9] D. Sharma *et al.*, "Development of an anti-clogging perforated plate atomizer for a zero liquid discharge humidification-dehumidification desalination system," *Desalination*, vol. 515, no. June, p. 115195, 2021, doi: 10.1016/j.desal.2021.115195.

[10] L. Yang *et al.*, "Photovoltaic-multistage desalination of hypersaline waters for simultaneous electricity, water and salt harvesting via automatic rinsing," *Nano Energy*, vol. 87, no. May, p. 106163, 2021, doi: 10.1016/j.nanoen.2021.106163.

[11] P. Rao *et al.*, “Energy considerations associated with increased adoption of seawater desalination in the United States,” *Desalination*, vol. 445, no. August, pp. 213–224, Nov. 2018, doi: 10.1016/j.desal.2018.08.014.

[12] A. Panagopoulos, K. J. Haralambous, and M. Loizidou, “Desalination brine disposal methods and treatment technologies - A review,” *Sci. Total Environ.*, vol. 693, p. 133545, 2019, doi: 10.1016/j.scitotenv.2019.07.351.

[13] H. Elcik *et al.*, “Multi-effect distillation brine treatment by membrane distillation: Effect of antiscalant and antifoaming agents on membrane performance and scaling control,” *Desalination*, vol. 493, no. August, 2020, doi: 10.1016/j.desal.2020.114653.

[14] M. N. Soliman, F. Z. Guen, S. A. Ahmed, H. Saleem, M. J. Khalil, and S. J. Zaidi, “Energy consumption and environmental impact assessment of desalination plants and brine disposal strategies,” *Process Saf. Environ. Prot.*, vol. 147, pp. 589–608, 2021, doi: 10.1016/j.psep.2020.12.038.

[15] A. Pistocchi, T. Bleninger, and C. Dorati, “Screening the hurdles to sea disposal of desalination brine around the Mediterranean,” *Desalination*, vol. 491, no. May, p. 114570, 2020, doi: 10.1016/j.desal.2020.114570.

[16] I. Sola *et al.*, “Sustainable desalination: Long-term monitoring of brine discharge in the marine environment,” *Mar. Pollut. Bull.*, vol. 161, no. October, 2020, doi: 10.1016/j.marpolbul.2020.111813.

[17] R. Riera, F. Tuya, A. Sacramento, E. Ramos, M. Rodríguez, and Ó. Monterroso, “The effects of brine disposal on a subtidal meiofauna community,” *Estuar. Coast. Shelf Sci.*, vol. 93, no. 4, pp. 359–365, 2011, doi: 10.1016/j.ecss.2011.05.001.

[18] N. Ahmad and R. E. Baddour, “A review of sources, effects, disposal methods, and regulations of brine into marine environments,” *Ocean Coast. Manag.*, vol. 87, pp. 1–7, 2014, doi: 10.1016/j.ocecoaman.2013.10.020.

[19] S. Ahirrao, *Zero Liquid Discharge Solutions*. Elsevier Ltd., 2014. doi: 10.1016/B978-0-08-099968-5.00013-1.

[20] Muhammad Yaqub and W. Lee, “Zero-liquid discharge (ZLD) technology for resource recovery from wastewater: A review,” *Sci. Total Environ.*, vol. 681, pp. 551–563, 2019, doi: 10.1016/j.scitotenv.2019.05.062.

[21] A. Panagopoulos, “Techno-economic assessment of zero liquid discharge (ZLD) systems for sustainable treatment, minimization and valorization of seawater brine,” *J. Environ. Manage.*, vol. 306, no. December 2021, p. 114488, 2022, doi: 10.1016/j.jenvman.2022.114488.

[22] G. Cipolletta, N. Lancioni, Ç. Akyol, A. L. Eusebi, and F. Fatone, “Brine

treatment technologies towards minimum/zero liquid discharge and resource recovery: State of the art and techno-economic assessment," *J. Environ. Manage.*, vol. 300, no. May, p. 113681, 2021, doi: 10.1016/j.jenvman.2021.113681.

[23] A. Al-Karaghouli and L. L. Kazmerski, "Energy consumption and water production cost of conventional and renewable-energy-powered desalination processes," *Renew. Sustain. Energy Rev.*, vol. 24, pp. 343–356, Aug. 2013, doi: 10.1016/j.rser.2012.12.064.

[24] Y. Ghalavand, M. S. Hatamipour, and A. Rahimi, "A review on energy consumption of desalination processes," *Desalin. Water Treat.*, vol. 54, no. 6, pp. 1–16, Mar. 2014, doi: 10.1080/19443994.2014.892837.

[25] D. E. López and J. P. Trembly, "Desalination of hypersaline brines with joule-heating and chemical pre-treatment: Conceptual design and economics," *Desalination*, vol. 415, no. March, pp. 49–57, 2017, doi: 10.1016/j.desal.2017.04.003.

[26] I. Prihatiningtyas, A. H. A. H. Al-Kebsi, Y. Hartanto, T. M. Zewdie, and B. Van der Bruggen, "Techno-economic assessment of pervaporation desalination of hypersaline water," *Desalination*, vol. 527, no. December 2021, p. 115538, 2022, doi: 10.1016/j.desal.2021.115538.

[27] S. Dehghani, A. Date, and A. Akbarzadeh, "An experimental study of brine recirculation in humidification-dehumidification desalination of seawater," *Case Stud. Therm. Eng.*, vol. 14, no. December 2018, 2019, doi: 10.1016/j.csite.2019.100463.

[28] V. Haluch, E. F. Zanoelo, and C. J. L. Hermes, "Experimental evaluation and semi-empirical modeling of a small-capacity reverse osmosis desalination unit," *Chem. Eng. Res. Des.*, vol. 122, pp. 243–253, Jun. 2017, doi: 10.1016/j.cherd.2017.04.006.

[29] R. Zhao, S. Porada, P. M. Biesheuvel, and A. van der Wal, "Energy consumption in membrane capacitive deionization for different water recoveries and flow rates, and comparison with reverse osmosis," *Desalination*, vol. 330, pp. 35–41, Dec. 2013, doi: 10.1016/j.desal.2013.08.017.

[30] A. Joseph and V. Damodaran, "Dynamic simulation of the reverse osmosis process for seawater using LabVIEW and an analysis of the process performance," *Comput. Chem. Eng.*, vol. 121, pp. 294–305, 2019, doi: 10.1016/j.compchemeng.2018.11.001.

[31] B. P.M., V. L. B., and V. D. W. A., "Dynamic adsorption/desorption process model for capacitive deionization," *J. Phys. Chem. C*, vol. 113, no. 14, pp. 5636–5640, 2009, doi: 10.1021/jp809644s.

[32] M. H. Sharqawy, M. A. Antar, S. M. Zubair, and A. M. Elbashir, “Optimum thermal design of humidification dehumidification desalination systems,” *Desalination*, vol. 349, pp. 10–21, 2014, doi: 10.1016/j.desal.2014.06.016.

[33] N. C. Wright, S. R. Shah, S. E. Amrose, and A. G. Winter, “A robust model of brackish water electrodialysis desalination with experimental comparison at different size scales,” *Desalination*, vol. 443, no. April, pp. 27–43, 2018, doi: 10.1016/j.desal.2018.04.018.

[34] M. K. Mansour and H. E. Fath, “A new and practical ε-NTU correlation for the humidification process under different Lewis number,” *Desalination*, vol. 395, pp. 72–78, 2016, doi: 10.1016/j.desal.2016.05.025.

[35] S. M. A. N. R. Abadi and R. Kouhikamali, “CFD-aided mathematical modeling of thermal vapor compressors in multiple effects distillation units,” *Appl. Math. Model.*, vol. 40, no. 15–16, pp. 6850–6868, 2016, doi: 10.1016/j.apm.2016.02.032.

[36] P. Behnam, M. Faegh, and M. Khiadani, “A review on state-of-the-art applications of data-driven methods in desalination systems,” *Desalination*, vol. 532, no. April, p. 115744, 2022, doi: 10.1016/j.desal.2022.115744.

[37] M. M. Farid, S. Parekh, J. R. Selman, and S. Al-Hallaj, “Solar desalination with a humidification-dehumidification cycle: Mathematical modeling of the unit,” *Desalination*, vol. 151, no. 2, pp. 153–164, 2003, doi: 10.1016/S0011-9164(02)00994-3.

[38] M. A. Sharaf, A. S. Nafey, and L. García-Rodríguez, “Thermo-economic analysis of solar thermal power cycles assisted MED-VC (multi effect distillation-vapor compression) desalination processes,” *Energy*, vol. 36, no. 5, pp. 2753–2764, 2011, doi: 10.1016/j.energy.2011.02.015.

[39] M. W. Saleem and W. S. Kim, “Parameter-based performance evaluation and optimization of a capacitive deionization desalination process,” *Desalination*, vol. 437, no. February, pp. 133–143, 2018, doi: 10.1016/j.desal.2018.02.023.

[40] K. M. Chehayeb, D. M. Farhat, K. G. Nayar, and J. H. Lienhard, “Optimal design and operation of electrodialysis for brackish-water desalination and for high-salinity brine concentration,” *Desalination*, vol. 420, no. March, pp. 167–182, Oct. 2017, doi: 10.1016/j.desal.2017.07.003.

[41] Y. Tanaka, “Irreversible thermodynamics and overall mass transport in ion-exchange membrane electrodialysis,” *J. Memb. Sci.*, vol. 281, no. 1–2, pp. 517–531, 2006, doi: 10.1016/j.memsci.2006.04.022.

[42] R. S. El-Emam and I. Dincer, “Thermodynamic and thermoeconomic analyses of seawater reverse osmosis desalination plant with energy

recovery," *Energy*, vol. 64, pp. 154–163, Jan. 2014, doi: 10.1016/j.energy.2013.11.037.

[43] J. G. Ji, R. Z. Wang, L. X. Li, and H. Ni, "Simulation and analysis of a single-effect thermal vapor-compression desalination system at variable operation conditions," *Chem. Eng. Technol.*, vol. 30, no. 12, pp. 1633–1641, 2007, doi: 10.1002/ceat.200700303.

[44] M. Ali, M. El Haj, E. Taha, and B. Soudan, "Recent progress in the use of renewable energy sources to power water desalination plants," *Desalination*, vol. 435, no. November 2017, pp. 97–113, 2018, doi: 10.1016/j.desal.2017.11.018.

[45] S. Loutatidou and H. A. Arafat, "Techno-economic analysis of MED and RO desalination powered by low-enthalpy geothermal energy," *Desalination*, vol. 365, pp. 277–292, 2015, doi: 10.1016/j.desal.2015.03.010.

[46] M. Methnani, "Influence of fuel costs on seawater desalination options," *Desalination*, vol. 205, no. 1–3, pp. 332–339, 2007, doi: 10.1016/j.desal.2006.02.058.

[47] D. Brogioli, F. La Mantia, and N. Y. Yip, "Thermodynamic analysis and energy efficiency of thermal desalination processes," *Desalination*, vol. 428, no. July 2017, pp. 29–39, Feb. 2018, doi: 10.1016/j.desal.2017.11.010.

[48] M. T. Ali, H. E. S. Fath, and P. R. Armstrong, "A comprehensive techno-economical review of indirect solar desalination," *Renew. Sustain. Energy Rev.*, vol. 15, no. 8, pp. 4187–4199, Oct. 2011, doi: 10.1016/j.rser.2011.05.012.

[49] K. V. Reddy and N. Ghaffour, "Overview of the cost of desalinated water and costing methodologies," *Desalination*, vol. 205, no. 1–3, pp. 340–353, Feb. 2007, doi: 10.1016/j.desal.2006.03.558.

[50] S. Ahmadvand, B. Abbasi, B. Azarfar, M. Elhashimi, X. Zhang, and B. Abbasi, "Looking Beyond Energy Efficiency: An Applied Review of Water Desalination Technologies and an Introduction to Capillary-Driven Desalination," *Water*, vol. 11, no. 4, p. 696, Apr. 2019, doi: 10.3390/w11040696.

[51] Z. Wang, Y. Wang, G. Xu, and J. Ren, "Sustainable desalination process selection: Decision support framework under hybrid information," *Desalination*, vol. 465, no. January, pp. 44–57, Sep. 2019, doi: 10.1016/j.desal.2019.04.022.

[52] R. Semiat, "Energy Issues in Desalination Processes," *Environ. Sci. Technol.*, vol. 42, no. 22, pp. 8193–8201, Nov. 2008, doi: 10.1021/es801330u.

[53] T. Altmann, J. Robert, A. Bouma, J. Swaminathan, and J. H. Lienhard, "Primary energy and exergy of desalination technologies in a power-water cogeneration scheme," *Appl. Energy*, vol. 252, no. January, p. 113319, Oct. 2019, doi: 10.1016/j.apenergy.2019.113319.

[54] G. P. Thiel, E. W. Tow, L. D. Banchik, H. W. Chung, and J. H. Lienhard, "Energy consumption in desalinating produced water from shale oil and gas extraction," *Desalination*, vol. 366, pp. 94–112, Jun. 2015, doi: 10.1016/j.desal.2014.12.038.

[55] N. C. Wright and A. G. Winter, "Justification for community-scale photovoltaic-powered electrodialysis desalination systems for inland rural villages in India," *Desalination*, vol. 352, pp. 82–91, 2014, doi: 10.1016/j.desal.2014.07.035.

[56] K. Mistry and J. Lienhard, "Generalized Least Energy of Separation for Desalination and Other Chemical Separation Processes," *Entropy*, vol. 15, no. 12, pp. 2046–2080, May 2013, doi: 10.3390/e15062046.

[57] M. H. Sharqawy, J. H. Lienhard, and S. M. Zubair, "Thermophysical properties of seawater: a review of existing correlations and data," *Desalin. Water Treat.*, vol. 16, no. 1–3, pp. 354–380, Apr. 2010, doi: 10.5004/dwt.2010.1079.

[58] K. G. Nayar, M. H. Sharqawy, L. D. Banchik, and J. H. Lienhard, "Thermophysical properties of seawater: A review and new correlations that include pressure dependence," *Desalination*, vol. 390, pp. 1–24, 2016, doi: 10.1016/j.desal.2016.02.024.

[59] I. Foxboro, "Conductivity Ordering Guide," *Price Sheet*. Invensys Foxboro, Foxboro, Massachusetts, pp. 1–2, 1999.

[60] H. Ucok, I. Ershaghi, and G. R. Olhoeft, "Electrical Resistivity of Geothermal Brines," *J. Pet. Technol.*, vol. 32, no. 04, pp. 717–727, Apr. 1980, doi: 10.2118/7878-PA.

[61] M. Holmgren, "X Steam, Thermodynamic properties of water and steam." MATLAB Central File Exchange, 2007. [Online]. Available: https://www.mathworks.com/matlabcentral/fileexchange/9817-x-steam-thermodynamic-properties-of-water-and-steam

[62] H. T. El-Dessouky and H. M. Ettouney, *Fundamentals of Salt Water Desalination*, 1st ed. Elsevier Science Ltd., 2002. doi: 10.1016/B978-044450810-2/50008-7.

[63] A. Picard, R. S. Davis, M. Gläser, and K. Fujii, "Revised formula for the density of moist air (CIPM-2007)," *Metrologia*, vol. 45, no. 2, pp. 149–155, Apr. 2008, doi: 10.1088/0026-1394/45/2/004.

[64] M. A. Darwish, F. Al-Juwayhel, and H. K. Abdulraheim, “Multi-effect boiling systems from an energy viewpoint,” *Desalination*, vol. 194, no. 1–3, pp. 22–39, 2006, doi: 10.1016/j.desal.2005.08.029.

[65] H. Ettouney, “Design and analysis of humidification dehumidification desalination process,” *Desalination*, vol. 183, no. 1–3, pp. 341–352, 2005, doi: 10.1016/j.desal.2005.03.039.

[66] J. Zhang, “Computational Modeling and Evaluation of Reverse Osmosis,” Stanford University, 2015.

[67] H. J. Lee, F. Sarfert, H. Strathmann, and S. H. Moon, “Designing of an electrodialysis desalination plant,” *Desalination*, vol. 142, no. 3, pp. 267–286, 2002, doi: 10.1016/S0011-9164(02)00208-4.

[68] M. Qin *et al.*, “Comparison of energy consumption in desalination by capacitive deionization and reverse osmosis,” *Desalination*, vol. 455, no. November 2018, pp. 100–114, 2019, doi: 10.1016/j.desal.2019.01.003.

[69] S. A. Romo, N. W. Mattise, and J. Srebric, “DESAL,” *City@UMD & The University of Maryland, College Park*, 2021. https://desal.city.umd.edu/

[70] W. EI-Mudir, “Performance evaluation of a small size TVC desalination plant,” *Desalination*, vol. 165, pp. 269–279, 2004, doi: 10.1016/j.desa1.2004.06.031.

[71] N. M. Al-Najem, M. A. Darwish, and F. A. Youssef, “Thermovapor compression desalters: energy and availability — Analysis of single- and multi-effect systems,” *Desalination*, vol. 110, no. 3, pp. 223–238, Sep. 1997, doi: 10.1016/S0011-9164(97)00101-X.

[72] S. Shen, S. Zhou, Y. Yang, L. Yang, and X. Liu, “Study of steam parameters on the performance of a TVC-MED desalination plant,” *Desalin. Water Treat.*, vol. 33, no. 1–3, pp. 300–308, Sep. 2011, doi: 10.5004/dwt.2011.2653.

[73] A. M. Bonanos, “Physical modeling of thermo-compressor for desalination applications,” *Desalination*, vol. 412, pp. 13–19, 2017, doi: 10.1016/j.desal.2017.03.004.

[74] A. O. Bin Amer, “Development and optimization of ME-TVC desalination system,” *Desalination*, vol. 249, no. 3, pp. 1315–1331, Dec. 2009, doi: 10.1016/j.desal.2009.06.026.

[75] H. El-Dessouky, “Modelling and simulation of the thermal vapour compression desalination process,” in *Nuclear Desalination of Sea Water*, 1997, pp. 315–338. [Online]. Available: https://inis.iaea.org/search/search.aspx?orig_q=RN:29023185

[76] R. R. B. Power, *Steam jet ejectors for the process industries.*, Second Edi. New York: McGraw-Hill Inc., 1994. [Online]. Available: http://www.osti.gov/scitech/biblio/6770303

[77] A. S. Hassan and M. A. Darwish, "Performance of thermal vapor compression," *Desalination*, vol. 335, no. 1, pp. 41–46, 2014, [Online]. Available: http://www.scopus.com/inward/record.url?eid=2-s2.0-84891656599&partnerID=40&md5=f6bb7d386d150da22dbd809b3ec3ca5a

[78] H. El-Dessouky, I. Alatiqi, S. Bingulac, and H. Ettouney, "Steady-state analysis of the multiple effect evaporation desalination process," *Chem. Eng. Technol.*, vol. 21, no. 5, pp. 437–451, 1998, doi: 10.1002/(SICI)1521-4125(199805)21:5<437::AID-CEAT437>3.0.CO;2-D.

[79] M. A. Darwish, "Thermal analysis of vapor compression desalination system," *Desalination*, vol. 69, no. 3, pp. 275–295, Jan. 1988, doi: 10.1016/0011-9164(88)80030-4.

[80] F. Al-Juwayhel, H. El-Dessouky, and H. Ettouney, "Analysis of single-effect evaporator desalination systems combined with vapor compression heat pumps," *Desalination*, vol. 114, no. 3, pp. 253–275, 1997, doi: 10.1016/S0011-9164(98)00017-4.

[81] H. T. El-Dessouky, I. M. Alatiqi, H. M. Ettouney, and N. S. Al-Deffeeri, "Performance of wire mesh mist eliminator," *Chem. Eng. Process. Process Intensif.*, vol. 39, no. 2, pp. 129–139, 2000, doi: 10.1016/S0255-2701(99)00033-1.

[82] H. El-Dessouky and H. Ettouney, "Single-effect thermal vapor-compression desalination process: Thermal analysis," *Heat Transf. Eng.*, vol. 20, no. 2, pp. 52–68, 1999, doi: 10.1080/014576399271583.

[83] K. H. Mistry, M. A. Antar, and J. H. Lienhard V, "An improved model for multiple effect distillation," *Desalin. Water Treat.*, vol. 51, no. 4–6, pp. 807–821, Jan. 2013, doi: 10.1080/19443994.2012.703383.

[84] M. Alahmad, "Factors Affecting Scale Formation in Sea Water Environments – An Experimental Approach," *Chem. Eng. Technol.*, vol. 31, no. 1, pp. 149–156, Jan. 2008, doi: 10.1002/ceat.200700062.

[85] M. Al-Ahmad and F. A. Aleem, "Scale formation and fouling problems and their predicted reflection on the performance of desalination plants in Saudi Arabia," *Desalination*, vol. 96, no. 1–3, pp. 409–419, Jun. 1994, doi: 10.1016/0011-9164(94)85190-5.

[86] M. A. Darwish and H. K. Abdulrahim, "Feed water arrangements in a multi-effect desalting system," *Desalination*, vol. 228, no. 1–3, pp. 30–54, 2008,

doi: 10.1016/j.desal.2007.05.039.

[87] P. Palenzuela, A. S. Hassan, G. Zaragoza, and D. C. Alarcón-Padilla, “Steady state model for multi-effect distillation case study: Plataforma Solar de Almería MED pilot plant,” *Desalination*, vol. 337, no. 1, pp. 31–42, 2014, doi: 10.1016/j.desal.2013.12.029.

[88] F. N. Alasfour, M. A. Darwish, and A. O. Bin Amer, “Thermal analysis of ME-TVC+MEE desalination systems,” *Desalination*, vol. 174, no. 1, pp. 39–61, 2005, doi: 10.1016/j.desal.2004.08.039.

[89] S. Casimiro, J. Cardoso, C. Ioakimidis, J. Farinha Mendes, C. Mineo, and A. Cipollina, “MED parallel system powered by concentrating solar power (CSP). Model and case study: Trapani, Sicily,” *Desalin. Water Treat.*, vol. 55, no. 12, pp. 3253–3266, 2015, doi: 10.1080/19443994.2014.940222.

[90] M. Shakouri, H. Ghadamian, and R. Sheikholeslami, “Optimal model for multi effect desalination system integrated with gas turbine,” *Desalination*, vol. 260, no. 1–3, pp. 254–263, 2010, doi: 10.1016/j.desal.2010.03.032.

[91] B. Ortega-Delgado, P. Palenzuela, and D. C. Alarcón-Padilla, “Parametric study of a multi-effect distillation plant with thermal vapor compression for its integration into a Rankine cycle power block,” *Desalination*, vol. 394, pp. 18–29, 2016, doi: 10.1016/j.desal.2016.04.020.

[92] H. T. El-Dessouky and H. M. Ettouney, “Multiple-effect evaporation desalination systems: Thermal analysis,” *Desalination*, vol. 125, no. 1–3, pp. 259–276, 1999, doi: 10.1016/S0011-9164(99)00147-2.

[93] M. Ameri, S. S. Mohammadi, M. Hosseini, and M. Seifi, “Effect of design parameters on multi-effect desalinationsystem specifications,” *Desalination*, vol. 245, no. 1–3, pp. 266–283, Sep. 2009, doi: 10.1016/j.desal.2008.07.012.

[94] A. Cipollina, G. Micale, and L. Rizzuti, “A critical assessment of desalination operations in Sicily,” *Desalination*, vol. 182, no. 1–3, pp. 1–12, 2005, doi: 10.1016/j.desal.2005.03.004.

[95] C. Temstet, G. Canton, J. Laborie, and A. Durante, “A large high-performance MED plant in Sicily,” *Desalination*, vol. 105, no. 1–2, pp. 109–114, 1996, doi: 10.1016/0011-9164(96)00064-1.

[96] D. Zhao, J. Xue, S. Li, H. Sun, and Q. dong Zhang, “Theoretical analyses of thermal and economical aspects of multi-effect distillation desalination dealing with high-salinity wastewater,” *Desalination*, vol. 273, no. 2–3, pp. 292–298, 2011, doi: 10.1016/j.desal.2011.01.048.

[97] M. M. Ashour, “Steady state analysis of the Tripoli West LT-HT-MED plant,” *Desalination*, vol. 152, no. 1–3, pp. 191–194, 2003, doi:

10.1016/S0011-9164(02)01062-7.

[98] P. Sharan and S. Bandyopadhyay, “Integration of thermo-vapor compressor with multiple-effect evaporator,” *Appl. Energy*, vol. 184, pp. 560–573, 2016, doi: 10.1016/j.apenergy.2016.10.037.

[99] V. Dvornikov, “Seawater multi-effect distillation energized by a combustion turbine,” *Desalination*, vol. 127, no. 3, pp. 261–269, 2000, doi: 10.1016/S0011-9164(00)00015-1.

[100] M. A. Sharaf, A. S. Nafey, and L. García-Rodríguez, “Exergy and thermo-economic analyses of a combined solar organic cycle with multi effect distillation (MED) desalination process,” *Desalination*, vol. 272, no. 1–3, pp. 135–147, 2011, doi: 10.1016/j.desal.2011.01.006.

[101] M. A. DARWISH, F. AL JUWAYHEL, and H. KAMAL, “MULTI-EFFECT BOILING SYSTEM MEB: AN ENERGY VIEWPOINT,” in *Sustainable Development of Energy, Water and Environment Systems*, Jun. 2007, vol. 194, no. 1–3, pp. 351–372. doi: 10.1142/9789812771285_0032.

[102] M. A. Sharaf, “Design and Simulation of Solar Desalination Systems,” Suez Canal University, 2011.

[103] M. Khedr, “Techno-Economic investigation of an air humidification-dehumidification desalination process,” *Chem. Eng. Technol.*, vol. 16, no. 4, pp. 270–274, Aug. 1993, doi: 10.1002/ceat.270160410.

[104] G. Al-Enezi, H. Ettouney, and N. Fawzy, “Low temperature humidification dehumidification desalination process,” *Energy Convers. Manag.*, vol. 47, no. 4, pp. 470–484, Mar. 2006, doi: 10.1016/j.enconman.2005.04.010.

[105] G. P. Narayan, M. H. Sharqawy, J. H. Lienhard V, and S. M. Zubair, “Thermodynamic analysis of humidification dehumidification desalination cycles,” *Desalin. Water Treat.*, vol. 16, no. 1–3, pp. 339–353, 2010, doi: 10.5004/dwt.2010.1078.

[106] S. Farsad and A. Behzadmehr, “Analysis of a solar desalination unit with humidification-dehumidification cycle using DoE method,” *Desalination*, vol. 278, no. 1–3, pp. 70–76, 2011, doi: 10.1016/j.desal.2011.05.008.

[107] M. Al-Sahali and H. M. Ettouney, “Humidification dehumidification desalination process: Design and performance evaluation,” *Chem. Eng. J.*, vol. 143, no. 1–3, pp. 257–264, 2008, doi: 10.1016/j.cej.2008.04.030.

[108] S. M. Zubair, M. A. Antar, S. M. Elmutasim, and D. U. Lawal, “Performance evaluation of humidification-dehumidification (HDH) desalination systems with and without heat recovery options: An experimental and theoretical investigation,” *Desalination*, vol. 436, no. October 2017, pp. 161–175, 2018,

doi: 10.1016/j.desal.2018.02.018.

[109] P. T. Tsilingiris, “Thermophysical and transport properties of humid air at temperature range between 0 and 100 °C,” *Energy Convers. Manag.*, vol. 49, no. 5, pp. 1098–1110, 2008, doi: 10.1016/j.enconman.2007.09.015.

[110] SFitz, “AirProperties.” GitHub, 2021. [Online]. Available: https://github.com/sjfitz/AirProperties

[111] S. Farsad, A. Behzadmehr, and S. M. H. Sarvari, “Numerical analysis of solar desalination using humidification—dehumidification cycle,” *Desalin. Water Treat.*, vol. 19, no. 1–3, pp. 294–300, 2010, doi: 10.5004/dwt.2010.1487.

[112] M. H. Hamed, A. E. Kabeel, Z. M. Omara, and S. W. Sharshir, “Mathematical and experimental investigation of a solar humidification-dehumidification desalination unit,” *Desalination*, vol. 358, pp. 9–17, 2015, doi: 10.1016/j.desal.2014.12.005.

[113] G. Franchini and A. Perdichizzi, “Modeling of a solar driven HD (humidification-dehumidification) desalination system,” *Energy Procedia*, vol. 45, pp. 588–597, 2014, doi: 10.1016/j.egypro.2014.01.063.

[114] E. H. Amer, H. Kotb, G. H. Mostafa, and A. R. El-Ghalban, “Theoretical and experimental investigation of humidification-dehumidification desalination unit,” *Desalination*, vol. 249, no. 3, pp. 949–959, 2009, doi: 10.1016/j.desal.2009.06.063.

[115] R. Santosh, G. Kumaresan, S. Selvaraj, T. Arunkumar, and R. Velraj, “Investigation of humidification-dehumidification desalination system through waste heat recovery from household air conditioning unit,” *Desalination*, vol. 467, no. May, pp. 1–11, 2019, doi: 10.1016/j.desal.2019.05.016.

[116] K. G. Tay and L. Song, “A more effective method for fouling characterization in a full-scale reverse osmosis process,” *Desalination*, vol. 177, no. 1–3, pp. 95–107, Jun. 2005, doi: 10.1016/j.desal.2004.11.017.

[117] S. A. Avlonitis, M. Pappas, and K. Moutesidis, “A unified model for the detailed investigation of membrane modules and RO plants performance,” *Desalination*, vol. 203, no. 1–3, pp. 218–228, 2007, doi: 10.1016/j.desal.2006.04.009.

[118] H. J. Oh, T. M. Hwang, and S. Lee, “A simplified simulation model of RO systems for seawater desalination,” *Desalination*, vol. 238, no. 1–3, pp. 128–139, 2009, doi: 10.1016/j.desal.2008.01.043.

[119] V. Geraldes, N. E. Pereira, and M. N. De Pinho, “Simulation and

optimization of medium-sized seawater reverse osmosis processes with spiral-wound modules," *Ind. Eng. Chem. Res.*, vol. 44, no. 6, pp. 1897–1905, 2005, doi: 10.1021/ie049357s.

[120] M. Khraisheh *et al.*, "Osmotic pressure estimation using the Pitzer equation for forward osmosis modelling," *Environ. Technol.*, vol. 41, no. 19, pp. 2533–2545, Aug. 2020, doi: 10.1080/09593330.2019.1575476.

[121] T. Kaghazchi, M. Mehri, M. T. Ravanchi, and A. Kargari, "A mathematical modeling of two industrial seawater desalination plants in the Persian Gulf region," *Desalination*, vol. 252, no. 1–3, pp. 135–142, 2010, doi: 10.1016/j.desal.2009.10.012.

[122] K. G. Nayar *et al.*, "Feasibility study of an electrodialysis system for in-home water desalination in urban India," *Dev. Eng.*, vol. 2, no. December 2016, pp. 38–46, 2016, doi: 10.1016/j.deveng.2016.12.001.

[123] M. Qasim, M. Badrelzaman, N. N. Darwish, N. A. Darwish, and N. Hilal, "Reverse osmosis desalination: A state-of-the-art review," *Desalination*, vol. 459, no. December 2018, pp. 59–104, Jun. 2019, doi: 10.1016/j.desal.2019.02.008.

[124] E.-S. Jang *et al.*, "Influence of concentration polarization and thermodynamic non-ideality on salt transport in reverse osmosis membranes," *J. Memb. Sci.*, vol. 572, no. October 2018, pp. 668–675, Feb. 2019, doi: 10.1016/j.memsci.2018.11.006.

[125] A. O. Sharif *et al.*, "A new theoretical approach to estimate the specific energy consumption of reverse osmosis and other pressure-driven liquid-phase membrane processes," *Desalin. Water Treat.*, vol. 3, no. 1–3, pp. 111–119, 2009, doi: 10.5004/dwt.2009.295.

[126] A. Altaee, "Computational model for estimating reverse osmosis system design and performance: Part-one binary feed solution," *Desalination*, vol. 291, pp. 101–105, 2012, doi: 10.1016/j.desal.2012.01.028.

[127] X. Jin, A. Jawor, S. Kim, and E. M. V. Hoek, "Effects of feed water temperature on separation performance and organic fouling of brackish water RO membranes," *Desalination*, vol. 239, no. 1–3, pp. 346–359, 2009, doi: 10.1016/j.desal.2008.03.026.

[128] J. C. Crittenden, R. R. Trussell, D. W. Hand, K. J. Howe, and G. Tchobanoglous, "Reverse Osmosis," in *MWH's Water Treatment - Principles and Design*, 3rd ed., John Wiley & Sons, 2012, pp. 1335–1414. [Online]. Available: https://app.knovel.com/hotlink/pdf/id:kt00AD5567/mwh-s-water-treatment/mwh-s-wate-reverse-osmosis

[129] N. M. Mazlan, D. Peshev, and A. G. Livingston, “Energy consumption for desalination — A comparison of forward osmosis with reverse osmosis, and the potential for perfect membranes,” *Desalination*, vol. 377, pp. 138–151, Jan. 2016, doi: 10.1016/j.desal.2015.08.011.

[130] D. E. Wiley and D. F. Fletcher, “Techniques for computational fluid dynamics modelling of flow in membrane channels,” *J. Memb. Sci.*, vol. 211, no. 1, pp. 127–137, 2003, doi: 10.1016/S0376-7388(02)00412-X.

[131] M. Ben Boudinar, W. T. Hanbury, and S. Avlonitis, “Numerical simulation and optimisation of spiral-wound modules,” *Desalination*, vol. 86, no. 3, pp. 273–290, 1992, doi: 10.1016/0011-9164(92)80038-B.

[132] G. Schock and A. Miquel, “Mass transfer and pressure loss in spiral wound modules,” *Desalination*, vol. 64, pp. 339–352, Jan. 1987, doi: 10.1016/0011-9164(87)90107-X.

[133] B. J. Mariñas and R. I. Urama, “Modeling Concentration-Polarization in Reverse Osmosis Spiral-Wound Elements,” *J. Environ. Eng.*, vol. 122, no. 4, pp. 292–298, Apr. 1996, doi: 10.1061/(ASCE)0733-9372(1996)122:4(292).

[134] M. Shakaib, S. M. F. Hasani, and M. Mahmood, “CFD modeling for flow and mass transfer in spacer-obstructed membrane feed channels,” *J. Memb. Sci.*, vol. 326, no. 2, pp. 270–284, Jan. 2009, doi: 10.1016/j.memsci.2008.09.052.

[135] F. Valero, A. Barcelo, and R. Arbos, “Electrodialysis Technology - Theory and Applications,” in *Desalination, Trends and Technologies*, vol. 189, no. 3, M. Schorr, Ed. InTech, 2011, pp. 1521–1535. doi: 10.5772/14297.

[136] T. Mohammadi, A. Moheb, M. Sadrzadeh, and A. Razmi, “Modeling of metal ion removal from wastewater by electrodialysis,” *Sep. Purif. Technol.*, vol. 41, no. 1, pp. 73–82, 2005, doi: 10.1016/j.seppur.2004.04.007.

[137] J. M. Ortiz *et al.*, “Brackish water desalination by electrodialysis: Batch recirculation operation modeling,” *J. Memb. Sci.*, vol. 252, no. 1–2, pp. 65–75, 2005, doi: 10.1016/j.memsci.2004.11.021.

[138] M. Sadrzadeh, A. Kaviani, and T. Mohammadi, “Mathematical modeling of desalination by electrodialysis,” *Desalination*, vol. 206, no. 1–3, pp. 538–546, 2007, doi: 10.1016/j.desal.2006.04.062.

[139] L. Karimi and A. Ghassemi, “An empirical/theoretical model with dimensionless numbers to predict the performance of electrodialysis systems on the basis of operating conditions,” *Water Res.*, vol. 98, pp. 270–279, 2016, doi: 10.1016/j.watres.2016.04.014.

[140] M. La Cerva *et al.*, "Determination of limiting current density and current efficiency in electrodialysis units," *Desalination*, vol. 445, no. July, pp. 138–148, 2018, doi: 10.1016/j.desal.2018.07.028.

[141] A. Campione, L. Gurreri, M. Ciofalo, G. Micale, A. Tamburini, and A. Cipollina, "Electrodialysis for water desalination: A critical assessment of recent developments on process fundamentals, models and applications," *Desalination*, vol. 434, no. October 2017, pp. 121–160, 2018, doi: 10.1016/j.desal.2017.12.044.

[142] M. Ben Sik Ali, A. Mnif, and B. Hamrouni, "Modelling of the limiting current density of an electrodialysis process by response surface methodology," *Ionics (Kiel).*, vol. 24, no. 2, pp. 617–628, 2018, doi: 10.1007/s11581-017-2214-7.

[143] V. Geraldes and M. D. Afonso, "Limiting current density in the electrodialysis of multi-ionic solutions," *J. Memb. Sci.*, vol. 360, no. 1–2, pp. 499–508, 2010, doi: 10.1016/j.memsci.2010.05.054.

[144] R. Valerdi-Pérez and J. Ibáñez-Mengual, "Current—voltage curves for an electrodialysis reversal pilot plant: determination of limiting currents," *Desalination*, vol. 141, no. 1, pp. 23–37, Dec. 2001, doi: 10.1016/S0011-9164(01)00386-1.

[145] Y. Tanaka, "Limiting current density of an ion-exchange membrane and of an electrodialyzer," *J. Memb. Sci.*, vol. 266, no. 1–2, pp. 6–17, 2005, doi: 10.1016/j.memsci.2005.05.005.

[146] H. J. Lee, H. Strathmann, and S. H. Moon, "Determination of the limiting current density in electrodialysis desalination as an empirical function of linear velocity," *Desalination*, vol. 190, no. 1–3, pp. 43–50, 2006, doi: 10.1016/j.desal.2005.08.004.

[147] A. Nakayama, Y. Sano, X. Bai, and K. Tado, "A boundary layer analysis for determination of the limiting current density in an electrodialysis desalination," *Desalination*, vol. 404, pp. 41–49, 2017, doi: 10.1016/j.desal.2016.10.013.

[148] D. Zhao, L. Y. Lee, S. L. Ong, P. Chowdhury, K. B. Siah, and H. Y. Ng, "Electrodialysis reversal for industrial reverse osmosis brine treatment," *Sep. Purif. Technol.*, vol. 213, no. December 2018, pp. 339–347, Apr. 2019, doi: 10.1016/j.seppur.2018.12.056.

[149] Y. Gong, X. L. Wang, and L. X. Yu, "Process simulation of desalination by electrodialysis of an aqueous solution containing a neutral solute," *Desalination*, vol. 172, no. 2, pp. 157–172, 2005, doi: 10.1016/j.desal.2004.06.200.

[150] Y. Tanaka, “A computer simulation of feed and bleed ion exchange membrane electrodialysis for desalination of saline water,” *Desalination*, vol. 254, no. 1–3, pp. 99–107, May 2010, doi: 10.1016/j.desal.2009.12.008.

[151] Y. Oren, “Capacitive deionization (CDI) for desalination and water treatment - past, present and future (a review),” *Desalination*, vol. 228, no. 1–3, pp. 10–29, 2008, doi: 10.1016/j.desal.2007.08.005.

[152] M. E. Suss, S. Porada, X. Sun, P. M. Biesheuvel, J. Yoon, and V. Presser, “Water desalination via capacitive deionization: What is it and what can we expect from it?,” *Energy Environ. Sci.*, vol. 8, no. 8, pp. 2296–2319, 2015, doi: 10.1039/c5ee00519a.

[153] J. E. Dykstra, J. Dijkstra, A. van der Wal, H. V. M. Hamelers, and S. Porada, “On-line method to study dynamics of ion adsorption from mixtures of salts in capacitive deionization,” *Desalination*, vol. 390, pp. 47–52, Jul. 2016, doi: 10.1016/j.desal.2016.04.001.

[154] J. Oladunni, J. H. Zain, A. Hai, F. Banat, G. Bharath, and E. Alhseinat, “A comprehensive review on recently developed carbon based nanocomposites for capacitive deionization: From theory to practice,” *Sep. Purif. Technol.*, vol. 207, no. March, pp. 291–320, 2018, doi: 10.1016/j.seppur.2018.06.046.

[155] M. Qin *et al.*, “Corrigendum to ‘Comparison of energy consumption in desalination by capacitive deionization and reverse osmosis’ [DES 455 (2019) 100–114],” *Desalination*, vol. 461, no. April, p. 55, Jul. 2019, doi: 10.1016/j.desal.2019.03.016.

[156] M. Qin *et al.*, “Response to comments on ‘comparison of energy consumption in desalination by capacitive deionization and reverse osmosis,’” *Desalination*, vol. 462, no. April, pp. 48–55, Jul. 2019, doi: 10.1016/j.desal.2019.04.004.

[157] M. E. Suss *et al.*, “Capacitive desalination with flow-through electrodes,” *Energy Environ. Sci.*, vol. 5, no. 11, pp. 9511–9519, 2012, doi: 10.1039/c2ee21498a.

[158] E. N. Guyes, A. N. Shocron, A. Simanovski, P. M. Biesheuvel, and M. E. Suss, “A one-dimensional model for water desalination by flow-through electrode capacitive deionization,” *Desalination*, vol. 415, pp. 8–13, 2017, doi: 10.1016/j.desal.2017.03.013.

[159] A. Rommerskirchen, B. Ohs, K. A. Hepp, R. Femmer, and M. Wessling, “Modeling continuous flow-electrode capacitive deionization processes with ion-exchange membranes,” *J. Memb. Sci.*, vol. 546, no. October 2017, pp. 188–196, 2018, doi: 10.1016/j.memsci.2017.10.026.

[160] J. E. Dykstra, R. Zhao, P. M. Biesheuvel, and A. Van der Wal, “Resistance

identification and rational process design in Capacitive Deionization," *Water Res.*, vol. 88, pp. 358–370, 2016, doi: 10.1016/j.watres.2015.10.006.

[161] R. Zhao, P. M. Biesheuvel, and A. Van Der Wal, "Energy consumption and constant current operation in membrane capacitive deionization," *Energy Environ. Sci.*, vol. 5, no. 11, pp. 9520–9527, 2012, doi: 10.1039/c2ee21737f.

[162] C. A. R. Perez, O. N. Demirer, R. L. Clifton, R. M. Naylor, and C. H. Hidrovo, "Macro Analysis of the Electro-Adsorption Process in Low Concentration NaCl Solutions for Water Desalination Applications," *J. Electrochem. Soc.*, vol. 160, no. 3, pp. E13–E21, Jan. 2013, doi: 10.1149/2.025303jes.

[163] A. Hemmatifar, M. Stadermann, and J. G. Santiago, "Two-Dimensional Porous Electrode Model for Capacitive Deionization," *J. Phys. Chem. C*, vol. 119, no. 44, pp. 24681–24694, 2015, doi: 10.1021/acs.jpcc.5b05847.

[164] J. E. Dykstra, S. Porada, A. van der Wal, and P. M. Biesheuvel, "Supplementary Information Energy consumption in capacitive deionization – Constant current versus constant voltage operation," *Water Res.*, vol. 143, pp. 367–375, 2018, doi: 10.1016/j.watres.2018.06.034.

[165] L. Wang and S. Lin, "Theoretical framework for designing a desalination plant based on membrane capacitive deionization," *Water Res.*, vol. 158, pp. 359–369, 2019, doi: 10.1016/j.watres.2019.03.076.

[166] S. Lin *et al.*, "Seawater desalination technology and engineering in China: A review," *Desalination*, vol. 498, no. October 2020, p. 114728, 2021, doi: 10.1016/j.desal.2020.114728.

[167] H. T. El-Dessouky, H. M. Ettouney, and F. Mandani, "Performance of parallel feed multiple effect evaporation system for seawater desalination," *Appl. Therm. Eng.*, vol. 20, no. 17, pp. 1679–1706, Dec. 2000, doi: 10.1016/S1359-4311(99)00098-8.

[168] D. Hasson, A. Drak, and R. Semiat, "Inception of CaSO4 scaling on RO membranes at various water recovery levels," *Desalination*, vol. 139, no. 1–3, pp. 73–81, Sep. 2001, doi: 10.1016/S0011-9164(01)00296-X.

[169] *Guidelines for drinking-water quality: fourth edition incorporating the first and second addenda*. Geneva: World Health Organization, 2017.

[170] M. Wakil Shahzad, M. Burhan, H. Soo Son, S. Jin Oh, and K. Choon Ng, "Desalination processes evaluation at common platform: A universal performance ratio (UPR) method," *Appl. Therm. Eng.*, vol. 134, no. October 2017, pp. 62–67, Apr. 2018, doi: 10.1016/j.applthermaleng.2018.01.098.

[171] G. Raluy, L. Serra, and J. Uche, "Life cycle assessment of MSF, MED and

RO desalination technologies," *Energy*, vol. 31, no. 13, pp. 2361–2372, 2006, doi: 10.1016/j.energy.2006.02.005.

[172] Y. Dreizin, "Ashkelon seawater desalination project - Off-taker's self costs, supplied water costs, total costs and benefits," *Desalination*, vol. 190, no. 1–3, pp. 104–116, 2006, doi: 10.1016/j.desal.2005.08.006.

[173] R. Valladares Linares *et al.*, "Life cycle cost of a hybrid forward osmosis – low pressure reverse osmosis system for seawater desalination and wastewater recovery," *Water Res.*, vol. 88, no. 7, pp. 225–234, Jan. 2016, doi: 10.1016/j.watres.2015.10.017.

[174] S. Senthil and S. Senthilmurugan, "Reverse Osmosis-Pressure Retarded Osmosis hybrid system: Modelling, simulation and optimization," *Desalination*, vol. 389, pp. 78–97, 2016, doi: 10.1016/j.desal.2016.01.027.

[175] R. Lokk, S. M. Alsadaie, and I. M. Mujtaba, "Dynamic simulation of once-through multistage flash (MSF-OT) desalination process: Effect of seawater temperature on the fouling mechanism in the heat exchangers," *Comput. Chem. Eng.*, vol. 155, p. 107515, 2021, doi: 10.1016/j.compchemeng.2021.107515.

[176] M. Di Martino, S. Avraamidou, J. Cook, and E. N. Pistikopoulos, "An optimization framework for the design of reverse osmosis desalination plants under food-energy-water nexus considerations," *Desalination*, vol. 503, no. May 2020, p. 114937, 2021, doi: 10.1016/j.desal.2021.114937.

[177] J. Kim, K. Park, and S. Hong, "Application of two-stage reverse osmosis system for desalination of high-salinity and high-temperature seawater with improved stability and performance," *Desalination*, vol. 492, no. June, p. 114645, 2020, doi: 10.1016/j.desal.2020.114645.

[178] E. Tayyeban, M. Deymi-Dashtebayaz, and D. Dadpour, "Multi objective optimization of MSF and MSF-TVC desalination systems with using the surplus low-pressure steam (an energy, exergy and economic analysis)," *Comput. Chem. Eng.*, vol. 160, p. 107708, 2022, doi: 10.1016/j.compchemeng.2022.107708.

[179] L. Huang *et al.*, "Industrial wastewater desalination under uncertainty in coal-chemical eco-industrial parks," *Resour. Conserv. Recycl.*, vol. 145, no. December 2018, pp. 370–378, 2019, doi: 10.1016/j.resconrec.2019.02.036.

[180] P. Wu, C. Xia, F. Liu, Y. Wu, and Y. He, "An integrated water strategy based on the current circumstances in China," *Appl. Math. Model.*, vol. 40, no. 17–18, pp. 8108–8124, 2016, doi: 10.1016/j.apm.2016.01.003.

[181] C. Papadaskalopoulou, E. Katsou, K. Valta, K. Moustakas, D. Malamis, and M. Dodou, "Review and assessment of the adaptive capacity of the water

sector in Cyprus against climate change impacts on water availability," *Resour. Conserv. Recycl.*, vol. 105, pp. 95–112, 2015, doi: 10.1016/j.resconrec.2015.10.017.

[182] D. Kumar, V. Kumar, and V. P. Singh, "Modeling and dynamic simulation of mixed feed multi-effect evaporators in paper industry," *Appl. Math. Model.*, vol. 37, no. 1–2, pp. 384–397, 2013, doi: 10.1016/j.apm.2012.02.039.

[183] D. R. Jones, "A Taxonomy of Global Optimization Methods Based on Response Surfaces," *J. Glob. Optim.*, vol. 21, no. 4, pp. 345–383, 2001, doi: 10.1023/A:1012771025575.

[184] A. Sóbester, S. J. Leary, and A. J. Keane, "On the design of optimization strategies based on global response surface approximation models," *J. Glob. Optim.*, vol. 33, no. 1, pp. 31–59, 2005, doi: 10.1007/s10898-004-6733-1.

[185] D. Huang, T. T. Allen, W. I. Notz, and N. Zeng, "Global optimization of stochastic black-box systems via sequential kriging meta-models," *J. Glob. Optim.*, vol. 34, no. 3, pp. 441–466, 2006, doi: 10.1007/s10898-005-2454-3.

[186] S. A. Romo, N. Mattise, and J. Srebric, "Desalination metamodels and a framework for cross-comparative performance simulations," *Desalination*, vol. 525, no. 1 March 2022, p. 115474, Mar. 2022, doi: 10.1016/j.desal.2021.115474.

[187] R. Stover and J. Martin, "Titan PX-1200 energy recovery device - test results from the inima Los Cabos, Mexico, seawater RO facility," *Desalin. Water Treat.*, vol. 3, no. 1–3, pp. 179–182, 2009, doi: 10.5004/dwt.2009.458.

[188] R. L. Stover, "Energy Recovery Device Performance Analysis," 2005, pp. 1–3. [Online]. Available: www.energy-recovery.com

[189] C. Desportes, "Experience and Operating Feed Back After 7 Years of Operation of a 10,000 M3/D MED Plant," 2013. doi: IDAWC/TIAN13-254.

[190] F. N. Team, "Desalination for Bahamian Resort," 2018. https://www.fluencecorp.com/desalination-for-bahamian-resort/ (accessed Oct. 07, 2021).

[191] Fluence, "Fluence achieves 2018 guidance with strong growth in Q4," 2018.

[192] "World Sea Water Temperatures." https://seatemperature.info/

[193] M. Ben Boudinar, "Performance prediction and optimisation of spiral wound modules," University of Glasgow, 1991.

[194] "LPG Prices," *Retail energy price data*, 2022.

https://www.globalpetrolprices.com

[195] "Electricity Prices," *Retail energy price data*, 2022. https://www.globalpetrolprices.com/

[196] M. O. Mavukkandy, C. M. Chabib, I. Mustafa, A. Al Ghaferi, and F. AlMarzooqi, "Brine management in desalination industry: From waste to resources generation," *Desalination*, vol. 472, no. September, p. 114187, Dec. 2019, doi: 10.1016/j.desal.2019.114187.

[197] A. Antony, J. H. Low, S. Gray, A. E. Childress, P. Le-Clech, and G. Leslie, "Scale formation and control in high pressure membrane water treatment systems: A review," *J. Memb. Sci.*, vol. 383, no. 1–2, pp. 1–16, 2011, doi: 10.1016/j.memsci.2011.08.054.

[198] I. G. Wenten, P. T. P. Aryanti, and A. N. Hakim, "Scale-up Strategies for Membrane-Based Desalination Processes: A Review," *J. Membr. Sci. Res.*, vol. 2, pp. 42–58, 2016, doi: 10.22079/JMSR.2016.19152.

[199] I. Sutzkover-Gutman and D. Hasson, "Feed water pretreatment for desalination plants," *Desalination*, vol. 264, no. 3, pp. 289–296, 2010, doi: 10.1016/j.desal.2010.07.014.

[200] J. Kavitha, M. Rajalakshmi, A. R. Phani, and M. Padaki, "Pretreatment processes for seawater reverse osmosis desalination systems—A review," *J. Water Process Eng.*, vol. 32, no. April, p. 100926, 2019, doi: 10.1016/j.jwpe.2019.100926.

[201] P. S. Goh, W. J. Lau, M. H. D. Othman, and A. F. Ismail, "Membrane fouling in desalination and its mitigation strategies," *Desalination*, vol. 425, pp. 130–155, Jan. 2018, doi: 10.1016/j.desal.2017.10.018.

[202] Q. She, R. Wang, A. G. Fane, and C. Y. Tang, "Membrane fouling in osmotically driven membrane processes: A review," *J. Memb. Sci.*, vol. 499, pp. 201–233, Feb. 2016, doi: 10.1016/J.MEMSCI.2015.10.040.

[203] E. M. V. Hoek, J. Allred, T. Knoell, and B.-H. Jeong, "Modeling the effects of fouling on full-scale reverse osmosis processes," *J. Memb. Sci.*, vol. 314, no. 1–2, pp. 33–49, Apr. 2008, doi: 10.1016/j.memsci.2008.01.025.

[204] M. Jafari *et al.*, "Cost of fouling in full-scale reverse osmosis and nanofiltration installations in the Netherlands," *Desalination*, vol. 500, no. December 2020, p. 114865, 2021, doi: 10.1016/j.desal.2020.114865.

[205] F. A. Essa, A. S. Abdullah, Z. M. Omara, A. E. Kabeel, and W. M. El-Maghlany, "On the different packing materials of humidification–dehumidification thermal desalination techniques – A review," *J. Clean. Prod.*, vol. 277, p. 123468, Dec. 2020, doi: 10.1016/j.jclepro.2020.123468.

[206] N. Heck, K. Lykkebo Petersen, D. C. Potts, B. Haddad, and A. Paytan, "Predictors of coastal stakeholders' knowledge about seawater desalination impacts on marine ecosystems," *Sci. Total Environ.*, vol. 639, pp. 785–792, Oct. 2018, doi: 10.1016/j.scitotenv.2018.05.163.

[207] B. Abbasi, M. A. E. Khalifa, D. Sharma, and X. Zhang, "Method and Apparatus for Desalinating Water," US 2021/0039008 A1, 2021 [Online]. Available: https://www.lens.org/lens/patent/178-685-600-736-733

[208] M. A. Elhashimi, X. Zhang, and B. Abbasi, "Empirical prediction of saline water atomization pressure loss and spray phase change using local flow pressure analysis," *Desalination*, vol. 514, p. 115156, Oct. 2021, doi: 10.1016/j.desal.2021.115156.

[209] M. A. Elhashimi, J. Shorb, M. Messer, and B. Abbasi, "Assessment of Humid Air-Solids Cyclone Separators in A Novel Humidification-Dehumidification Desalination," 2021.

[210] J. Jedelsky and M. Jicha, "Energy conversion during effervescent atomization," *Fuel*, vol. 111, pp. 836–844, 2013, doi: 10.1016/j.fuel.2013.03.053.

[211] A. C. Hoffmann and L. E. Stein, *Gas Cyclones and Swirl Tubes*. Berlin, Heidelberg: Springer Berlin Heidelberg, 2007. doi: 10.1007/978-3-540-74696-6.

[212] N. de Nevers, *Air Pollution Control Engineering*, Second Edi. McGraw-Hill, 2000.

[213] M. A. Elhashimi, M. Gee, and B. Abbasi, "Unconventional Desalination: The Use of Cyclone Separators in HDH Desalination to Achieve Zero Liquid Discharge," *Desalination*, 2022, doi: https://doi.org/10.1016/j.desal.2022.115932.

[214] D. Sharma, D. P. Ghosh, S. J. Dennis, and B. Abbasi, "Fouling mechanism in airblast atomizers and its suppression for water desalination," *Water Res.*, vol. 221, no. December 2021, p. 118726, 2022, doi: 10.1016/j.watres.2022.118726.

[215] M. Ochowiak *et al.*, "The concept design and study of twin-fluid effervescent atomizer with air stone aerator," *Chem. Eng. Process. Process Intensif.*, vol. 124, no. November 2017, pp. 24–28, 2018, doi: 10.1016/j.cep.2017.11.020.

[216] A. Kourmatzis, A. Lowe, and A. R. Masri, "Combined effervescent and airblast atomization of a liquid jet," *Exp. Therm. Fluid Sci.*, vol. 75, pp. 66–76, Jul. 2016, doi: 10.1016/j.expthermflusci.2016.02.002.

[217] V. Tesař, “New concept: Low-pressure, wide-angle atomiser,” *Chem. Eng. Process. Process Intensif.*, vol. 82, pp. 19–29, Aug. 2014, doi: 10.1016/j.cep.2014.05.004.

[218] G. B. Abdelaziz, M. A. Dahab, M. A. Omara, S. W. Sharshir, A. M. Elsaid, and E. M. S. El-Said, “Humidification dehumidification saline water desalination system utilizing high frequency ultrasonic humidifier and solar heated air stream,” *Therm. Sci. Eng. Prog.*, vol. 27, no. June 2021, p. 101144, Jan. 2022, doi: 10.1016/j.tsep.2021.101144.

[219] A. E. Tourab, A. M. Blanco-Marigorta, A. M. Elharidi, and M. J. Suárez-López, “A Novel Humidification Technique Used in Water Desalination Systems Based on the Humidification–Dehumidification Process: Experimentally and Theoretically,” *Water*, vol. 12, no. 8, p. 2264, Aug. 2020, doi: 10.3390/w12082264.

[220] Z. Xiong, M. Lu, M. Wang, H. Gu, and X. Cheng, “Study on flow pattern and separation performance of air-water swirl-vane separator,” *Ann. Nucl. Energy*, vol. 63, pp. 138–145, 2014, doi: 10.1016/j.anucene.2013.07.026.

[221] J. Miller, “Ideal Air Properties,” *MATLAB Central File Exchange*, 2020. https://www.mathworks.com/matlabcentral/fileexchange/25030-ideal-air-properties (accessed Nov. 24, 2020).

[222] S. A. Romo, M. Storch Jr., and J. Srebric, “Operation Modeling of Actual Desalination Plants,” *Desalination*, 2022, doi: Under peer-review.

[223] P. Ziemkiewicz, J. Hause, R. Lovett, D. L. Harry Johnson, and D. Patchen, “Zero Discharge Water Management for Horizontal Shale Gas Well Development,” Pittsburgh, PA, and Morgantown, WV (United States), Mar. 2012. doi: 10.2172/1054519.

[224] US Energy Information Administration, “Electric Sales, Revenue, and Average Price,” 2020. https://www.eia.gov/electricity/sales_revenue_price/ (accessed Jan. 06, 2021).

[225] F. Evangelista, “A Short Cut Method for the Design of Reverse Osmosis Desalination Plants,” *Ind. Eng. Chem. Process Des. Dev.*, vol. 24, no. 1, pp. 211–223, 1985, doi: 10.1021/i200028a036.

[226] A. R. Hussain and A. H. Ahmed, “The Addur SWRO desalination plant towards a full plant production,” *Desalination*, vol. 120, no. 1–2, pp. 143–152, 1998, doi: 10.1016/S0011-9164(98)00212-4.

[227] K. Burashid and A. R. Hussain, “Seawater RO plant operation and maintenance experience: addur desalination plant operation assessment,” *Desalination*, vol. 165, no. SUPPL., pp. 11–22, Aug. 2004, doi: 10.1016/j.desal.2004.06.002.

[228] F. van Rooij, P. Scarf, and P. Do, “Planning the restoration of membranes in RO desalination using a digital twin,” *Desalination*, vol. 519, no. June 2021, p. 115214, 2022, doi: 10.1016/j.desal.2021.115214.

[229] S. Xiao, Q. Guan, W. Zhang, and L. Wu, “Optimal scheduling of the combined power and desalination system,” *Energy Reports*, vol. 8, pp. 661–669, 2022, doi: 10.1016/j.egyr.2021.11.253.

[230] C. Bailey, *Hyperfocus: How to Be More Productive in a World of Distraction*, 2018th ed. New York: Viking, 2018.

[231] C. Newport, *Deep Work: Rules for Focused Success in a Distracted World*, 2016th ed. London: Piatkus, 2016.

[232] J. D. Birkett, “A brief illustrated history of desalination,” *Desalination*, vol. 50, pp. 17–52, Jan. 1984, doi: 10.1016/0011-9164(84)85014-6.

[233] M. Paidar, V. Fateev, and K. Bouzek, “Membrane electrolysis—History, current status and perspective,” *Electrochim. Acta*, vol. 209, pp. 737–756, 2016, doi: 10.1016/j.electacta.2016.05.209.